

Dipl.-Phys. Ole Hölck

Gas Sorption and Swelling in Glassy Polymers

**Combining Experiment, Phenomenological Models
and Detailed Atomistic Molecular Modeling**

Die vorliegende Arbeit entstand an der Bundesanstalt für Materialforschung und -prüfung (BAM).

Impressum

Gas Sorption and Swelling in Glassy Polymers

Combining Experiment, Phenomenological Models
and Detailed Atomistic Molecular Modeling

2008

Herausgeber:
Bundesanstalt für Materialforschung und -prüfung (BAM)
Unter den Eichen 87
12205 Berlin
Telefon: +49 30 8104-0
Telefax: +49 30 8112029
E-Mail: info@bam.de
Internet: www.bam.de

Copyright © 2008 by Bundesanstalt für
Materialforschung und -prüfung (BAM)

Layout: BAM-Arbeitsgruppe Z.64

ISSN 1613-4249
ISBN 978-3-9812072-5-5

Gas Sorption and Swelling in Glassy Polymers
Combining Experiment, Phenomenological Models and Detailed
Atomistic Molecular Modeling

von der
Fakultät III Prozesswissenschaften
der Technischen Universität Berlin
genehmigte

DISSERTATION

zur Erlangung des akademischen Grades
doctor rerum naturalium
(Dr. rer. nat.)

vorgelegt von
Herrn Dipl.-Phys. Ole Hölck
geboren am 06.06.1972 in Kiel

Promotionsausschuss:

- Vorsitzender: Prof. Dr. Bernhard Senge
1. Gutachter: Prof. Dr.-Ing. Manfred H. Wagner
2. Gutachter: Prof. Dr. Dieter Hofmann

Tag der wissenschaftlichen Aussprache: 22.01.2008

Berlin 2008
D 83

Zusammenfassung

Durchgeführte Arbeiten: In der vorliegenden Arbeit werden grundlegende Fragen zur Gas-Sorption und der damit verbundenen Quellung von glasigen Polymeren untersucht. Dabei wurde eine kombinierte Analyse aus experimenteller Charakterisierung, detailliert atomistischer Modellierung und phänomenologisch-theoretischer Betrachtung angewandt.

Drei unterschiedliche Polymere, ein Polysulfon (PSU), ein Polyimid (PI4) und ein neuartiges Polymermaterial (PIM-1), wurden experimentell bezüglich ihrer Sorptions- und Quellungseigenschaften unter CO_2 - und CH_4 -Atmosphären bis zu 50 bar charakterisiert. Die Kinetik der Prozesse der experimentell gemessenen Gasaufnahme und Volumendilatation wurde analysiert, wobei zwei Anteile unterschieden werden konnten: Ein diffusiv/elastischer Anteil und ein relaxiver Anteil, der bei längerer Messzeit und höheren Drücken signifikant wird. Zusätzlich zu dieser Ermittlung von Konzentrations-Druck- bzw. Dilatations-Druck-Isothermen (differentielle Messung) wurden sogenannte integrale Sorptions- und Dilatationsmessungen (‘Ein-Schritt’-Messungen) durchgeführt, die als Referenz für eine entsprechende molekulardynamische (MD) Simulation elastischer Dilatationseffekte dienten.

Für die detailliert atomistischen MD Simulationen wurden equilibrierte Packungsmodelle der (ungequollenen) Polymere erstellt. Für jeweils einen weiteren Referenzzustand, charakterisiert durch Druck, aufgenommene Gasmenge und Quellung, wurden CO_2 - und CH_4 -beladene (gequollene) Packungsmodelle erstellt und durch NpT -MD Simulation equilibriert. Die Packungsmodelle der reinen (ungequollenen) Polymere und der CO_2 -gequollene Zustand wurden jeweils bezüglich ihres freien Volumens quantitativ charakterisiert. Die gefundenen Unterschiede konnten weiterhin durch eine detaillierte 3D-Visualisierung des Freien Volumens veranschaulicht werden.

Für alle Packungsmodelle wurden großkanonische Monte Carlo (GCMC) Simulationen durchgeführt, die jeweils zu Konzentrations-Druck-Isothermen führten. Experimentelle Daten und Simulationsergebnisse wurden in Bezug auf drei theoretische Modelle (*Dual Mode Sorption* Model (DM), *Site Distribution* Model (SD), und *Non-Equilibrium Thermodynamics of Glassy Polymers* (NET-GP)) ausgewertet und diskutiert.

Außerdem wurden die ungequollenen Packungsmodelle nach experimenteller Spezifikation aus integralen Sorptionsmessungen mit dem jeweiligen Gas beladen und die elastische Dilatation während der folgenden NpT -MD Equilibrierung beobachtet.

Ergebnisse: Die konsistente Anwendung der Ergebnisse der kinetischen Analyse führt zu einer verbesserten Übereinstimmung theoretischer Modelle mit dem Experiment und deutlich zuverlässigerer Bestimmung von Modellparametern. Deren physikalische Bedeutung ermöglicht erste Ansätze für eine universelle Beschreibung grundlegender Stofftransporteigenschaften. Eine mögliche Limitierung des SD Modells bezüglich der Anwendbarkeit auf hochfreivolumige Polymere, wie sie im Rahmen dieser Arbeit festgestellt wurde, konnte dahingehend erklärt werden, daß die Gas-Matrix

Wechselwirkung eine andere Besetzungsreihenfolge von Sorptionsplätzen bedingt, als bisher vom SD Modell angenommen.

Die simulierten Isothermen konnten durch die Einführung eines linearen Übergangs zwischen der jeweils für ungequollenes und gequollenes Packungsmodell berechneten GCMC-Isothermen in gute Übereinstimmung mit dem Experiment gebracht werden. Die Verwandtschaft der Methode mit dem NET-GP Modell wird erörtert und die Ergebnisse mit der Vorhersage der Sorption des Modells verglichen.

Die Freie-Volumen-Analyse zeigt deutliche Unterschiede zwischen den Polymeren PSU und PI4 einerseits und PIM-1 andererseits. In PIM-1 liegt ein großer Teil des Freien Volumens in einer Art loseem Verbund einzelner ‘Löcher’ vor, der in dieser Arbeit als ‘Lochphase’ (*‘void phase’*) diskutiert wird. Im Gegensatz zu den gequollenen Packungen von PSU zeigen diejenigen von PI4 bereits Ansätze zur Bildung einer solchen Lochphase. Diese ist in gequollenen PIM-1 Packungen stärker ausgeprägt. Die gefundenen Größenverteilungen Freier Volumen-Elemente in den ungequollenen Packungsmodellen zeigen eine gute Übereinstimmung mit den aus der SD Analyse erhaltenen Gaußverteilungen.

Außerdem konnte die elastische Dilatation, die in integralen Messungen experimentell beobachtet wird, erfolgreich in entsprechenden MD-Simulationen nachempfunden werden. Ein Zusammenhang zwischen den Abweichungen der Absolutwerte und möglichen anelastischen Reaktionen der Polymermatrix wird diskutiert.

Die gute Übereinstimmung experimenteller Ergebnisse mit den Resultaten aus der Simulation sorgfältig ausgewählter Aspekte der Gas-Sorption und Quellung in glasigen Polymeren bestätigt sowohl die Qualität der erstellten Packungsmodelle als auch die Vorteile der generellen Herangehensweise. Die Ergebnisse dieser Arbeit zeigen, dass die Diskrepanz in Zeitskalen von Experiment und Simulation und die daraus resultierende scheinbare Inkompatibilität mit Hilfe phänomenologischer Modelle überbrückt werden kann, und damit wertvolle Erkenntnisse über die zugrunde liegenden Phänomene gewonnen werden.

Contents

1	Introduction	1
2	Background	6
2.1	Glassy Polymers and Free Volume	6
2.2	Permeability, Solubility and Diffusion	8
2.3	Partial Molar Volume	10
2.4	Stress-strain Relationships	11
3	Theoretical Models	15
3.1	Dual Mode Sorption Model	15
3.2	NET-GP Model	17
3.3	Site Distribution Model	20
3.4	Summary	24
4	Experimental	25
4.1	Materials	25
4.1.1	Gases	25
4.1.2	Polymers	25
4.2	Sorption Measurements	28
4.3	Dilation Measurements	29
4.4	Kinetic Analysis	30
4.5	Experimental Results and Discussion	33
4.5.1	Sorption and Dilation Isotherms	33
4.5.2	Integral Sorption and Dilation	44

5	Modeling	50
5.1	Forcefield based Molecular Modeling	51
5.1.1	The Forcefield	51
5.1.2	Molecular Dynamics (MD)	53
5.1.3	The Concept of Ensembles	53
5.1.4	Periodic Boundary Conditions	55
5.1.5	Packing Procedure	56
5.2	Modeling Techniques	58
5.2.1	Free Volume Analysis	58
5.2.2	Grand Canonical Monte Carlo Calculations	60
5.2.3	Integral Dilation Simulation	61
5.3	Modeling Results and Discussion	62
5.3.1	Detailed Atomistic Molecular Packing Models	62
5.3.2	<i>Free Volume</i> Analysis	65
5.3.3	Sorption Isotherms	72
5.3.4	Integral Dilation Simulation	78
6	Combined Discussion	84
6.1	Sorption Isotherms	84
6.2	<i>Free Volume</i> Distributions	91
6.3	Integral Dilation	98
7	Synopsis	102
	Bibliography	106
A	Appendix	115
A.1	Abbreviations	115
A.2	Selected Notations	116
A.3	Slices of Packing Models	117
A.4	Rotation Analysis of Bond Angles	120

Preliminary Remarks

This work was prepared in the framework of a joint project between the Federal Institute for Materials Research and Testing (Bundesanstalt für Materialforschung und -prüfung, BAM) and the GKSS-Forschungszentrum Geesthacht (GKSS Research Center). The project was financially supported by the Deutsche Forschungsgemeinschaft (DFG, German Research Foundation). All experimental measurements were conducted at the BAM, which also hosted the author of this work. All simulation efforts were performed at the Institut für Polymerforschung of the GKSS in Teltow (Institute for Polymer Research). Data analysis was carried out at both project partners' facilities. Experiments and data analysis of both, simulated and experimental results were predominantly conducted by the author of this work. However, operation of the simulations, in particular the procedure of packing detailed atomistic molecular models, strongly depended on the expertise of the project partners at the GKSS Research Center in Teltow, where the author could resort to the basic procedures of packing detailed models, as well as existing analyzing scripts. The packing and equilibration of the models of *PSU* and *PSU80*, *PIM*, *PIM95* and *PIM206*, as well as the bond angle analysis on *PSU* and *PI4* were realized by the modeling group of Prof. D. Hofmann of the GKSS Research Center in Teltow, as part of the joint research project. The packing of the models *PSU35*, *PI4*, *PI76* and *PI156* was operated under the supervision of Dr. M. Heuchel (GKSS) by the author of this thesis.

Besides the publication of two abstracts for the Conference Proceedings of the Euromembrane 2006 (Heuchel et al., *Desal.* 199(1):443, 2006 and Hölck et al., *Desal.* 200(1):166, 2006), some of the results of this work have already been published or have been accepted for publication in peer reviewed scientific journals:

[1]: M. Heuchel, M. Böhning, O. Hölck, M. R. Siegert, and D. Hofmann. *J. Polym. Sci. B: Polym. Phys.*, 44(13):1874-1897, 2006.

[2]: O. Hölck, M. R. Siegert, M. Heuchel, and M. Böhning. *Macromolecules*, 39(26):9590-9604, 2006.

[3] O. Hölck, M. Heuchel, M. Böhning, and D. Hofmann. *J. Polym. Sci. B: Polym. Phys.*, (in press), 2007.

The concept of preswollen packing models was introduced in [1] where also sorption isotherms were calculated using the GCMC technique. In the second publication [2], the experimental sorption and dilation data were kinetically and phenomenologically analyzed and results were compared to nonswollen and swollen packing models of PSU with respect to CO₂-sorption, free volume and integral dilation. The experimental and simulated integral dilation results of the polymers PSU and PI4, induced by CO₂ and CH₄ sorption and insertion, respectively, were published in reference [3]. However, these aspects are presented and discussed in full context for the first time in this work.

1 Introduction

The behavior of amorphous polymers in contact with gas atmospheres is still an area of both fundamental scientific and applied industrial research. Applications range from the use as barrier materials or protective coatings to active layers in sensor applications (‘artificial nose’) and the large field of gas separation membranes. In all these applications, high concentrations of small penetrant molecules may lead to a plasticization of the polymer. This effect is utilized in processing applications, where supercritical carbon dioxide (CO_2) can be used as a plasticizer.⁴ The phenomenon of penetrant induced plasticization of glassy polymers is also observed in gas separation membranes.⁵ In the process of natural gas sweetening, the CO_2 content of the gas mixture is reduced by separation of the CO_2 from the fuel gas methane (CH_4) to avoid corrosion of pipelines and to enhance the fuel value. Solubility and diffusivity of the respective gas determine the separation performance of the membrane material, i.e., the permselectivity. Both parameters are connected to the internal structure of the polymer and its *free volume*. To achieve high throughputs, e.g. to enhance cost-effectiveness, it is desirable to increase the CO_2 solubility and mobility. However, the observed plasticization and the associated relaxations in the polymer matrix change its structure and *free volume*, and thereby affect the selectivity of the material.⁶ In addition, other properties of the polymer are influenced, e.g. a reduction of glass transition temperature,⁷ yield stress⁸ and creep compliance⁹ have been observed. The origin and mechanism of these structural relaxations are poorly understood, as are the factors that influence solubility and mobility of the plasticizing penetrant. This lack of knowledge leads to a development of new or optimized materials, which is in part determined by trial and error. A deeper understanding of the phenomena that accompany gas sorption on the molecular level is therefore needed to control material properties and enable a targeted design of functional materials. Therefore, in this work, laboratory experiments are combined with detailed atomistic molecular simulations.

Modeling. In detailed atomistic molecular modeling, the interactions of an assembly of atoms, e.g. a polymer molecule, are calculated according to known physical laws. Several established analysis methods allow an indirect determination of certain properties of such assemblies, others can even be directly calculated.¹⁰ However,

CPU-power limits both the size and the simulation time of such assemblies. The size of the simulated packing models used in this work (~ 5000 atoms) ranges among the larger models found in the literature. Forcefield based Molecular Dynamics (MD) simulations are calculated in femtosecond steps, but reliable results are usually not obtained until a nanosecond of net simulation time has been performed. Millions of interactions need to be calculated, making the time effort for these ‘virtual experiments’ comparable to laboratory experiments. However, increasing speed of single processors and the possibility of parallel processing will further reduce the evaluation times for such simulations in the future. The goal of computer simulations is therefore to establish reliable methods to predict material properties. Properties of new materials could then be assessed by simulations first and only the most promising materials need to be synthesized for further testing, reducing the expense of trial and error.

Although some methods already exist to predict polymer/gas properties from simulations, which show well agreeing results in ideal circumstances, they frequently fail when applied to less moderate conditions, e.g., high penetrant concentrations, long time scales, large penetrants etc. The aforementioned gas induced plasticization of polymers presents such a case where the gap of time scales between experiment and available simulation time amounts to several orders of magnitude. The time scale of simulations is limited to a few nanoseconds and therefore it is not possible to directly simulate relaxations of the glassy matrix as they are observed experimentally. Experiments, on the other hand, yield results of the real macroscopic system, and though molecular details cannot be observed individually, the accumulated effects permit the analysis through models on a statistical or phenomenological basis. It is the aim of this work to survey new approaches of a combined analysis of experimental and modeling results and to establish, where possible, a convergence of boundary conditions or, alternatively, an identification and isolation of comparable aspects of these seemingly incompatible methods of research. To this effect, phenomenological models are utilized as a means of interpretation of experimental data as well as to construe modeling results and thereby putting the assumptions and implications of these models to the test.

Phenomenological Models. The well known *Dual Mode Sorption Model* (DM model),^{11, 12} is the most widely used model to describe gas sorption in glassy polymers, due to its easy applicability and the ability to successfully describe sorption in a wide variety of polymer/gas systems. Though the initial assumption of two distinct penetrant populations could not unambiguously be confirmed,¹³ the concept has proven to be flexible, and the parameters are beyond their physical interpretation a valuable means to interpolate or exchange data.

Several other authors successfully developed phenomenological models to describe or predict penetrant concentration in glassy polymers.⁵ Most of these models approach sorption from the thermodynamic point of view,^{13–16} often treating the system of polymer matrix, free volume and penetrants as a lattice of partly occupied sites,^{17–19}

extending earlier models of lattice fluids²⁰ by introducing order parameters that describe the non-equilibrium nature of the glassy state.

This is done in the *Non-Equilibrium Thermodynamics of Glassy Polymers* (NET-GP) model, by considering the density as a parameter indicating the deviation from equilibrium. Using an equation of state, applying suitable mixing rules for the two components, polymer and penetrant, and assuming the density of the matrix to decrease linearly with penetrant concentration, a quasi-equilibrium concentration can be calculated for each pressure (chemical potential) of the penetrant gas. The calculation of Grand Canonical Monte Carlo (GCMC) isotherms in conjunction with the transition between discrete swollen states which will be introduced later in this work, correspond exactly to the NET-GP procedure and the respective results will be compared accordingly.

Free Volume. It is agreed upon in the literature, that the *free volume* plays a major role in penetrant solubility, transport and matrix mobility.²¹ A better understanding of its structure, volume fraction and distribution will also contribute to the understanding of sorption and swelling phenomena. The *Site Distribution* (SD) model explicitly constitutes a conception of the *free volume*. Though this model does not incorporate relaxational swelling of the matrix, its main feature comprises the penetrant-induced elastic stresses, which have been recognized by Newns.²² Newns suggested that the second-stage-sorption of vapors into glassy polymers is controlled by the rates of relaxations in the polymer. The rapid initial stage of sorption, following Fickian diffusion kinetics until a quasi-equilibrium is reached, was thought to induce stresses within the polymer matrix. Limited mobility of the matrix would lead to a relaxation of the stresses and hence a decrease in chemical potential of sorbed penetrant molecules, relatively to the gas or vapor phase. This again would lead to a self sustaining cycle of sorption-induced stresses and relaxations which is only limited by the ability of the matrix to relax stresses and thus by the (concentration dependent) plasticizing ability of the penetrant molecule. Following this interpretation, in order to understand relaxational swelling behavior, the forces that lead to the softening and subsequent relaxation need to be understood. In contrast to the thermodynamic approach, the SD model relates the distribution of sorption site volumes to a distribution of corresponding site energies. In this mechanical view, the partial molar volume connects the solubility of penetrant molecules to the structure of the *free volume* of the polymer matrix. It thus provides a favorable basis of comparison to detailed atomistic packing models, which can be analysed with respect to the *free volume* by the insertion of a small probe sphere, scanning the static polymer matrix following a grid pattern to detect non-occupied space.

Laboratory Experiments. Gas separation with polymeric membranes is a rather complex process, involving a gas mixture and a steady-state concentration gradient through the membrane. Properties of the membrane material and its changes as well

as transport properties of the gases are therefore not easily attributed to individual phenomena. The fundamental processes of penetrant sorption, transport (diffusion) and relaxation of the matrix which are underlying the gas separation are, with regard to the combined analysis of experiment, phenomenology and simulation, better investigated utilizing sorption and dilation isotherms of single gases. Here, the step by step procedure of increasing the pressure allows a thorough kinetic analysis and the determination of (quasi-) equilibrium conditions. In addition to the comparison of sorption isotherms and size distributions, this thesis presents an attempt to further investigate the experimentally observed dilation induced by *integral* gas sorption. The volume change of specially prepared packing models of binary mixtures under molecular dynamics simulations (NpT) show satisfying agreement to the experimental results and opens promising possibilities to investigate the elastic nature of the dilation process in its initial state, as well as the partial molar volumes of the penetrant gases in the polymers investigated in this work.

Investigated Systems. Six polymer/gas systems were selected for investigation in this work. CO_2 and CH_4 were selected as penetrant gases because of their vital roles in industrial applications, as mentioned in the beginning. Polysulfone (PSU) is a widely investigated conventional glassy polymer with regard to CO_2 sorption,^{23–29} and can therefore be used to validate the experimental procedures used in this work. Polymers of the class of 6FDA-polyimides, generally exhibiting a larger *free volume* than PSU, are known to show excellent transport and solubility characteristics with respect to gas separation applications. They furthermore tend to be susceptible to plasticization,³⁰ making the 6FDA-TrMPD (PI4) an ideal choice for the desired investigations. Still larger *free volume* is expected to be present in *Polymers of Intrinsic Microporosity* (PIMs). This new class of polymers, with structures of varying degree of order, shows promising features which have yet to be fully investigated.³¹ The selection of PIM1 (see Section 4.1.2) as an amorphous, membrane forming polymer allows for this work to contribute to a very recent field of research.

Outline. In this thesis, three different polymers are investigated with respect to the sorption of two gases and the induced dilation effects, involving three phenomenological models to analyze the experimental data and several simulation techniques and analysis methods regarding the modeling data. To provide some background to the general subject, the following chapter briefly summarizes some general features of polymer/gas systems and gas separation. Chapter 3 addresses the phenomenological models and the relevant formulae are established. In Chapter 4, the investigated polymers and experimental methods are introduced and, to retain lucidity, the immediate experimental results are presented at the end of this chapter, along with the related results of phenomenological model analyses. Correspondingly, Chapter 5 introduces to detailed atomistic molecular simulations, the applied techniques and analysis methods, followed by the presentation of the results. The discussion of Chapter 6 is reserved to the combined interpretation and comparison of experiment,

simulation and phenomenological models. If convenient, results that were presented in the preceding chapters may be shown again, in some cases introducing enhancements of the presentation or evaluation of data. This work is summarized and concluded in Chapter 7, where a short outlook will be given as well.

2 Background

The polymer/gas applications named in the Introduction highly depend on the sensitivity of the material to particular gases. Especially gas separation membranes are required to meet high standards regarding the *selectivity* while at the same time the *permeability* of the target gas species should be high enough to allow effective separation on an industrial scale. Glassy dense, i.e., non-porous, polymeric materials are ‘frozen’ into a non-equilibrium state. Between the disordered and in their mobility quite limited polymer chains, they contain some *excess free volume* which provides the room (‘sorption sites’) to accommodate penetrants and to allow movement within the polymer matrix (‘diffusion paths’). Differing size and interaction with the matrix allows the separation of small penetrants in a *solution-diffusion process*, the basics of which will be shortly recapitulated below.

2.1 Glassy Polymers and Free Volume

In the thermodynamic description of materials, it is generally distinguished between first and second order transitions.³² The first order transitions are marked by a continuous free energy function of state variables (e.g. pressure p or temperature T) which is discontinuous in the first partial derivatives with respect to the relevant state variables. At a melting point, a typical first order transition, the Gibbs Free energy G is continuous, but there is a discontinuity in entropy S , volume V and enthalpy H :

$$\left(\frac{\partial G}{\partial T}\right)_p = -S \quad \left(\frac{\partial G}{\partial p}\right)_T = V \quad \left(\frac{\partial(G/T)}{\partial(1/T)}\right)_p = H \quad (2.1)$$

Second order transitions are classically defined³³ by discontinuities in the second partial derivatives of the free energy function while the function itself as well as the first partial derivatives S , V or H are continuous, leading to discontinuities in the heat capacity C_p , compressibility κ and the thermal expansion coefficient γ :

$$\left(\frac{\partial S}{\partial T}\right)_p = \frac{C_p}{T} \quad \left(\frac{\partial V}{\partial p}\right)_T = -\kappa V \quad \left(\frac{\partial H}{\partial T}\right)_p = C_p \quad \left(\frac{\partial V}{\partial T}\right)_p = -\gamma V \quad (2.2)$$

The nature of the glass transition is still the subject of discussions. Though it exhibits features of a second order transition, there is still disagreement whether it is purely kinetic or if it is a kinetic manifestation of an underlying thermodynamic transition.³² However, when a liquid is cooled to form a glassy solid, it transforms from an *equilibrium* state (liquid) to a *nonequilibrium* state (glass), and its appearance, i.e., the glass transition temperature T_g , is dependent on the rate or time scale of the experiment (see Figure 2.1), contradicting the definition of thermodynamic phase transitions. A way to determine the glass transition temperature T_g is provided by differential scanning calorimetry (DSC). Here, the heat flow of the sample to a reference is monitored and at the glass transition temperature T_g a step is observed that is caused by the discontinuity of the heat capacity C_p .

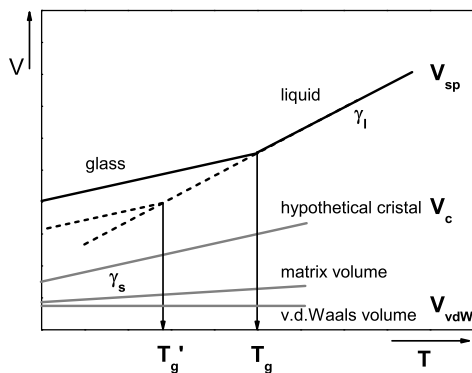


Figure 2.1:

Schematic diagram of volume definitions in polymers and temperature dependencies. The *glass transition* T_g depends on the cooling rate of the liquid state.

Above the glass transition temperature, glass forming amorphous polymers are in a liquid-like or rubbery state. At these temperatures, the enhanced molecular motion permits assemblies of polymer chain-segments to move in a coordinated manner, and hence allowing the material to flow,³⁴ the degree of cooperative movement depending on temperature and molecular weight. The enhanced molecular mobility mutually depends on the presence of *free volume* which provides the space that is required for the rearrangement of the polymer segments to take place.

With decreasing temperature, the mobility of the polymer segments decreases and hence the specific volume V_{sp} of the polymer decreases according to the thermal expansion coefficient of the liquid state γ_l , see Fig. 2.1. At the glass transition temperature, long range cooperative movement of polymer segments ceases, and while short-ranged rearrangements of individual mobile units of the polymer chain may still be possible, the restricted coordinated movement of the entangled macromolecu-

lar chains below the glass transition temperature turns the polymer into a solid glass, preserving the amorphous structure of the liquid or rubbery state.

Volume changes now follow the thermal expansion coefficient of the solid γ_s . The transition temperature T_g depends on the rate of cooling, as does the amount of frozen-in free volume. At slower rates, the glass transition temperature decreases (T'_g) and less *free volume* is conserved. Figure 2.1 also serves to illustrate different concepts of *free volume*. Starting from the specific volume of the polymer V_{sp} different *occupied* volumes may be subtracted to give a measure of the *free volume*:

- i) $V_{sp} - V_{vdW}$, the van der Waals volume of the polymer chains, gives the *free volume* at 0 K.
- ii) $V_{sp} - V_c$, the volume of a hypothetical, close packed crystal, gives the *excess free volume*
- iii) $V_{sp} - V_l$, the extrapolated volume of an undercooled liquid, gives the amount of unrelaxed *free volume*

Commonly glassy polymers are characterized with respect to the free volume by calculation of the *fractional free volume* using the method of Bondi:³⁵

$$\Phi_{FV} = \frac{V_{free}}{V_{sp}} = 1 - 1.3 \frac{V_{vdW}}{V_{sp}} \quad (2.3)$$

2.2 Permeability, Solubility and Diffusion

Gas separation with membranes made from dense amorphous polymers under a concentration gradient is based on a *solution-diffusion* mechanism,⁵ that is the sorption and transport of small molecules (penetrants), which essentially depends on the *free volume* and its size distribution. The *solution-diffusion* mechanism comprises the three steps of (i) sorption of the gas molecules at the so called ‘feed’ or ‘upstream’ side of the membrane, (ii) diffusion of the molecules through the dense matrix and (iii) desorption of the gas molecules at the ‘permeate’ or ‘downstream’ side. Mass transport of a penetrant species i through a membrane of thickness d is given by the flux J_i .³⁶

$$J_i = P_i \frac{p_{up} - p_{down}}{d} \quad (2.4)$$

where p_{up} and p_{down} denote the feed and permeate pressure and P_i is the coefficient of permeability of species i . Characteristic for the separating performance of a membrane with respect to a gas pair i, j is the ratio of permeabilities, called the ideal selectivity α_{ij} :

$$\alpha_{ij} = \frac{P_i}{P_j} \quad (2.5)$$

The ideal selectivity α_{ij} is determined by separate measurements of the permeabilities for the two gases i, j ; for real gas mixtures different partial pressures and competitive sorption have to be taken into account.^{37, 38}

Driving force of the permeation process is the pressure difference between up- and downstream side of the membrane $\Delta p = p_{up} - p_{down}$, which leads to a difference of the concentration ΔC between the gas/polymer interfaces

$$\Delta C = S(p_{up} - p_{down}) \quad (2.6)$$

where S denotes the solubility of the gas in the polymer. The flux within the polymer membrane is, according to Fick's first law for an isotropic material

$$J = -D \left(\frac{\partial C}{\partial x} \right) \quad (2.7)$$

where x is the direction perpendicular to the membrane plane. The constant D is called the diffusion coefficient[‡] and gives a measure of the penetrant mobility in the polymer matrix. Equation 2.7 is valid only in the steady state, when in the process of permeation a constant concentration gradient is established. In this case, the time dependency formulated in Fick's second law

$$\left(\frac{\partial C}{\partial t} \right) = \left(\frac{\partial^2 C}{\partial x^2} \right) \quad (2.8)$$

vanishes and, assuming a linear concentration gradient (D independent of concentration), the flux is

$$J = -D \left(\frac{dC}{dx} \right) = -D \frac{\Delta C}{\Delta x} = D \frac{C_{up} - C_{down}}{d} \quad (2.9)$$

At constant upstream pressure p_{up} and small downstream pressure $p_{down} \approx 0$, as is usually the case in permeation setups, equations 2.4, 2.6 and 2.9 yield the permeability coefficient

$$P_i = S_i D_i \quad (2.10)$$

In a typical permeation measurement, the pressure increase with time in a small downstream volume is monitored at nearly constant upstream pressure. Assuming the steady state condition, the permeability P is then retrieved from the slope of the curve, whereas the diffusion coefficient can be calculated from the time lag (zero pressure extrapolation of the steady state regime). However, the aforementioned conditions are not necessarily valid in longtime experiments and at high concentrations. The phenomenon of swelling alters the structure of the free volume making the direct

[‡]Throughout this work, by 'diffusion coefficient' the coefficient of *mutual* diffusion is meant. In contrast to the *tracer* diffusion, which describes the statistical motion of a single particle, the driving force for mutual diffusion is a concentration gradient.

observation of the application relevant property P difficult. Equation 2.10 emphasizes that solubility and diffusion are the fundamental processes which determine the permeability. Therefore, in this work, experiments were performed which allow more reliable assertions of the fundamental processes in question. In the sorption measurements, which will be discussed in more detail in Section 4.2, the phenomenon of mass uptake (sorption) is observed directly and time resolved, allowing the determination of the diffusion coefficient D . For a plane sheet geometry, Fick's second law has been solved by Crank:³⁹

$$\frac{M(t)}{M_\infty} = 1 - \sum_{n=0}^{\infty} \frac{8}{(2n+1)^2 \pi^2} \exp(-D(2n+1)^2 \pi^2 t / d^2) \quad (2.11)$$

where $M(t)$ and M_∞ denote the total mass uptake at time t and at infinite time, respectively. By variation of M_∞ and the diffusion coefficient D , equation 2.11 can be fitted to sorption data, yielding the information on solubility (using eq. 2.6) and diffusion for a polymer/gas system (see also Section 4.4).

2.3 Partial Molar Volume

The molar volume $V_{m,i}$ of a pure species i may be defined as the ratio between its volume V_i and its quantity n_i , measured in moles, at a given temperature and pressure:

$$V_{m,i} = \left(\frac{V_i}{n_i} \right)_{T,p} \quad (2.12)$$

Formally, the partial molar volume (PMV) $\tilde{V}_{m,i}$ of a species i in a mixed system of volume V is defined as the variation of the volume with the amount of substance n_i of species i and constant amount of other species $n_{j \neq i}$

$$\tilde{V}_{m,i} = \left(\frac{\partial V}{\partial n_i} \right)_{T,p,n_{j \neq i}} \quad (2.13)$$

In practice, it may be measured as the ratio of the change in the volume of the system ΔV , and in the number of molecules Δn_i of species i :

$$\tilde{V}_{m,i} = \frac{\Delta V}{\Delta n_i} \quad (2.14)$$

In liquids or rubbery polymers, the mobility of the matrix is sufficient to compensate the insertion of a penetrant molecule into a site of *free volume* such that the latter is kept nearly constant. In this case the relaxation around a penetrant molecule is complete and the PMV $\tilde{V}_{m,i}$ may be regarded as a 'dynamic volume' $V_{g,i}$, and thus as a property of the penetrant phase of species i :

$$\tilde{V}_{m,i} = V_{g,i} \quad (2.15)$$

In glassy polymers the situation is different. The mobility of the matrix is limited, and therefore occupation of free volume cannot be fully compensated within reasonable time scales. The consumption of free volume by the penetrant molecules leads to a smaller partial molar volume which must now be regarded as a property of the matrix/penetrant system. A mechanical interpretation of this phenomenon is provided by Eshelby:⁴⁰

The volume change ΔV of an elastic continuum containing a spherical hole of volume V_h , upon occupation of this hole with an elastic sphere of volume $V_g \geq V_h$ is given by

$$\Delta V = \text{const}(V_g - V_h) = \tilde{V}_i \quad (2.16)$$

where $\text{const} = 1$ if penetrant and matrix have the same elastic properties. The partial molar volume \tilde{V}_i therefore reveals information about the structure of the free volume, provided that the penetrant phase volume $V_{g,i}$ of species i is known and the matrix can be regarded as an elastic continuum. For convenience, the ‘tilde’, indicating *partial* molar volumes will be omitted in the following. V_g will be used to indicate the molar ‘dynamic volume’ of the penetrants (CO_2 and CH_4) and $V_p \equiv \tilde{V}_{m,i}$ for their *partial* molar volumes. V_h denotes the molar volume of sorption sites (see Section 3.3). On rare occasions, for the sake of a simplified discussion, the denominations are used to describe *single* holes or penetrants, their meaning being easily recognized out of the context. In addition, Appendix A.2 provides a list of selected notations used in this thesis.

2.4 Stress-strain Relationships

Polymers below their glass transition temperature T_g exhibit complex behavior when subjected to an external stress. While chemical bonds and physical entanglements of the polymer chain prevent long range cooperative motion and ensure a certain form stability that gives rise to an *elastic* reaction of the polymer matrix, localized rearrangements of smaller subunits may still take place below the glass transition and lead to a limited relaxation. This behavior is called *viscoelastic*. For viscoelastic materials, the mechanical behavior, that is, the response to a (uniaxial) stress with a strain closely resembles that of models built from discrete elastic and viscous elements.⁴¹ If a material is linear-elastic, the relationship between the stress σ and the strain ϵ is described by Hooke’s law

$$\sigma = E\epsilon \quad (2.17)$$

where E is the Young’s modulus. The reaction of a purely elastic material is therefore instantaneous, proportional to the stress. The element representing elastic behavior is a spring. When the applied stress is removed, the strain recovers in full as depicted in Figure 2.2.

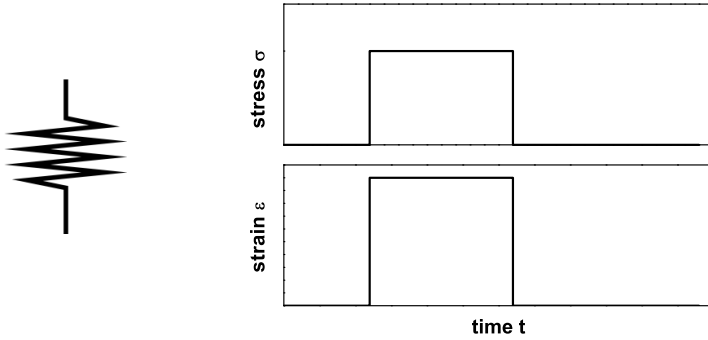


Figure 2.2: The stress-strain relationship of a spring module is proportional and instantaneous.

In materials exhibiting viscous flow, on the other hand, the stress is proportional to the strain rate, according to Newton's law

$$\sigma = \eta \frac{d\epsilon}{dt} \quad (2.18)$$

where η is the viscosity.³⁴ Viscous flow, represented by a dashpot, corresponds to a plastic deformation of the polymer matrix and is not recovered upon removal of the stress (Figure 2.3).

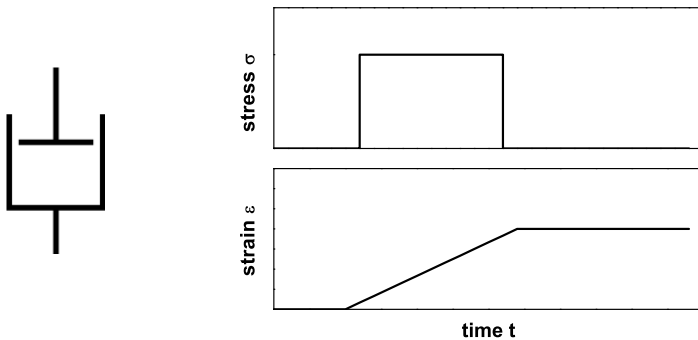


Figure 2.3: The strain of a dashpot module is proportional to the stress rate and linear in time.

The two models may be connected in various ways, depending on the nature of viscoelasticity specific to the material. A common combination to describe a single retardational process of a glassy polymer, is the ‘Kelvin’ model (sometimes called the ‘Voigt’ model), where spring and dashpot are connected in parallel (Figure 2.4). The stress-strain relationship becomes³⁴

$$\sigma = \eta \frac{d\epsilon}{dt} + E\epsilon \quad (2.19)$$

and under conditions of constant stress, equation 2.19 can be integrated to

$$\epsilon = \frac{\sigma}{E}(1 - \exp(-t/\tau)), \quad \tau = \frac{\eta}{E} \quad (2.20)$$

where τ denotes the retardation time. Generally, deformations in glassy polymers are not recovered upon removal of the stress. However, the Kelvin model implies a reversibility of the strain. This apparent contradiction can be solved, if different time constants are assumed for strain and recovery.

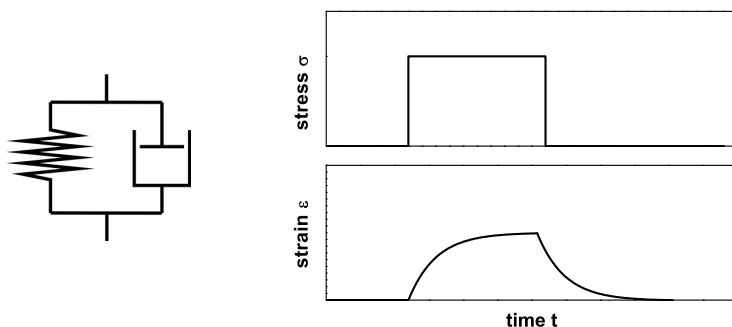


Figure 2.4: The Kelvin module is a combination of spring and dashpot. Its response to a stress is reversible but nonlinear in time.

In this work, the term ‘relaxational’ will be used in a more general sense as the generic term for *retardational* (viscoelastic behaviour under constant stress) as well as *relaxational* behaviour (constant strain), as is common in the literature regarding sorption induced swelling of glassy polymers. Since most often relaxational behavior cannot be attributed to one single process but a spectrum of relaxation times has to be assumed in addition to an elastic response of the polymer matrix, a superposition of an infinite sum of Kelvin models seems more appropriate to completely describe the complex behavior of viscoelastic polymers. However, in most cases one or two Kelvin models in series with a spring are sufficient to describe experimental data^{42, 43} as is

the case in this work, where a spring and two Kelvin models are connected in series (eq. 4.3) to kinetically analyse experimental sorption and dilation data (see Section 4.4).

The Kelvin model (Fig. 2.4) may also serve to describe *anelastic* behavior. Anelastic materials, e.g. metals,⁴⁴ are known to exhibit a time dependent but completely reversible contribution to the strain that is usually observed on short time scales. With respect to polymers, anelastic behavior has been discussed in the context of the secondary relaxation processes by Boyd et al.⁴⁵, and in the context of internal friction caused by small molecules (Snoek effect) by Böhm et al.⁴⁶. In this work, possibly anelastic effects will be considered in Section 6.3.

3 Theoretical Models

3.1 Dual Mode Sorption Model

Of the several phenomenological models that have been developed to describe sorption of small molecules in glassy polymers and the induced swelling behavior, the *Dual Mode Sorption Model* (DM model) is the one most commonly used. It combines the two independent processes of *Henry solution*, as it is observed in liquids or rubbery polymers, with the *Langmuir adsorption* process on inner surfaces of microporous materials. In the framework of this model, a penetrant molecule is either sorbed into a Henry-type sorption site, which is believed to be in the intermediate space of neighboring polymer segments, or adsorbing onto the surface of Langmuir type sites, microcavities which considerably contribute to the *excess Free Volume* of a glassy polymer. For solution according to Henry's law, the solubility coefficient k_D connects the penetrant concentration C_D in the polymer linearly with the pressure p :

$$C_D(p) = k_D p \quad (3.1)$$

The linear relationship between concentration and pressure of Henry mode sorption is depicted by a dotted line in Figure 3.1. The Langmuir isotherm C_H can be viewed as a sort of 'hole filling' of the microcavities with a saturation capacity C'_H and the quotient of ad- and desorption rate b is called the affinity constant:

$$C_H(p) = \frac{C'_H b p}{1 + b p} \quad (3.2)$$

In total, the pressure dependent concentration $C(p)$ amounts to

$$C(p) = C_D + C_H = k_D p + \frac{C'_H b p}{1 + b p} \quad (3.3)$$

The total concentration, i.e., the resulting sorption isotherm depicted by a compact line in Figure 3.1, is dominated by the steep increase of Langmuir mode sorption in the low pressure regime (dashed line), while at higher pressures it reaches saturation and the influence of Henry mode sorption is more pronounced. Originally, the DM

model was only intended to describe sorption of small penetrants in glassy polymers. Property changes of the matrix like plasticisation were neglected. There were several attempts to modify the DM model or incorporate other models,⁴⁷ since the implied existence of two distinct populations of sorbed molecules could not unambiguously be validated,¹³ nor could the parameters be ascribed to physical parameters in a straightforward way. However, due to its easy applicability and frequent use, the DM model of the form 3.3 remains the most important model to interpolate and exchange sorption data. If the Langmuir adsorption eq. 3.2 is interpreted as a mechanism of filling up microcavities or rather covering their surfaces, dilation should only be caused by Henry type sorption 3.1. This linear volume change is then related to the concentration of penetrants via their partial molar volume V_p :

$$\frac{\Delta V}{V_0} = \frac{V_p}{V_{id}} C_D = \frac{V_p}{V_{id}} k_D p \quad (3.4)$$

where V_0 is the volume of the dry polymer and V_{id} the volume of an ideal gas at standard conditions (STP). To be able to also describe dilation isotherms that are concave to the pressure axis, Kamiya et al.⁴⁸ introduced the factor $0 \leq f \leq 1$, to capture the contribution of penetrants sorbed in microcavities to the dilation:

$$\frac{\Delta V}{V_0} = \frac{V_p}{V_{id}} C_D + f \frac{V_p}{V_{id}} C_H = \frac{V_p}{V_{id}} k_D p + f \frac{V_p}{V_{id}} \frac{C'_H b p}{(1 + b p)} \quad (3.5)$$

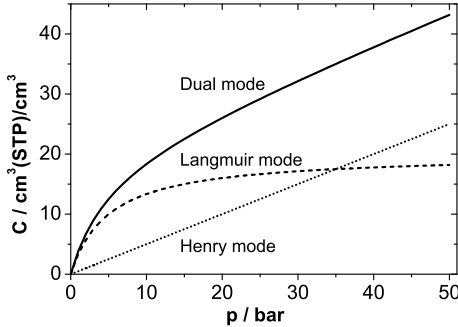


Figure 3.1:

According to the DM model, the total concentration (solid line) is a superposition of Henry mode and Langmuir mode sorption.

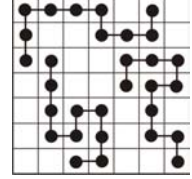
In other words, the two populations of sorbed penetrants exhibit different *partial molar volumes* (p.m.v.):

The p.m.v. of the Henry population $V_p = V_D$ as also observed in liquid or rubbery polymers, and the smaller p.m.v. $fV_p = V_H$ of the penetrants sorbed in microcavities.

3.2 NET-GP Model

The Non Equilibrium Thermodynamics of Glassy Polymers model (NET-GP)^{19, 49–51} is based on the description of liquid polymer/gas systems as lattice fluids. It presents a modification of the ‘Lattice Fluid Theory’ (LF) of Sanchez and Lacombe:^{20, 52}

The polymer/gas system is treated as a partially occupied lattice for which the equilibrium chemical potential of the components can be calculated from parameters of the lattice, statistical considerations of possible configurations of gas and polymer, and their interaction energies. Sanchez and Lacombe consider a polymer of N r -mers, each mer occupying a lattice site of molar volume[‡] v^* , and the number of N_0 unoccupied lattice sites. The total number N_r of lattice sites and the total volume V of the system are then given by



$$N_r = N_0 + rN \quad V = (N_0 + rN)v^* = V^* \frac{N_r}{rN} \quad (3.6)$$

Here, V^* is the volume of the ideally packed polymer ‘crystal’ (i.e., no vacant sites in the lattice), which is related to the characteristic density ρ^*

$$V^* = N(rv^*) \quad rv^* = M/\rho^* \quad (3.7)$$

where M is the molar mass of the pure polymer. For n mole of a pure polymeric fluid at temperature T , pressure p and density ρ , the expression for the Gibbs free energy is²⁰

$$G = rnRT^* \left\{ -\tilde{\rho} + \frac{\tilde{p}}{\tilde{\rho}} + \frac{\tilde{T}}{\tilde{\rho}} \left[(1 - \tilde{\rho}) \ln(1 - \tilde{\rho}) + \frac{\tilde{\rho}}{r} \ln(\tilde{\rho}) \right] \right\} \quad (3.8)$$

where r is the number of lattice sites occupied by a molecule and R is the universal gas constant. The reduced quantities of density $\tilde{\rho}$, temperature \tilde{T} and pressure \tilde{p} are defined by

$$\tilde{\rho} = \rho/\rho^* \quad \tilde{p} = p/p^* \quad \tilde{T} = T/T^* \quad (3.9)$$

where p^* and T^* are the characteristic pressure and temperature, respectively. The molar volume v^* of the closely packed polymer is assumed independent of temperature and pressure

$$v^* = \frac{RT^*}{p^*} \quad (3.10)$$

In the case of thermodynamic equilibrium (EQ)

$$\left(\frac{\partial G}{\partial \rho} \right)_{T,p,n} = 0 \quad (\text{at EQ}) \quad (3.11)$$

[‡]The denominations of the NET-GP model somewhat differ from the notations used in this thesis. However, since the quantities are discussed only once outside this section in an unambiguous context, the notation of the authors of the model is used to conveniently stay in compliance with the literature.

holds. To fulfill the condition for equilibrium 3.11 at a given temperature and pressure, the density can be varied.

For a two-component system, the LF theory can be expanded by combining the model parameters ρ^* , p^* , T^* and v^* using appropriate mixing rules²⁰:

(1) The reduced molar volume becomes

$$v^* = \phi_1^0 v_1^* + \phi_2^0 v_2^* \quad (3.12)$$

where the concentration variable ϕ_1^0 is defined by the number of moles n_i of component i ($i = 1, 2$)

$$\phi_1^0 = \frac{r_1^0 n_1}{r_1^0 n_1 + r_2^0 n_2} \quad (3.13)$$

(2) For the ratio of the number of sites occupied by a molecule of species 1 in the mixture (r_1) to the number of sites occupied by the same molecule in the pure state (r_1^0), the following assumption is made:

$$\frac{r_1}{r_1^0} = \frac{v_1^*}{v^*} \quad (3.14)$$

(3) For the characteristic pressure p^*

$$p^* = \phi_1 p_1^* + \phi_2 p_2^* - \phi_1 \phi_2 \Delta p^* \quad (3.15)$$

where ϕ_1 is the volume fraction of the penetrant species which is defined by

$$\phi_1 = \phi_1^0 \frac{v_1^*}{v^*} \quad (3.16)$$

The mixing rules result in a relation of the characteristic density ρ^* and the composition of the mixture which is expressed by the mass fraction ω_i ($i = 1, 2$) of the components

$$\frac{1}{\rho^*} = \frac{\omega_1}{\rho_1^*} + \frac{\omega_2}{\rho_2^*} \quad (3.17)$$

The expression for the Gibbs free energy of a mixture containing n_1 moles (penetrant) and n_2 moles of the polymer then becomes

$$G = RT^*(r_1 n_1 + r_2 n_2) \left\{ -\tilde{\rho} + \frac{\tilde{P}}{\tilde{\rho}} + \frac{\tilde{T}}{\tilde{\rho}} \left[1(1 - \tilde{\rho}) \ln(1 - \tilde{\rho}) + \frac{\phi_1}{r_1} \tilde{\rho} \ln(\phi_1 \tilde{\rho}) \right] \right\} \quad (3.18)$$

For a given temperature, pressure and composition, the equilibrium value of the density minimizes the Gibbs energy:

$$\left(\frac{\partial G}{\partial \rho} \right)_{T, p, n_1, n_2} = 0 \quad (\text{at EQ}) \quad (3.19)$$

However, since the molecular mobility is limited, glassy polymers are not at equilibrium. On the contrary, the density may be utilized to describe the nonequilibrium character of the system. Doghieri and Sarti¹⁹ introduced the density of the polymer matrix ρ_2 as an internal state variable which is related to the reduced density $\tilde{\rho}$ of the system as

$$\tilde{\rho} = \frac{\rho_2}{\omega_2} \frac{1}{\rho^*} \quad (3.20)$$

The chemical potential of the penetrant in the sorbed phase

$$\mu_1^S = \left(\frac{\partial G}{\partial n_1} \right)_{T, p, n_2, \rho_2} \quad (3.21)$$

can now be expressed as a function of temperature, pressure, concentration and density of the matrix using 3.18:

$$\frac{\mu_1^S}{RT} = \ln(\tilde{\rho}\phi_1) - [r_1^0 + (r_1 - r_1^0)/\tilde{\rho}] \ln(1 - \tilde{\rho}) - r_1 - \tilde{\rho}[r_1^0 v_1^*(p_1^* + p^* - \phi_2^2 \Delta p^*)]/(RT) \quad (3.22)$$

Equation 3.22 provides the means to calculate the solubility of a penetrant phase at a given temperature, matrix density and pressure (chemical potential of the gas phase of the penetrant). Only one binary parameter, Δp^* , and the variation of matrix density with pressure is needed to predict a concentration/pressure isotherm from otherwise pure-component parameters only. The former may be approximated by the arithmetic mean value¹⁹

$$\Delta p^* = (\sqrt{p_1^*} - \sqrt{p_2^*})^2 \quad (3.23)$$

For the density change of the matrix with pressure, i.e., the dilation isotherm corresponding to the concentration isotherm, a linear relationship is assumed:

$$\rho_2^\infty(p) = \rho_2^0(1 - k_s p) \quad (3.24)$$

where $\rho_2^\infty(p)$ is the pseudo-equilibrium matrix density at pressure p , ρ_2^0 the initial density and k_s the swelling coefficient, which can be used as the single free parameter to fit sorption data. Moreover, the resulting swelling coefficient k_s may be used to entirely predict swelling behavior or vice versa, predict sorption from known swelling behavior. Only the latter will be done in this work, since this way the procedure is more closely related to the method of calculating sorption isotherms using modeling techniques presented later in this work. The NET-GP calculations were performed using the Microsoft Excel sheet *xIEOS.xls* and the library *EOS.dll* that are freely available for download in the internet as *Nonequilibrium package*.⁵³ The necessary pure-component data of the gases CO₂ and CH₄ are contained within this package and were published in reference [54]. The pure component data of the polymers were calculated using equation 3.22 from experimental solubility data of three gases⁵⁴ and are listed in Table 3.1.⁵⁵

Table 3.1: Pure component parameters used for NET-GP calculations.

polymer	ρ_0 g/cm ³	p^* MPa	T^* K	ρ^* g/cm ³
PSU	1.240	503	899	1.310
PI4	1.320	421	864	1.603
PIM	1.124	624	728	1.554

3.3 Site Distribution Model

The *site distribution* model of Kirchheim^{56, 57} considers the localized free volume of an amorphous polymer (‘holes’) as possible sorption sites for penetrants. It is the size distribution of these holes which, by way of an additional energy term caused by elastic deformation upon occupation of a penetrant, leads to a distribution of sorption energies as well. Once the parameters of this energy distribution have been obtained from sorption data, dilation data can be used to obtain the parameters of the size distribution of ‘holes’ and hence information of the structure of the *free volume* is gained.

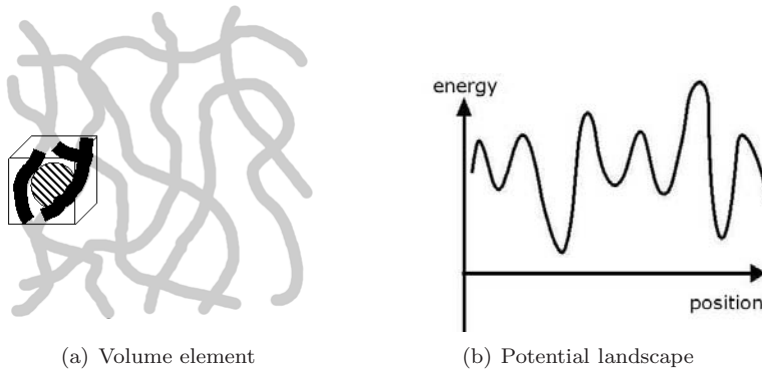


Figure 3.2: a): Sketch of a volume element V occupied by polymer segments (cube) and the enclosed free volume site V_h (hatched). b): Sketch of a potential landscape as seen by penetrant molecules, caused by a distribution of site volumes V_h .

The shape of the distribution is deduced from above T_g considerations following the treatment of Bueche.⁵⁸ A number of polymer segments in a polymer matrix occupy a certain volume V (see Figure 3.2(a)). Above T_g , thermal fluctuations lead to the

probability to find this volume in an interval $[V, dV]$

$$P(V)dV \propto \exp\left(-\frac{G_0(V)}{kT}\right) dV \quad (3.25)$$

where the Gibbs free energy is $G_0 = E_0 - T_0S + p_0V$ at constant pressure p_0 and temperature T_0 . The most probable state is when $G_0 = G_{min}$ is at a minimum. For small volume fluctuations $\Delta V = V - V_{min}$, G_0 can be expanded to yield

$$\Delta G = G_0 - G_{min} = \left(\frac{\partial G_0}{\partial V}\right)_T \cdot \Delta V + \frac{1}{2} \left(\frac{\partial^2 G_0}{\partial V^2}\right)_T \cdot \Delta V^2 + \dots \quad (3.26)$$

Dropping higher order terms and taking into account the conditions for the minimum

$$\left(\frac{\partial G_0}{\partial V}\right)_T = 0 \text{ and } \left(\frac{\partial^2 G_0}{\partial V^2}\right)_T = -\left(\frac{\partial p}{\partial V}\right)_T \geq 0 \quad (3.27)$$

it follows, that

$$G_0(V) = G_{min} + \left(\frac{(\Delta V)^2}{2V_0K}\right) \quad (3.28)$$

and hence the probability for the volume to be in the interval $[V, dV]$ becomes

$$P(V)dV = B \exp\left(-\frac{(V - V_0)^2}{2kT_0V_0K}\right) dV \quad (3.29)$$

where $K = -1/V(\partial V/\partial p)_T$ is the compressibility, k the Boltzman constant and B is a factor to be determined from the normalization condition. If the probability 3.29 holds true for a number of segments occupying a volume V , it should also be valid for the ‘hole’ volume V_h which is enclosed by the segments, because the volume of the segments does not vary (Fig. 3.2(a)). The distribution of ‘holes’, $n(V_h)$, enclosed by polymer segments, becomes

$$n(V_h) = \frac{N_0}{\sqrt{\pi}\sigma_V} \exp\left(-\frac{(V_h - V_{h0})^2}{\sigma_V^2}\right) \quad (3.30)$$

with the number of ‘holes’ per unit volume N_0 . The width of the distribution σ_V is deduced from the normalization condition

$$\int_{-\infty}^{\infty} \frac{n(V)}{N_0} dV = 1 \rightarrow \sigma_V = \sqrt{2kT_0V_{h0}K} \quad (3.31)$$

Below the glass transition temperature T_g , the segmental mobility of the polymer is limited and the distribution of free volumes is quenched-in, providing the space to accommodate penetrants (*sorption sites*). To account for the size effect of the sorption sites on the Gibbs free energy of sorption G , it is considered as the sum of an

elastic contribution G_{el} and the total of all other interactions G_r ('rest'), the latter is assumed to be independent of site volume V_h and equal for all sites:

$$G = G_{el} + G_r \quad (3.32)$$

To assess the elastic contribution, Kirchheim simplifies by idealizing the polymer matrix as an elastic continuum, containing the free volume in the form of spherical holes. If an elastic sphere (penetrant) of volume $V_g > V_h$ is inserted into a hole of volume V_h , the elastic energy of the sphere E_g can be derived from the distortion ΔV_g of the sphere⁴⁰

$$E_g = \frac{K_g(\Delta V_g)^2}{2V_g} \quad (3.33)$$

where K_g is the compressibility of the sphere. The energy E_m stored in the matrix is derived from the distortion field surrounding the deformed hole V_h

$$E_m = \frac{\mu_m(\Delta V_h)^2}{3V_h} \quad (3.34)$$

with the shear modulus μ_m of the matrix. Comparison of the pressures acting on sphere and hole, 3.33 and 3.34 lead to a relation between the misfit $(V_g - V_h)$ and the macroscopic volume change, i.e., the partial molar volume V_p

$$V_p = \frac{\gamma}{\gamma'}(V_g - V_h) \quad (3.35)$$

where γ and γ' contain the elastic properties of sphere and matrix

$$\gamma = 1 + \frac{4\mu_m}{3K_m} \quad \gamma' = 1 + \frac{4\mu_m}{3K_g} \quad (3.36)$$

The total energy stored in the polymer/penetrant system by occupation of a sorption site adds up to

$$G_{el} = E_g + E_m = \frac{2\mu_m}{3\gamma'} \frac{(V_g - V_h)^2}{V_h} \quad (3.37)$$

Inserting 3.37 into 3.32 and expanding around V_{h0} and dropping higher order terms leads to

$$G(V) = G_r + G_{el}(V) \quad (3.38)$$

$$= G_r + G_{Vh0} + \frac{2\mu_m}{3\gamma'} \frac{(V_g^2 - V_{h0}^2)}{V_{h0}^2} (V_{h0} - V_h) + \dots \quad (3.39)$$

$$\approx G_0 + \text{const.}(V_{h0} - V_h) \quad (3.40)$$

G_{Vh0} denotes the elastic energy needed to occupy a sorption site of volume V_{h0} , and G_0 the total sorption energy of a sorption site of average volume V_{h0}

$$G_0 = G_r + G_{Vh0} \quad (3.41)$$

The expression 3.40 can now be inserted into the distribution of site volumes 3.30, which leads to a distribution of sorption energies

$$n(G) = \frac{N_0}{\sqrt{\pi}\sigma_G} \exp\left(-\frac{(G - G_0)^2}{\sigma_G^2}\right) \quad (3.42)$$

The width σ_G of the distribution satisfies the normalization condition and is connected to σ_V (cf. Equation 3.31) as

$$\sigma_G = \sigma_V \frac{2\mu_m(V_g^2 - V_{h0}^2)}{3\gamma V_{h0}^2} \quad (3.43)$$

The distribution of site volumes of Gaussian form 3.30 obviously leads to a similar distribution of site energies 3.42 as well. For a penetrant, the polymer matrix presents itself as a potential landscape (see Figure 3.2(b)) of sorption sites (energy minima) and ‘bottlenecks’, energy barriers that might be considered as diffusion paths. Assuming thermal occupancy of the sorption sites following Fermi-Dirac statistics, the concentration of the penetrant is given by

$$C(\mu) = \int_{-\infty}^{\infty} n(G) dG / (1 + \exp[(G - \mu)/kT]) \quad (3.44)$$

where μ is the chemical potential of the gas phase of the penetrant, which is related to the pressure p via

$$\mu = \mu_0 + kT \ln\left(\frac{p}{p_0}\right) \quad (3.45)$$

with μ_0 being the standard value for $p = p_0 = 1$ atm. The parameters G_0 and σ_G are varied to fit the sorption isotherms, their values result in a Gaussian distribution of site energies. In order to calculate the elastic volume dilation, equation 3.32 and 3.41 are subtracted and equation 3.37 inserted:

$$G = G_0 + \frac{2}{3}\mu_s \left(\frac{(V_g - V_h)^2}{V_h} - \frac{(V_g - V_{h0})^2}{V_{h0}} \right) \quad (3.46)$$

The latter equation can be solved for V_h , yielding⁵⁷

$$V_h(G) = V_g + \frac{3(G - G_0)}{4\mu_s} + \frac{(V_g - V_{h0})^2}{2V_{h0}} - \sqrt{\left(\frac{3(G - G_0)}{4\mu_s} + \frac{(V_g - V_{h0})^2}{2V_{h0}} \right)^2 - V_g^2} \quad (3.47)$$

The macroscopic volume change ΔV can now be calculated combining equation 3.35 and 3.44, considering the contribution of all molecules occupying sorption sites of free enthalpy G by integrating over all sites

$$\begin{aligned} \frac{\Delta V}{V_0} &= \int_{-\infty}^{\infty} V_p(G) C(G) dG \\ &= \int_{-\infty}^{\infty} \frac{\gamma[V_g - V_h(G)]}{\gamma'} \frac{n(G)}{(1 + \exp[(G - \mu)/kT])} dG \end{aligned} \quad (3.48)$$

Equation 3.48 contains only one unknown parameter, provided that the parameters of the energy distribution are known from a fit of eqn. 3.44 to sorption data and reasonable values for the volume of the penetrants V_g , the elastic properties γ and γ' as well as the number of sorption sites N_0 can be assumed. Following Kirchheim,⁵⁶ for the volume V_g of the penetrants their partial molar volumes in liquids or rubbery polymers, which may be viewed as *dynamic* or *relaxed partial molar volume* of the penetrants, are used in this work. Gotthardt et al.⁵⁹ proposed that the bulk moduli of liquid gases and glassy polymers are about equal, yielding $\gamma/\gamma' \approx 1$ and simplifying equations 3.35 and 3.48. The number of sorption sites per unit volume N_0 has been estimated to be in the range of $3 \cdot 10^{21}$ to $6 \cdot 10^{21} \text{ cm}^3/\text{mol}$, and a value of $6.7 \cdot 10^{21} \text{ cm}^3/\text{mol}$ was chosen for easy unit conversion.⁵⁶ In this thesis however, an analysis of detailed atomistic molecular packing models is utilized to determine the value of N_0 for each polymer individually. This will be discussed in more detail in Section 6.2. The fit of equation 3.44 to sorption and of equation 3.48 to dilation data was performed using the numerical integration algorithm of the package ‘Statistics_NonlinearFit’ of the Mathematica 5.2 software of Wolfram Research Inc., Champaign (USA).

3.4 Summary

In the above sections, the details of three theoretical models were provided which will be used later to analyse the experimental data of this work (see Section 4.5). Selected aspects of the results will be compared to simulated data in Section 5.3. All three models approach the phenomenon of gas sorption and sorption induced dilation in glassy polymers from different viewpoints. The DM model combines, in a more or less empirical way, the observation of sorption in liquid or rubbery polymers (Henry part) with the adsorption process on inner surfaces (Langmuir part); while this intuitive combination seemed to fit sorption data rather well, the attempt to connect the parameters of the model to independently determinable physical parameters was only partly successful.⁶⁰ In contrast, the NET-GP approach and the *site distribution* model arise from physical considerations, enabling a view on the phenomena of a more substantiated nature. However, both models show limitations regarding their applicability which are inherent in the model assumptions and can therefore not be accounted as ‘general’, as will be shown later in this work.

4 Experimental

4.1 Materials

4.1.1 Gases

Carbon dioxide (CO₂) and methane (CH₄) of purity > 99.5 % were used as received from Air Liquide Deutschland GmbH. As ‘dynamic volume’ V_g in terms of a relaxed partial molar volume of the gas dissolved in liquids or rubbery polymers, the values of 46.2 cm³/mol and 52 cm³/mol were used that were reported by Pope et al.⁶¹ for CO₂ and CH₄ in silicone rubbers, respectively. For unit conversion, the value of $V_{id} = 22413.6$ cm³/mol was used as the volume of an ideal gas at standard conditions (STP: $T = 273.15$ K, $p = 1.013$ bar).

4.1.2 Polymers

Polysulfone

Poly(sulfone) is an amorphous high-performance thermoplast used in a variety of applications and therefore readily available from a number of different suppliers. In this work, Ultrason S was obtained from BASF AG, Germany, as a melt extruded film of $d = 100$ μm thickness. The repeat unit (see Figure 4.1) has a molecular weight of 469.8 g/mol and the supplier reports an average molecular weight of 400 kg/mol. Measurements in a differential-scanning-calorimeter (DSC), heating rate 10 K/min showed non-crystallinity and a glass transition at 462 K (190 °C). The density was determined in a density-gradient column (DGC, Ca(NO₃)₂-solution) at 295 K (23 °C) to $\rho = 1.240$ g/cm³, agreeing well with the value given by the supplier (1.24 g/cm³). From the density a value of $\Phi_{free} = 13.5$ % results for the fraction of *free volume*, calculated by the Synthia software of Accelrys Inc.,⁶² using the Bondi method.³⁵

Polyimide 4 (6FDA-TrMPD)

The polyimide 6FDA-TrMPD (named PI4 as in ref. [63]) was synthesized⁶⁴ at the GKSS research center, resulting in chains of an average molecular weight of about 300 kg/mol. The chemical structure of the repeat unit, which has a molecular weight of 558.4 g/mol, is shown in Figure 4.2. Films were cast from a dichloromethane solution onto a glass plate and spread by a coating knife. After slow solvent evaporation in a chamber of decreasing solvent vapor atmosphere, the films were shortly immersed in water to detach them from the glass plate. The thickness of the resulting dry and transparent films was determined to $d = 120 \mu\text{m}$. DSC measurements showed some residual water contents in the film and a glass transition of 650 K (380 °C). After several days of degassing of the sample inside the pressure cell (prior to sorption and dilation measurements), no significant influence of the residual water on volume or weight of the sample could be detected. The density of the cast film was determined to be $\rho = 1.352 \text{ g/cm}^3$ and the *free volume* fraction to be $\Phi_{free} = 18.7 \%$.

PIM-1

The Polymer of Intrinsic Microporosity (PIM-1), a recent development of Budd et al.,^{31, 65–67} was synthesized at the GKSS research center, resulting in an average molecular weight of 150 kg/mol.⁶⁸ The chemical structure of the repeat unit with 460.5 g/mol is shown in Fig. 4.3. Films were cast from a chloroform solution into a petri dish situated inside a chamber of decreasing solvent vapor atmosphere for slow evaporation. Immediately after detaching the films in a water bath for some hours, they were immersed in ethanol for 8 h to reduce the water content and then dried in vacuum and 552 K (150 °C) for 12 h. The transparent film of yellow color had a thickness of $d = 150 \mu\text{m}$ and a density of $\rho = 1.124 \text{ g/cm}^3$. As reported in ref. [65], no glass transition could be observed by DSC below the degradation temperature of $T_{deg} = 722 \text{ K}$ (350 °C). From the density, the *free volume* fraction was calculated to $\Phi_{free} = 19.2 \%$.

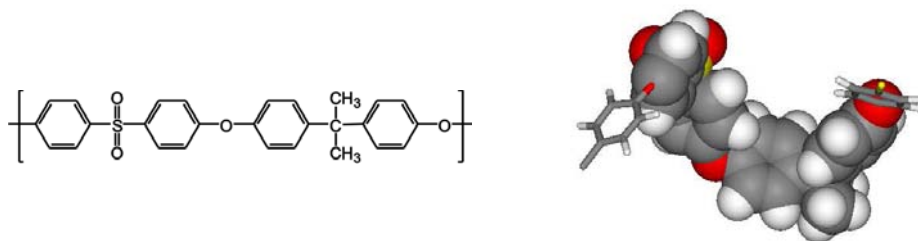


Figure 4.1: Chemical structure of PSU and representation of the repeat unit by Van-der-Waals spheres.

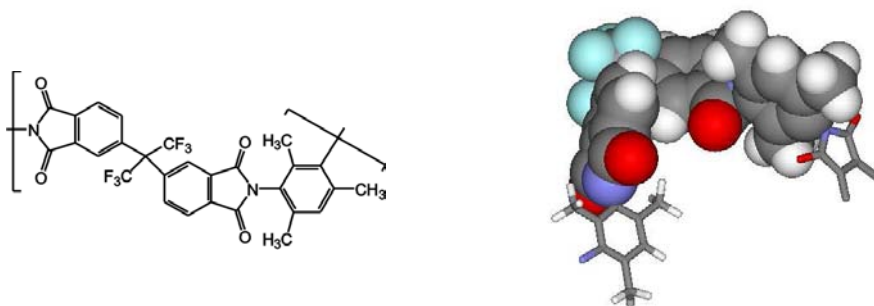


Figure 4.2: Chemical structure of PI4 and representation of the repeat unit by Van-der-Waals spheres.

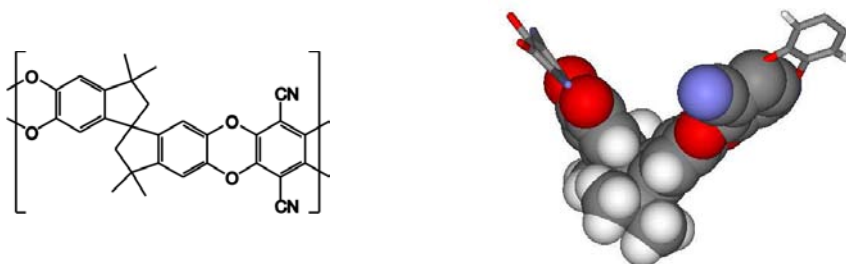


Figure 4.3: Chemical structure of PIM-1 and representation of the repeat unit by Van-der-Waals spheres.

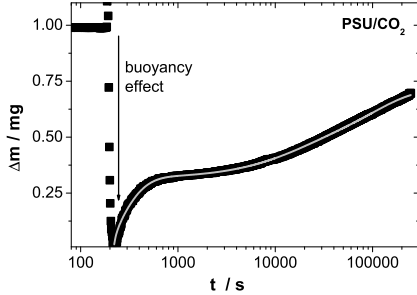


Figure 4.4:

Typical mass uptake curve on logarithmic time scale following a gas pressure step. The buoyancy effect is easily identified. Data points are shown with a fit according to the kinetic analysis (cf. Section 4.4).

4.2 Sorption Measurements

Gravimetric Sorption Balance

Gravimetric sorption measurements were carried out using an electronic microbalance Sartorius M25D-P of Sartorius GmbH, Göttingen. Details of the setup may be found in reference [69]. The balance is situated in a pressure cell designed to bear pressures well over 50 bar. The temperature of the setup is held constant by an air-bath at 35 ± 0.1 °C. Deviating from ref. [69], in this work data acquisition was computer aided, recording the signal of the microbalance automatically at a rate of 0.5 s^{-1} . The film sample of uniform thickness is cut into several pieces ($\sim 10 \times 10 \times 0.1 \text{ mm}^3$) and put onto the balance pan inside the cell, which is then evacuated at $p < 10^{-5} \text{ mbar}$ until any significant weight change has ceased. After thorough degassing of the sample, the gas-pressure is increased in a series of stepwise increments and the weight gain Δm of the sample is observed for at least 24 hours at each step (Figure 4.4); in the literature, this procedure is referred to as *differential* sorption measurement. For the so called *integral* sorption measurements, the gas-pressure is increased in a single integral step to (in this work) 10 bar and the weight gain of the sample is observed for at most 4 hours to ensure that a quasi-equilibrium is reached but no significant relaxations take place. Afterwards, the pressure cell is evacuated and the desorption process is observed. The effect of buoyancy is either eliminated from the data or estimated using Archimedes law. The weight gain is converted into the commonly used units of $\text{cm}^3(\text{STP})/\text{cm}^3(\text{polymer})^\#$ using

$$\Delta C = \frac{V_{id} \Delta m}{M_{\text{gas}}} \cdot \frac{\rho_0}{m_0} \quad (4.1)$$

[#]Throughout this work, for better readability the unit $\text{cm}^3(\text{STP})/\text{cm}^3(\text{polymer})$ will be expressed by cm^3/cm^3 .

where V_{id} is the molar volume of an ideal gas at standard conditions (STP), M_{gas} the molar mass of the penetrant gas and ρ_0 and m_0 the density and mass of the polymer prior to any measurement.

4.3 Dilation Measurements

Gas pressure Dilatometer

A number of different techniques to measure sorptive dilation of glassy polymers are reported in the literature. While earlier methods were based on visual readouts,^{70, 71} more recently induction gauges,^{59, 72, 73} ellipsometry³⁰ or image analysis⁷⁴ are utilized to monitor the swelling of polymer/gas systems. In this work, the volume changes in the sample due to sorption of gas molecules were investigated using a gas-pressure-dilatometer, whose principle is shown in Figure 4.5 and which has been described in more detail in references [69] and [29]. It is based on a capacitive distance measuring system:

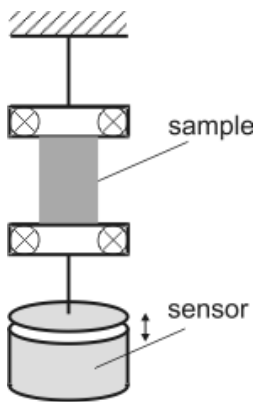


Figure 4.5:
Principle of the capacitive dilatometer.

A strip ($\sim 20 \times 10 \times 0.1 \text{ mm}^3$) of the sample film is clamped at both ends. The upper clamp is fixed to the cell-wall, while at the lower end a small metal disk is attached perpendicular to the film plane. Thus the disk is suspended freely above the capacitance-sensor, serving as its counter plate. Distance changes between the two plates of this capacitor can be measured linearly within a range of $1000 \mu\text{m}$ and with an accuracy of $0.25 \mu\text{m}$. The weight of lower clamp and metal disk ($< 10 \text{ g}$) is not expected to significantly influence the measurement as the exerted stress is almost three orders of magnitude below the yield stress of the polymer specimen. Similar to the sorption setup, the dilatometer is placed in a pressure cell which is held at constant temperature by an air bath. In contrast to ref. [69], a second sensor has been added to the chamber with a well defined distance to its fixed counter plate; its signal is used to eliminate the effects due to dielectric changes

of the gas atmosphere resulting from its variations in the density upon each pressure step. The Labview-based software allows data-acquisition rates of up to 1 s^{-1} , limited by the instruments and interfaces. Following the same procedure as in the sorption measurements, after thorough degassing, the length change of the sample is recorded for a series of pressure increments, and at least 24 hours observation time per step were scheduled for the differential dilation isotherms, and accordingly a pressure step to 10 bar for several hours and subsequent degassing for 24 hours following the integral dilation procedure. Assuming isotropic swelling, the length change Δl of the

sample can be easily converted to volume change ΔV using

$$\Delta V/V_0 = (1 + \Delta l/l_0)^3 - 1 \quad (4.2)$$

where l_0 and V_0 denote the initial length and volume of the sample.

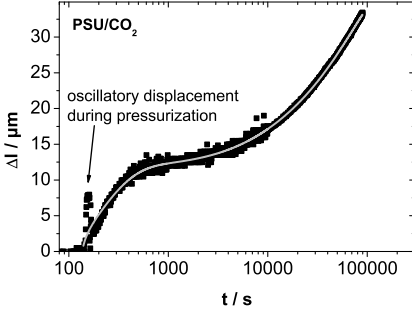


Figure 4.6:

Typical length change curve on logarithmic time scale following a gas pressure step. At times larger than 10^4 s, the sample rate is decreased and the data is smoothed by an averaging algorithm. Data points are shown with a fit according to the kinetic analysis (cf. Section 4.4).

4.4 Kinetic Analysis

According to Crank,³⁹ three cases of diffusion of penetrants in glassy polymers are distinguished:

- i Case I or Fickian diffusion in which the rate of diffusion is much less than the rate of relaxations;
- ii Case II diffusion in which diffusion is very rapid compared with the relaxation processes;
- iii Non-Fickian or anomalous diffusion which occurs when diffusion and relaxation rates are at a comparable level.

For the obtained data of all investigated polymer/gas systems at 308 K, the shape of the mass uptake curve implies anomalous diffusion with a two-stage sorption process, where the initial rapid stage is controlled by Fickian diffusion, whereas the second stage is dominated by relaxational processes of the polymer matrix. A typical example for the PSU/CO₂ system is shown in Figure 4.4. The same two-stage behavior is observed for the dilation curve (Figure 4.6). Thus, for a detailed analysis of the kinetics of sorption and dilation, the following model function has been fitted to the sorption and dilation data, respectively:

$$\Delta X(t) = \Delta X_f \cdot f(t, D) + \Delta X_{g1} \cdot g_1(t, \tau_1^*) + \Delta X_{g2} \cdot g_2(t, \tau_2^*) \quad (4.3)$$

where

$$f(t, D) = 1 - \sum_{n=0}^{\infty} \frac{8}{(2n+1)^2 \pi^2} \exp(-D(2n+1)^2 \pi^2 t / d^2) \quad (4.4)$$

and

$$g_i(t, \tau_i^*) = 1 - \exp(-t / (d^2 \tau_i^*)) \quad (4.5)$$

$\Delta X(t)$ denotes the time dependent change of mass or length, respectively. The first term on the right side of eq.4.3 reflects Fickian diffusion kinetics into a plane sheet of thickness $d/2$ as derived by Crank³⁹ (eq.4.4 \equiv eq.2.11). It contains the diffusion coefficient D and the diffusive fraction of the mass uptake ΔX_f as fit-parameters. Sufficient accuracy was achieved using the first ten terms in the summation of eq.4.4 for calculations while higher order terms were dropped for practical reasons ($n \leq 9$). To account for non-Fickian diffusion, two exponential relaxation functions g_1 and g_2 are implemented with the relaxational fractions ΔX_{gi} and the thickness normalized relaxation times[‡] τ_i^* as fit-parameters. This approach was proposed by Berens and Hopfenberg,⁴² based on the treatment of solvent-vapor sorption in glassy polymers. In their model, the kinetics of vapor sorption are considered to be a linear superposition of independent contributions from Fickian diffusion and sorption controlled by relaxational processes of the polymer matrix. In general the relaxational contribution may be written as an infinite sum of exponential functions representing first order relaxations. However, one or two relaxational terms have proven to successfully describe even complex sorption data.^{42, 43} Wessling et al.⁴³ applied this method to CO₂-sorption in glassy polyimides, and suggested to use the same kinetic model to fit the corresponding CO₂-induced dilation.

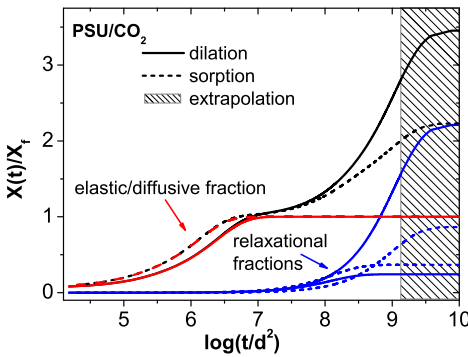


Figure 4.7:

Thickness normalized kinetics of mass uptake and dilation on logarithmic time scale, normalized to the elastic/diffusional fraction and extrapolated to large times (hatched area).

[‡]Strictly speaking, the τ_i^* are reciprocal (effective) diffusion coefficients; however, this stage of sorption is kinetically controlled by relaxations of the polymer matrix, characterized by a relaxation time $\tau_i = (d^2 \tau_i^*)$. The normalization of the relaxation times to the film thickness is done for convenient comparison to the diffusion coefficient and should not imply a thickness dependence.

As a typical example for the behavior in the PSU/CO₂-system, Figure 4.7 on the previous page shows mass uptake and dilation of the pressure step 25 to 30 bar, that were shown in Figures 4.4 and 4.6, normalized to the diffusive/elastic fraction and on a thickness-normalized logarithmic time scale. As can be easily seen,

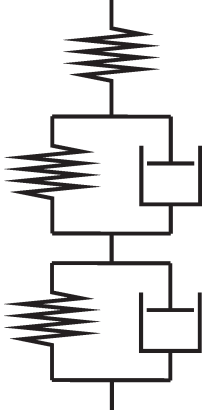


Figure 4.8:
Spring-dashpot model
to describe viscoelastic
behavior.

there is a clear relation between the time scales of the different processes involved in sorption and dilation, respectively. This leads to the viscoelastic interpretation by Newns²² as discussed in the introduction: Equation 4.3 is the mathematical representation of a spring and dashpot model (cf. Section 2.4) as shown in Figure 4.8. A spring accounts for the elastic stresses imposed during the initial, rapid stage of sorption of penetrant molecules. Because this reaction of the matrix is nearly instantaneous, the slower kinetics of diffusion into the matrix is controlling the process and eq.4.4 applies to this elastic fraction of dilation. Two Kelvin modules (see also Section 2.4) represent the viscoelastic relaxations of the polymer matrix. Their time constants τ_i^* , normalized to the film-thickness d , are of the order $\tau_i^* \approx 10^8 \dots 10^9 \text{ s/cm}^2$, whereas the reciprocal diffusion coefficient D^{-1} is about 10^7 s/cm^2 for CO₂ in PSU at 308 K at a CO₂ pressure of 30 bar (see Figure 4.7). In the following, the first part, with kinetics controlled by Fickian diffusion, will be referred to as the *diffusive* fraction of sorption and *elastic* fraction of dilation, respectively. As there is

no explicit relation of the relaxation functions g_i to specific molecular motions or processes assumed here, both relaxational contributions will be discussed in terms of one *relaxational* fraction of sorption or dilation, meaning the sum of both relaxational functions at the end of an experimental measurement cycle ($t = t_e = 24 \text{ h}$):

$$\Delta X_r(t_e) = \Delta X_{g1}(t_e) + \Delta X_{g2}(t_e) \quad (4.6)$$

The respective contributions to sorption ($\Delta C_f(t_e)$ and $\Delta C_r(t_e)$) and dilation ($\Delta V_f(t_e)$ and $\Delta V_r(t_e)$) for each pressure step may now be added up resulting in separate isotherms of the *diffusive/elastic* and the *relaxational* fraction, which may be further analyzed:

$$C_{diff} = \sum_{steps} \Delta C_f(t_e) \quad (4.7)$$

$$\Delta V_{elast} = \sum_{steps} \Delta V_f(t_e) \quad (4.10)$$

$$C_{relax} = \sum_{steps} \Delta C_r(t_e) \quad (4.8)$$

$$\Delta V_{relax} = \sum_{steps} \Delta V_r(t_e) \quad (4.11)$$

$$C_{total} = C_{diff} + C_{relax} \quad (4.9)$$

$$\Delta V_{total} = \Delta V_{elast} + \Delta V_{relax} \quad (4.12)$$

4.5 Experimental Results and Discussion

4.5.1 Sorption and Dilation Isotherms

The application of the kinetic analysis (eq. 4.3) that was described in the previous section, yields the fractions of mass uptake (sorption) and volume change (dilation) that follow diffusive/elastic and relaxational kinetics for each experimental step, respectively. The resulting values for each pressure step are added, resulting in two separate contributions (diffusive/elastic and relaxational) to the total isotherm. Summation of the two parts gives the total sorption or dilation isotherm, respectively, as it is usually presented. In the following, the data acquired for the PSU/CO₂ system will be thoroughly discussed exemplarily in terms of the *Dual Mode* (DM) and the *site distribution* (SD) model. The quality of the fits and the reliability of the fitparameters will be addressed and the kinetic analysis will be consistently implemented with regard to the origin of the SD model.

Polysulfone - CO₂

A number of authors have published data on CO₂ sorption in polysulfone.^{24–29} Erb and Paul²³ examined polysulfone samples that were aged (*free volume* reduction by sub- T_g annealing) or conditioned (*free volume* increase by high pressure CO₂ treatment). The resulting isotherms, emphasized by DM-fitcurves in Figure 4.9 (solid lines), approximately mark the lower and upper boundaries of sorption data at a temperature of 35 °C. Aside from a variety of different experimental setups, the sample prehistory, which is not always known, and the experimental time scale seem to be the main causes of the observed differences. As can be seen from Figure 4.9, the primary sorption data gathered in this work (displayed in red) are well within the limits of the variation of reported literature data.²

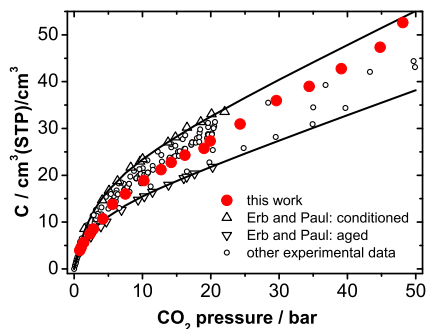


Figure 4.9:

Sorption data of CO₂ in PSU at 35 °C of this work (red) and literature data (○) from refs.^{24–29} The data of Erb and Paul²³ on conditioned (△) and aged (▽) samples mark the upper and lower boundary of the variation found in the literature.

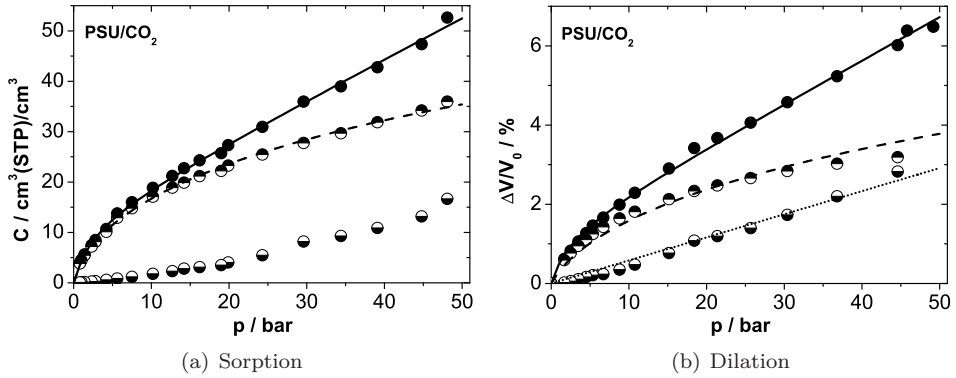


Figure 4.10: Isotherms of CO₂ in PSU. The solid lines represent a best fit of the DM model through the total isotherms (●). The dashed line through the diffusive/elastic fraction (◐) represents a best fit of the SD model. The relaxational fraction (○) of the dilation is fitted linearly (cf. text).

For the CO₂-induced dilation there is no literature data available to a similar extent. However, Wang and Kamiya²⁵ arrived at a dilation of 0.5 % at a pressure of 2.3 bar and Böhning and Springer⁶⁹ measured a dilation of 5 % and 8.5 % for short- and long-term measurements, respectively, in an isotherm up to 50 bar CO₂ pressure using the same experimental setup as in this work.

Figure 4.10 shows the experimental results of sorption and dilation in the PSU/CO₂ system obtained in this thesis. In Figure 4.10(a) the increase of concentration with pressure is shown. The total mass uptake is shown in full circles (●), at each pressure step indicating the content of CO₂ within the polymer sample. The second isotherm that is displayed shows the diffusive/elastic part of the sorption (◐). At each pressure step, only the fraction of sorbed CO₂ following Fickian diffusion kinetics is added to the isotherm. It should be noted that this ‘diffusive isotherm’ indicates the amount of penetrant gas that was sorbed at short time scales following Fickian diffusion kinetics; however, the classification as diffusive (and relaxational) isotherm should not imply different populations of sorbed CO₂.[‡] At low pressures both, the total and the diffusive isotherm coincide, because no significant relaxations take place within the time scale of the experiment. At pressures above 10 bar, the diffusive isotherm deviates from the total isotherm and the relaxational fraction (○) can be obtained by subtraction of the diffusive part. It should be noted that the relaxational fraction and hence the total isotherm result from relaxational processes that are still in progress at the end of a measurement step ($t_e = 24$ h). The concentration, total or relaxational, at each pressure is therefore not at a quasi-equilibrium, as is the diffusive fraction of sorption.

[‡]To illustrate this point, imagine a room with a door and a window. It is possible to count how many people entered through the door, and how many entered through the window; but once inside it is impossible to tell who entered through the door.

In Figure 4.10(b) the corresponding dilation isotherms are shown, using the same symbols for the total (●), elastic (◐) and relaxational (◑) isotherm. Comparison of the concentration and dilation isotherm (Figure 4.10) and of the time dependent sorption and dilation of individual pressure steps (Figure 4.7) shows a clear correlation between the diffusive sorption and elastic dilation and the respective relaxational fractions, which may be interpreted in the following way:^{2, 22, 43}

Following the pressure step, the chemical potential of the CO₂ in the gas phase and within the polymer matrix is balanced by a mass flux, following Fickian diffusion kinetics (eq. 4.4), until a (pseudo-) equilibrium concentration is reached in the polymer. The elastic dilation that is caused by the misfit between gas molecule and sorption site (hole) in the matrix (cf. Section 2.3) appears instantaneously upon occupation of a sorption site, which is the reason why the elastic/diffusive process is kinetically controlled by the slower sorption kinetics (Fickian diffusion). Since in the glassy polymer PSU (at a low concentration level) the mobility of the matrix is quite limited, any sorption induced stresses are conserved and the system remains in a metastable state. At higher pressures (concentration levels) of CO₂ the PSU-matrix is plasticized, the mobility of the polymer chains is enhanced and sorption induced stresses are partly reduced, resulting in relaxational dilation. The reduction of sorption induced stresses lowers the chemical potential of the sorbed gas molecules, which again leads to a diffusive mass flux into the matrix. The characteristic times of the relaxational processes are larger than that of diffusion ($\tau_i^* > D^{-1}$) and therefore the relaxational dilation dominates the sorption kinetics.

Dual Mode Sorption Model

In Chapter 3, three different phenomenological descriptions of sorption and concomitant swelling behavior of polymer/gas systems were introduced. The *Dual Mode Sorption Model* (DM model) describes sorption as two superposing processes, one describing a ‘hole filling’ of microcavities within the polymer matrix (Langmuir mode) and the other the occupation of interstitial space (Henry mode) (see Section 3.1). Equation 3.3 was fitted to the total concentration pressure isotherm. The resulting fit parameters are listed in Table 4.1 on page 36, along with the results of the extended DM model to fit the gas induced dilation (Section 3.1 eq. 3.5). The fit curves of the DM model are in excellent agreement with the experimental data (Fig. 4.10, solid lines). However, the dual mode sorption parameters show a clear dependence on the maximum pressure.⁷⁵ Figure 4.11 on page 37 shows the variation of model parameters with pressure. On the y-axis, the parameter value is plotted against the maximum pressure (Fig. 4.10) of which the data pair $[C, p]$ was included in the fit (as if the measurement was finished at this pressure)[‡]. The dependence of the DM model parameters (k_D, C'_H, b) on this maximum pressure is quite strong at pressures below

[‡]Note that the DM-parameters at the highest pressure correspond to the DM-fit in Fig. 4.10, i.e., all datapoints were included in the fit.

20 bar and levels off at higher pressures. Speaking in terms of the model, Langmuir-type sorption sites are saturated at this pressure and the Henry parameter k_D may be determined with reasonable certainty. Anyhow, due to the uncertainty of the exact pressure of Langmuir site saturation and the physical ambiguity of the parameters it is recommended to use DM parameters for interpolation only.

At first glance, a comparison of Figure 3.1 and the three sorption isotherms of Figure 4.10 suggest a correlation between Henry mode sorption and the relaxational fraction of sorption on the one hand and between Langmuir mode and diffusional sorption on the other. However, the separate display of Henry mode sorption (dotted line) and Langmuir mode sorption (dashed line) in Figure 4.12, as obtained by a best fit of eq. 3.3, shows that the observed similarity with the kinetic separation of diffusive and relaxational fractions of sorption is misleading, and a connection of the observed kinetic processes and the two sorption modes of the model cannot be made in a straightforward way.

Table 4.1: Dual Mode Sorption model parameters (cf. eqs. 3.3 and 3.5).

polymer/ gas	$k_D/$ $\text{cm}^3/\text{cm}^3\text{bar}^{-1}$	$C'_H/$ cm^3/cm^3	$b/$ bar^{-1}	$V_p/$ cm^3/mol	f
PSU /CO ₂	0.805	12.8	0.384	30.1	0.79
PSU /CH ₄	0.381	3.35	0.206	10.7	1.6
PI4 /CO ₂	1.56	54.6	0.544	75.2	0.16
PI4 /CH ₄	0.482	31.5	0.153	29.5	0.13
PIM-1/CO ₂	1.64	78.6	0.480	37.6	0.29
PIM-1/CH ₄	0.116	76.4	0.109	312	0.00

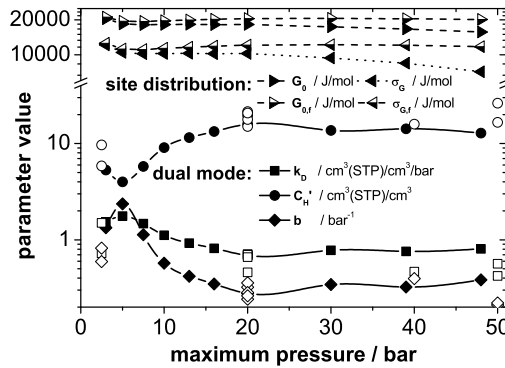


Figure 4.11: Model parameters in dependence on the maximum pressure included in a fit to sorption data of CO₂/PSU. The strong dependency of the *dual mode* parameters (k_D , C_H , b) levels off at higher pressures. Reported literature data^{23, 25–28} (open symbols) fit well into this scheme.

Site distribution parameters from the total sorption (\blacktriangleright , \blacktriangleleft) lose reliability with the onset of relaxational swelling, while parameters obtained from diffusive fraction (\blacktriangleright , \blacktriangleleft) are stable over the whole pressure range.

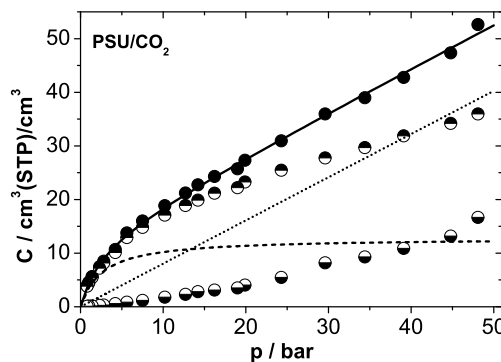


Figure 4.12: DM fit (—) to the experimental sorption data of CO₂/PSU. Obviously, there is no connection between the diffusive sorption (\bigcirc) and the Langmuir mode (---) or the relaxational fraction (\bullet) and the Henry mode (\cdots).

Site Distribution model

The *site distribution* model is derived using the assumption of a continuous, elastic polymer matrix (see Section 3.3). The concentration of penetrants within the matrix is calculated, assuming that elastic energy, resulting from the deformation of a sorption site, is stored in the matrix. Ideally, the SD model then yields parameters of a size distribution of sorption sites of the pure polymer matrix. Relaxational swelling processes are not considered by the model, which is why the author of the model disregards any sorption and dilation data beyond the pressure at which relaxational swelling typically sets in (20 bar).⁵⁶ But the omission of data points always involves a loss of reliability or accuracy, as Figure 4.11 has already shown for the DM parameters. Figure 4.11 also contains the pressure dependent parameters of the SD model, obtained in the same fashion as the DM model parameters. Obviously, the pressure dependence of the SD model is not as pronounced. However, if all data of the total isotherm are included in the fit, the parameters of the SD-model decrease slightly with pressure. This result is consistent with the model: if relaxational swelling takes place, the average site volume should rise and therefore the elastic energy which is necessary to occupy the site decreases; hence additional sorption occurs. Also, as plasticization is progressing, i.e. the mobility of the matrix is significantly increased, stresses induced in the matrix upon gas sorption are easier to be relaxed and, as the differences in site energy lessen, the distribution of Gaussian shape decays to a Dirac-delta function (one site energy for all sites). As more and more data points are included in the fit, both effects, swelling and plasticization, change the structure of the amorphous polymer matrix, and the result of the SD model fit that should give information about the original structure of the matrix is altered.

Therefore it seems reasonable to exclusively use the *diffusive/elastic* fraction of sorption and dilation over the whole pressure range and thus abiding by the supposed origin of the SD model (i.e., elastic deformation).² It must be noted that, even if only the diffusive fraction is taken into account, the structural changes of the matrix are taking place nonetheless, increasing the width of the size distribution of sorption sites. Yet, at the regarded levels of concentration, this change does not lead to significant differences in the diffusive fraction of sorption. Therefore it is justified to utilize the complete diffusive fraction of the sorption isotherm to obtain structural information of the original matrix. The dashed lines in Figure 4.10 show the best fit of eqs. 3.44 and 3.48 to the sorption and dilation data, respectively. The sorption data (left) was fitted resulting in best-fit-parameters of the energy distribution G_0 and σ_G (center and width of the Gaussian distribution). These values are used as input for eq. 3.48, where only the average volume of a sorption site V_{h0} is varied to give a best fit to the dilation data. The fit curves agree well with the experimental data. The resulting parameters of Gaussian size and energy distributions are compiled in Table 6.2 on page 91 and will be discussed in the context of *free volume* distributions (Sec. 6.2).

NET-GP

The third model that was discussed in Chapter 3 is called Non-Equilibrium Thermodynamics of Glassy Polymers (NET-GP) or Non-Equilibrium Lattice Fluids (NELF). As will be argued in Section 6.1, the model only takes into account irreversible volume changes. Since the elastic dilation is not considered by this model, besides using the total dilation, in Section 6.1 the exclusive use of the relaxational dilation isotherms will also be discussed to determine the swelling factor k_s needed for the prediction of sorption isotherms. As can be seen in Figure 4.10, the relaxational dilation resembles far better a linear relationship with pressure, which is assumed by the model, than the diffusive or total isotherms do. Figure 4.10 shows the best fitting straight line (through zero, dotted line). It results in a swelling coefficient k_{sr} that was used to predict sorption isotherms according to equation 3.22 (cf. Table 3.1). Owing to the close relationship of the procedures, the results of the sorption prediction by the NELF model will be presented in Section 6.1 in the context of GCMC isotherms (see Section 5.2.2), including a more thorough discussion of the exclusive use of relaxational dilation.

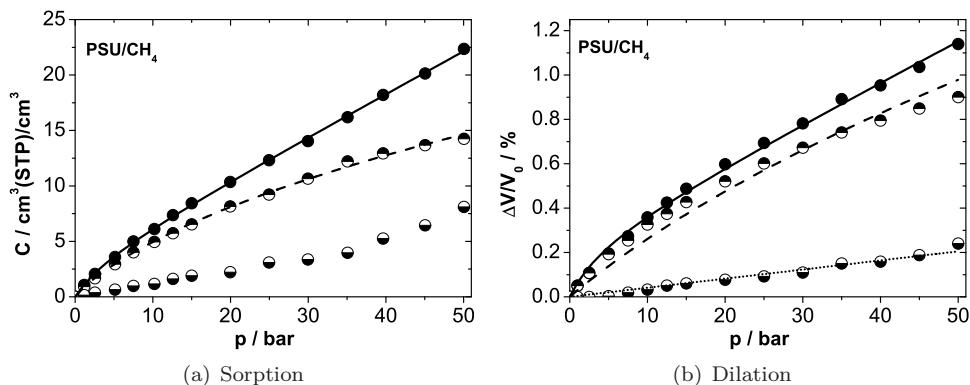


Figure 4.13: Sorption and dilation isotherms of CH₄ in PSU. (—): DM model through the total isotherms (●). (---): SD model fit through the diffusive/elastic fraction (○). The relaxational fraction (◐) of the dilation is fitted linearly (···)(cf. text).

Polysulfone - CH₄

Figure 4.13 shows the sorption and dilation isotherms of CH₄ in polysulfone. Expectedly, the concentration level reached is much lower than that for CO₂. This is expressed by the lower values of the DM model parameters (Tab. 4.1 on page 36), which represent a well agreeing fit through the (total) sorption data. The diffusive/elastic fraction of sorption and dilation was fitted by the site distribution model, in compli-

ance with the arguments discussed in the previous paragraph. The curves fit the data reasonably well and the resulting size distribution of sorption sites will be discussed in Section 6.2.

PI4 - CO₂

Figure 4.14 shows the sorption and dilation isotherms of CO₂ in 6FDA-TrMPD polyimide (PI4). Due to technical reasons, the measurement had to be aborted at a pressure of 35 bar. The CO₂ solubility is extraordinarily high, as is the accompanying dilation. It is worth mentioning that at the maximum pressure of 35 bar, the relaxational fraction of dilation reaches the level of elastic dilation, indicating the strong plasticizing ability of CO₂. The DM parameters reflect this sorption and dilation behavior and again yield excellent fit curves. While the diffusive sorption is well represented by the SD model, the dilation, where only one parameter (V_{h0}) is adjusted, overestimates the dilation at low pressures and underestimates at high pressures. However, the agreement between fit curve and data is still acceptable. The unexpectedly low value for the average site volume V_{h0} , when compared to polysulfone, will be discussed in Section 6.2.

PI4 - CH₄

In Figure 4.15 the sorption and dilation isotherms of the PI4/CH₄ system are presented. Again, a considerably lower concentration and dilation level is observed for methane in comparison to CO₂, but the solubility is higher in PI4 than in PSU. The DM model fits the data quite well. The total dilation seems, in contrast to both dilation isotherms in PSU, to be almost linear, which is, same as for CO₂, reflected by the small value of f , denoting the fraction of Langmuir mode sorption contributing to the dilation. The site distribution model yields excellent fits to the diffusive fraction of sorption and the elastic fraction of dilation, respectively.

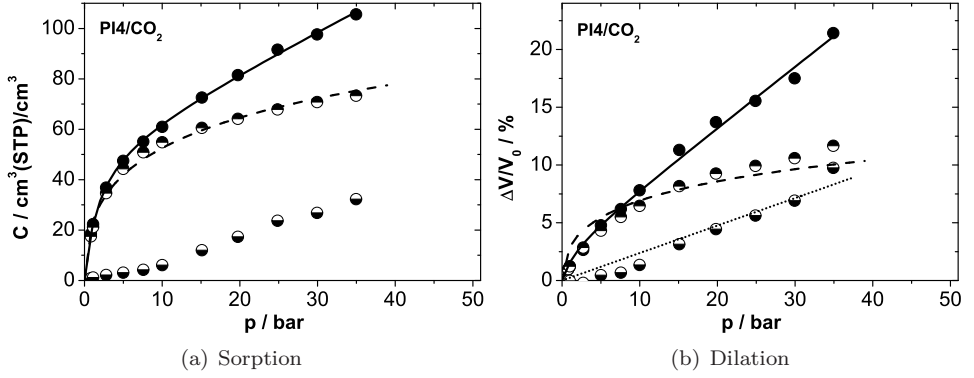


Figure 4.14: Sorption and dilation isotherms of CO₂ in PI4. (—): DM model through the total isotherms (●). (---): SD model fit through the diffusive/elastic fraction (●). The relaxational fraction (●) of the dilation is fitted linearly (····)(cf. text).

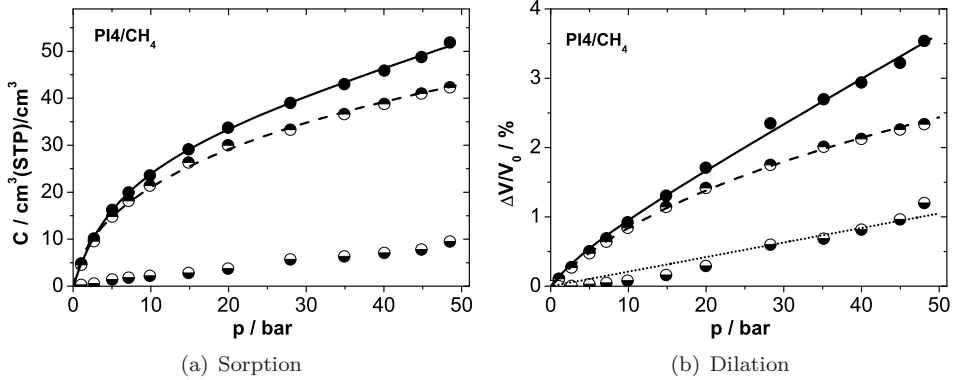


Figure 4.15: Sorption and dilation isotherms of CH₄ in PI4. (—): DM model through the total isotherms (●). (---): SD model fit through the diffusive/elastic fraction (●). The relaxational fraction (●) of the dilation is fitted linearly (····)(cf. text).

PIM-1 - CO₂

Sorption and dilation isotherms of the PIM-1/CO₂ system are presented in Figure 4.16. The solubility of CO₂ in PIM-1 exceeds even that of CO₂ in PI4, while at the same time exhibiting less pronounced dilation. Also the comparatively low relaxational fraction suggests a high fractional free volume (only little dilation necessary to accommodate penetrants) as well as a relatively rigid matrix (poor plasticisation ability), as is expected for a ‘polymer of intrinsic microporosity’. The DM model yields a nice fit and the highest value for the Langmuir capacity C'_H . The SD model again fits the sorption very well, while the dilation fit is of poorer quality (see also the discussion in Section 6.2).

PIM-1 - CH₄

Figure 4.17 shows the sorption and dilation isotherms of the PIM-1/CH₄ system. Similar to the methane isotherms in PI4, a high level of concentration is reached. The low value of the Henry parameter k_D entails an unusually high Langmuir capacity C'_H . In combination with the linear dilation, unreasonable values of the partial molar volume V_p and fV_p result. The SD model fit curve does not represent the experimental data as well as in all other cases. However, the agreement can still be called fairly well.

Despite the fact that all experimental data may be well fitted by the discussed models, the following observations can be made:

- E1) Overall sorption is represented very well by the DM model. The Langmuir capacity C'_H as well as the Henry solubility k_D arrange in the order PSU < PIM-1 < PI4, giving a measure of the concentration level reached by CO₂ and CH₄. The only exception presents the PIM-1/CH₄ sorption. A reliability analysis of DM parameters of data of this work and literature data suggests their use for interpolation only.
- E2) By way of kinetic analysis, the sorption and dilation process can be successfully divided into a fraction following Fickian diffusion kinetics and a relaxational fraction. Dilation which is induced in the former, more rapid stage appears instantly upon sorption of a penetrant and is therefore regarded as elastic. The slower process is dominated by viscoelastic or plastic deformation kinetics of the polymer matrix and therefore regarded as irreversible (on a similar time scale).
- E3) The SD model, which is based on the assumption of an elastic deformation, fits the diffusive/elastic fraction of sorption and dilation fairly well, allowing to make use of the full pressure range of the data. The reliability analysis of the PSU/CO₂ justifies this approach.
- E4) The relaxational fraction can be fitted linearly to derive a swelling parameter to be used for NET-GP sorption predictions (see Section 6.1).

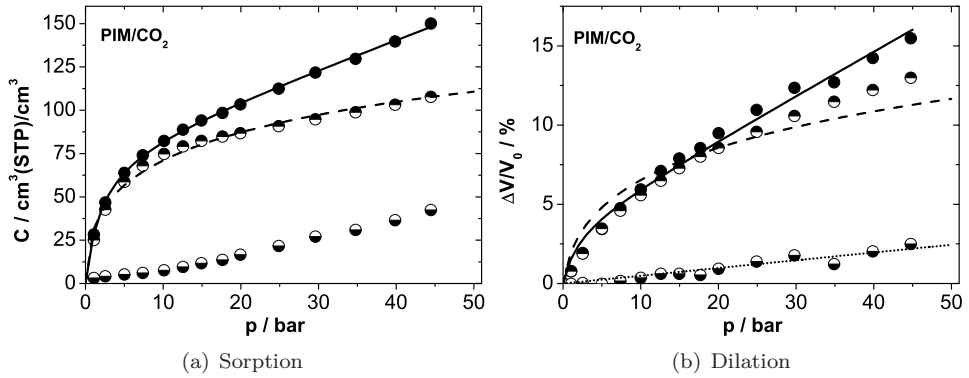


Figure 4.16: Sorption and dilation isotherms of CO_2 in PIM-1. (—): DM model through the total isotherms (\bullet). (---): SD model fit through the diffusive/elastic fraction (\bullet). The relaxational fraction (\circ) of the dilation is fitted linearly (\cdots) (cf. text).

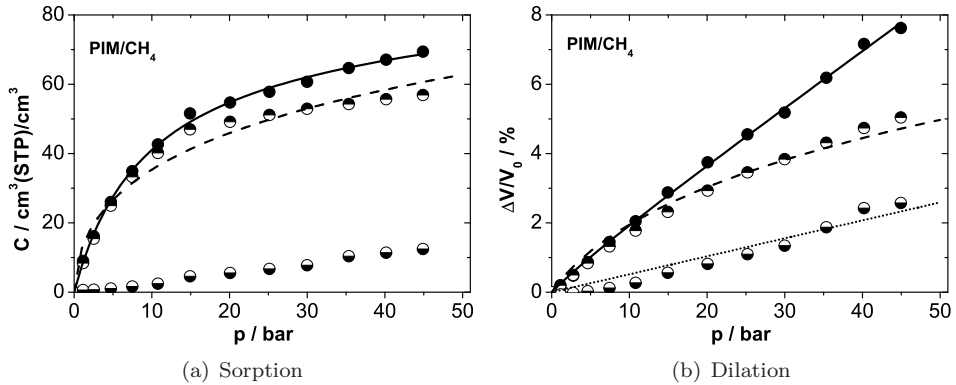


Figure 4.17: Sorption and dilation isotherms of CH_4 in PIM-1. (—): DM model through the total isotherms (\bullet). (---): SD model fit through the diffusive/elastic fraction (\bullet). The relaxational fraction (\circ) of the dilation is fitted linearly (\cdots) (cf. text).

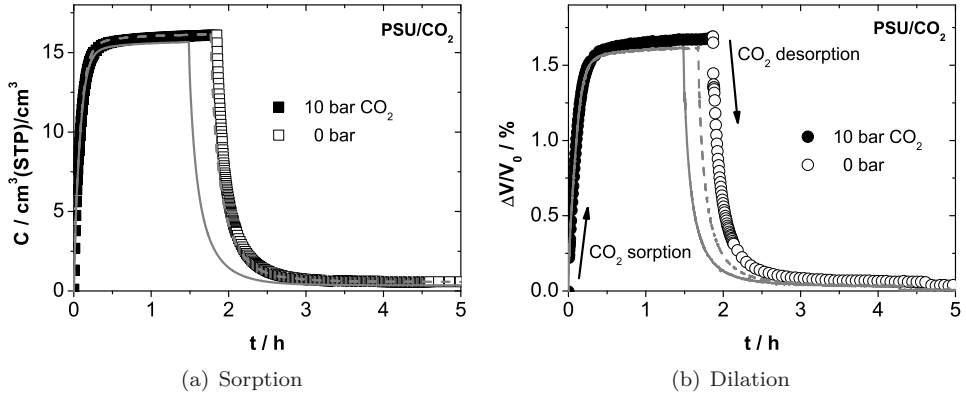


Figure 4.18: (a) Integral sorption of CO₂ at 10 bar gas pressure in PSU (■) and subsequent desorption at 0 bar (□). (b) Corresponding dilation (●) and contraction (○). Lines denote second and third measurement in each diagram.

4.5.2 Integral Sorption and Dilation

In contrast to *differential* sorption and dilation measurements, where a series of relatively small pressure increments at regular time intervals lead to sorption and dilation isotherms as described in the previous section, *integral* sorption and dilation refers to the experimental procedure of a single, larger pressure step.⁴² In this work, a step to 10 bar is reversed after a given time to be repeated following the desired pattern. This procedure bears the advantage of a relatively quick assertion of the concentration and dilation level for one individual pressure, although a point by point scan of a complete isotherm would take considerably more time, due to the necessity of relatively long degassing times in-between steps. Anyway, it should be noted that the latter method of measuring a sorption or dilation isotherm not necessarily leads to the same result as a differentially measured isotherm, because of the difference in sample history and the difference in the rate of stress application. In this work, the integral sorption and dilation procedure was utilized to assess the diffusive concentration level of the penetrant gases at 10 bar and use this information as input for ‘integrally loaded’ packing models in preparation to integral dilation simulation (see Section 5.2.3). The observed experimental dilation is then compared to the volume dilation of thusly prepared packing models in NpT -MD simulations.

Figure 4.18 shows the integral sorption and dilation of polysulfone (PSU) under 10 bar CO₂ pressure. At the start of the measurement, following thorough degassing, the pressure is raised quickly in one single step. The increase in concentration is following Fickian diffusion kinetics, reaching a (quasi-) equilibrium after a few hours. The pressure step is then reversed and desorption is observed. Three consecutive measurements (No. 2 and 3 shown as lines; note the slightly different starting point

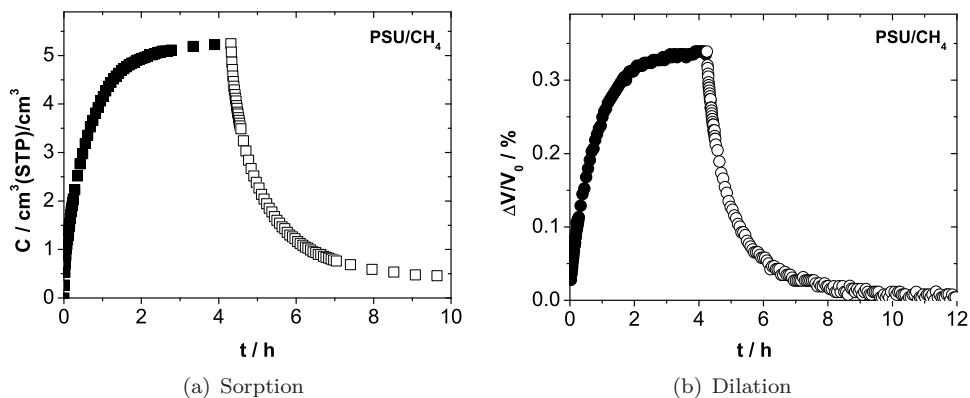


Figure 4.19: (a) Integral sorption of CH₄ at 10 bar gas pressure in PSU (■) and subsequent desorption at 0 bar (□). (b) Corresponding dilation (●) and contraction (○). Lines for the second and third measurement are omitted here and in subsequent diagrams.

of the desorption) show the reproducibility of the measurement. The desorption of the penetrant gas is complete but somewhat slower than the sorption. This is due to the concentration dependency of the diffusion coefficient caused by penetrant induced plasticization, decreasing the rate of desorption in the process. The dilation is following the same kinetics as the sorption and is, upon desorption, completely recovered. Qualitatively, these are the two major results of the experimental measurements of integral sorption and dilation: The congruent kinetics of sorption and dilation suggest that the dilation appears instantly (within experimental resolution) upon sorption of a penetrant. Furthermore, the gas induced dilation is reversible on the same time scale. Both results confirm the interpretation as *elastic* deformation (=instant and reversible, see Section 3.3), induced by penetrant sorption in the rapid stage, and justify the splitting of the isotherms (see previous section) into diffusive/elastic and relaxational parts. The mass uptake and dilation were fitted using equation 4.3, yielding the (quasi-) equilibrium values of CO₂ in PSU concentration $C = 15.6 \text{ cm}^3/\text{cm}^3$ at 10 bar and the induced elastic dilation $\Delta V/V_0 = 1.62 \%$ as well as the diffusion coefficient $D = 2.6 \cdot 10^{-8} \text{ cm}^2\text{s}^{-1}$. The ratio of sorption and dilation may be regarded as a measure of the partial molar volume V_p (eq. 2.14), which will be further discussed in Section 6.3. All values are the averaged result of three subsequent measurements and are compiled in Table 4.2 on page 46, along with the results of the following integral measurements.

Figure 4.19 shows the results of integral sorption and dilation in the PSU/CH₄ system. Only one representative measurement of each, sorption and dilation, is shown in the graph for clarity. The concentration level reached by CH₄ at 10 bar pressure is significantly lower than that for CO₂, and the partial molar volume V_p reveals a smaller dilation effect per CH₄ molecule than for CO₂. The diffusion coefficient D is

lower by an order of magnitude. This relatively slow diffusion of CH₄ in PSU gave rise to the longest sorption and desorption times needed to ensure the determination of the (quasi) equilibrium concentration and dilation, compared to the other investigated polymer gas systems.

Figure 4.20 shows the integral sorption and dilation of CO₂ in PI4. The high level of concentration is reached very fast, due to a large value of the diffusion coefficient. The low partial molar volume V_p indicates a considerably higher amount of free volume in PI4 than in PSU. This is confirmed by the integral sorption and dilation measurement of PI4/CH₄ shown in Figure 4.21. Again, diffusion of CH₄ is slower than CO₂ in PI4 by an order of magnitude, and the concentration level reaches only about a quarter of that of CO₂. The low partial molar volume compared to CH₄ in PSU suggests a higher free volume in PI4, as stated above. It is interesting to note that a small fraction of the CO₂ induced dilation seems to recover following kinetics that differ from the (faster) desorption kinetics. This could be due to anelastic effects that are discussed in more detail in Section 6.3. The dilation effect of methane is obviously too small to induce such mechanisms and appears therefore purely elastic.

Table 4.2: Results of integral sorption and dilation.

polymer/ gas	$C/$ cm^3/cm^3	$\Delta V/V_0/$ %	$V_p/$ cm^3/mol	$D/$ $10^{-8} \text{ cm}^2/\text{s}$
PSU /CO ₂	15.6	1.62	23.29	2.6
PSU /CH ₄	5.6	0.35	14.18	0.44
PI4 /CO ₂	81.4	6.13	16.89	32.2
PI4 /CH ₄	20.8	0.89	9.60	5.6
PIM-1/CO ₂	99.5	7.75	17.45	34.6
PIM-1/CH ₄	40.4	1.94	10.79	46.3

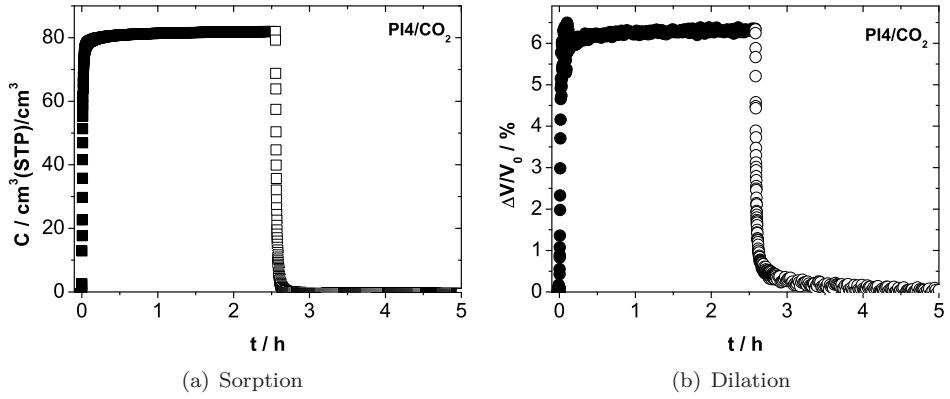


Figure 4.20: (a) Integral sorption of CO₂ in PI4 (■) and subsequent desorption (□). (b) Corresponding dilation (●) and contraction (○).

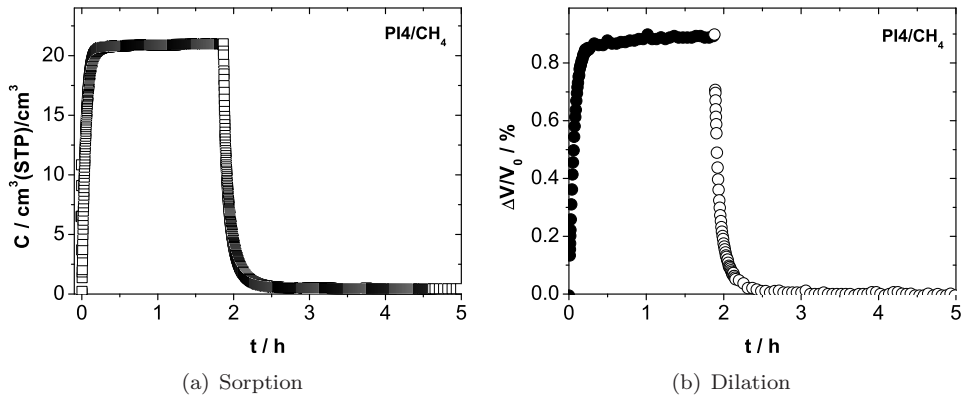


Figure 4.21: (a) Integral sorption of CH₄ in PI4 (■) and subsequent desorption (□). (b) Corresponding dilation (●) and contraction (○).

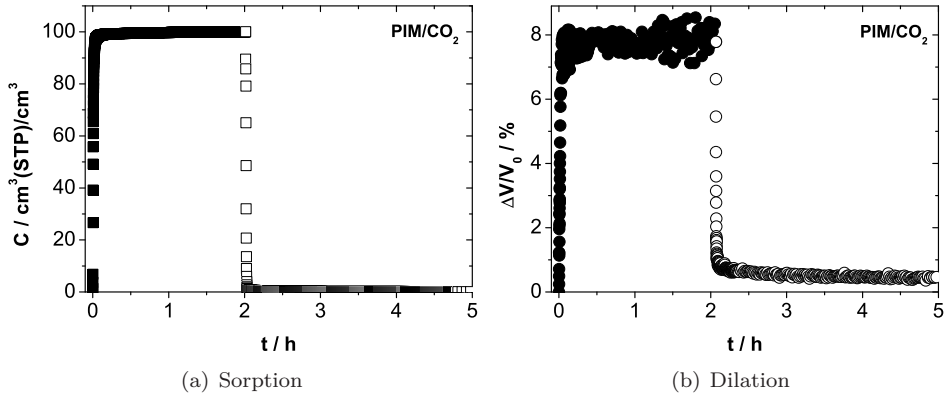


Figure 4.22: (a) Integral sorption of CO₂ in PIM-1 (■) and subsequent desorption (□). (b) Corresponding dilation (●) and contraction (○).

Figure 4.22 shows the results of integral CO₂ sorption and dilation in PIM-1. The concentration level exceeds that of CO₂ in PI4. The dilation[‡] effect is rather large and the larger value of the partial molar volume in comparison with PI4/CO₂ suggests a smaller fractional free volume in PIM-1 than in PI4. This unexpected result will be discussed in the context of the size distribution of the free volume in Section 6.2. Again, the differing kinetics of desorption (faster) and contraction (slower) reveal the existence of some anelastic effects, which in the case of PIM-1 also occur in the CH₄ measurements. However, in all cases (PI4/CO₂, PIM-1/CO₂, PIM-1/CH₄) the dilation is completely recovered within several hours. Diffusion of CH₄ in PIM-1 is quite fast, the determined value of the diffusion coefficient at 10 bar is even slightly higher than that for CO₂.

[‡]The poor quality of the signal of the volume dilation of the PIM-1 sample is due to a resonance vibration of the freely suspended metal disc, which does not lead to significant errors due to its regular sinusoidal form.

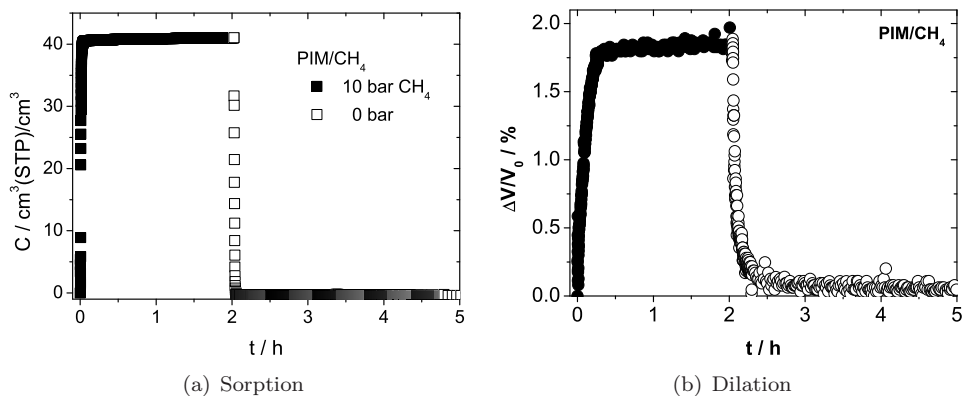


Figure 4.23: (a) Integral sorption of CH₄ in PIM-1 (■) and subsequent desorption (□). (b) Corresponding dilation (●) and contraction (○).

In continuation of experimental results, measured integral sorption and dilation can be summarized as follows:

- E5) In all cases, the dilation follows the kinetics of sorption, implying an instantaneous reaction to sorption of penetrants.
- E6) In all cases, the dilation is completely recovered upon desorption, implying a reversible dilation effect, although in some cases it is not instantaneously reversible.
- E7) The findings E5) and E6) suggest the gas induced dilation to be of elastic nature. Better time resolution or slower processes (as in some cases the contraction) might reveal an anelastic nature of the dilation.
- E8) As may be expected from the calculated free volume (Bondi³⁵, cf. Section 4.1) of the different polymers, the concentration level of CO₂ and CH₄ at 10 bar gas pressure order as follows: PSU < PI4 < PIM-1.
- E9) The same order holds true for the dilation.
- E10) Unexpectedly, the partial molar volume of the gases, which might be expected in reversed order, arrange as PSU > PIM-1 \gtrsim PI4.
- E11) Equally unexpected is the fast diffusion of CH₄ in PIM-1; while for the other polymers the ratio of the diffusion coefficients is $D_{\text{CO}_2} / D_{\text{CH}_4} \gg 1$, for PIM-1 it is $D_{\text{CO}_2} / D_{\text{CH}_4} < 1$.

5 Modeling

Atomistic molecular modeling is a field of growing importance in the investigation of molecular phenomena and development of innovative materials. Its potential lies within the detailed description of the behavior of ensembles under a set of given conditions. The elaborate representation of molecular systems allows a detailed insight into individual, small scale processes which can otherwise only be grasped collectively as a statistical and thermodynamic accumulation of individual effects. Although the physical description cannot be called ‘complete’, relying on approximations and simplifications to reduce complexity, it is nevertheless able to predict basic properties with reasonable certainty and, by analysis and visualization of individual aspects, advertises ideas of interpretation and conception of the investigated phenomena. Once a procedure is validated, the performance of ‘virtual experiments’ may allow the characterization of new materials beforehand, saving a great deal of effort and expenses associated with the synthesis and experimental characterization.

It will become clear in the following paragraphs, that processes with large time constants are impossible to simulate for large systems and with the available CPU-power and -time. It was a goal of this work to establish ways to work around the alleged incompatibility of experimentally observed long term processes and the simulation of large systems. As was presented in Section 4.5.1 as a result of the kinetic analysis (section 4.4), relaxational processes on large time scales take place during sorption. In fact, sorption that is kinetically controlled by Fickian diffusion must be called a long term process with regard to simulation times, too, as the following estimation⁷⁶ shows:

A typical value for a single diffusional step, as e.g. obtained from MD-simulations,⁷⁷ is $a \approx 5 \cdot 10^{-8} \text{ cm}$ (5 Å), a typical small molecule diffusion coefficient for conventional glassy polymers is $D \approx 10^{-8} \text{ cm}^2 \text{ s}^{-1}$ and a common MD-simulation covers a simulation time of $t \approx 10^{-9} \text{ s}$ (1 ns). Random walk of a particle with this diffusion coefficient D in a cubic lattice of grid spacing a leads, via the Einstein equation,⁷⁸ to a number of observable penetrant jumps $n = 6Dt/a^2 \ll 1$.

Obviously, sorption processes on these time scales cannot be directly simulated nor is it possible to simulate relaxational processes on even larger time scales. However,

in the course of this work, the concept of *preswollen* packing models was developed,¹ proposing to construct and analyse two separate states of a polymer/gas system with respect to the volumetric dilation of the matrix and penetrant concentration. In combination with Grand Canonical Monte Carlo simulations (section 5.2.2), sorption isotherms on static packing models of two reference states can be calculated and combined² and thus be compared to experimental data.

The same argument as above impedes the direct simulation of *integral* sorption. However, as was shown in Section 4.5.2, the dilation which is accompanied by the sorption of penetrants, seems to be of elastic nature, i.e., it is (nearly) instantaneous and reversible with regard to the experimental resolution. The method of setting the penetrant concentration according to experimental results within a static packing model and subsequently simulating the volumetric dilation³ is described in Section 5.2.3. A short introduction to the background of the applied molecular modeling techniques will be given first, followed by a simple analysis technique to characterize the free volume of the packing models. For the molecular simulations described in detail in the following paragraphs, the Insight II (4.0.0p), Cerius², as well as the Materials Studio (3.2) software of Accelrys, Inc. (San Diego, CA), were used. To prepare the three-dimensional visualizations, the DS Viewer Pro 6.0 of Accelrys Inc. was used.

5.1 Forcefield based Molecular Modeling

The interaction of particles, bonded or nonbonded, is subject to a quantum mechanical description. In principle, for the physically most accurate description available, the Schrödinger-equation for each particle (electrons and nuclei) must be devised, leading to a complex set of equations. Its solution is, though possible, beyond reasonable effort for the size of the systems and the CPU-power available. However, the properties which are under investigation in this work, i.e., static, thermodynamic and dynamic (transport and relaxational) properties of non-reactive organic polymers, are well described using forcefield based molecular mechanics (MM), molecular dynamics (MD) and classical Monte Carlo (MC) simulations,^{79, 80} methods based on classical mechanics of multi-particle systems. Needless to say, some quantum mechanical information and experimental data are needed to establish the forcefield in the first place. The information is obtained for relatively small units and is, by extrapolation, assumed to be valid for larger systems of equal classes.

5.1.1 The Forcefield

Forcefields allow the calculation of the potential energy U of an ensemble of N atoms, as a function of their coordinates ($r_1 \dots r_N$). It is composed of individual contributions which describe the interactions of bonded atoms (bond-lengths, -angles, conformation

angles) and nonbonded interactions (van der Waals, electrostatic).

$$\begin{aligned}
U(\mathbf{r}_1, \mathbf{r}_2, \dots, \mathbf{r}_N) = & \sum_{bonds} \text{bond-length-deformations} \\
& + \sum_{angles} \text{bond-angle-deformations} \\
& + \sum_{conf. angles} \text{torsional-deformation} \\
& + \sum_{atom-pairs} \text{nonbonded-interactions} \quad (5.1)
\end{aligned}$$

The contributions of bonded interactions are represented by anharmonic oscillators of the form⁸¹

$$\begin{aligned}
U_{ij}(r_{ij}) &= k_1(r_{ij} - r_{ij}^0)^2 + k_2(r_{ij} - r_{ij}^0)^3 + k_3(r_{ij} - r_{ij}^0)^4 & (\text{stretch}) \\
U_{ijk}(\theta_{ijk}) &= k_1(\theta_{ijk} - \theta_{ijk}^0)^2 + k_2(\theta_{ijk} - \theta_{ijk}^0)^3 + k_3(\theta_{ijk} - \theta_{ijk}^0)^4 & (\text{angle}) \\
U_{ijkl}(\Phi_{i-l}) &= k_1[1 - \cos(\Phi_{i-l} - \Phi_1^0)]^2 + k_2[1 - \cos(\Phi_{i-l} - \Phi_2^0)]^3 & (\text{torsion}) \\
&+ k_3[1 - \cos(\Phi_{i-l} - \Phi_3^0)]^4 & (5.2)
\end{aligned}$$

The force constants k_i and the equilibrium positions r_{ij}^0 , θ_{ijk}^0 and Φ_{i-l}^0 are based e.g. on results of quantum mechanics and constitute the integral part of the forcefield. The nonbonded interactions are expressed in the applied forcefield by a van der Waals term with a 9,6-potential and a coulomb-term

$$U_{ij}(r_{ij}, q_i, q_j) = \left(\frac{A_{ij}}{r_{ij}^9} - \frac{B_{ij}}{r_{ij}^6} \right) + \frac{q_i q_j}{\epsilon_0 r_{ij}} \quad (\text{nonbonded}) \quad (5.3)$$

where A_{ij} and B_{ij} are parameters describing the strength of the repulsive and attractive force, q_i and q_j are the partial charges of the interacting atoms and ϵ_0 is the vacuum permittivity. The forcefield is defined by the functional form (eqns. 5.2, 5.3) and a set of parameters k_i, r_{ij}^0, \dots which are specific to types of atoms, i.e., account for different bonded states of the atoms. For a given molecular structure, the forcefield results in a potential energy surface, which can be evaluated with respect to local energy minima. These methods are known as *molecular mechanics* (MM).⁸¹ In the course of optimization, geometrically reasonable (static) structures can be obtained from the initially guessed geometry by varying the atom positions and minimizing the potential energy of the system.

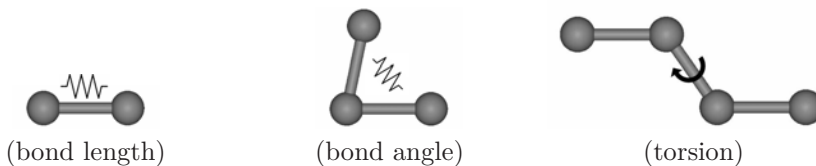


Figure 5.1: Illustration of (bonded) forcefield contributions.

5.1.2 Molecular Dynamics (MD)

To perform *molecular dynamics* (MD) simulations, the forces that result from the forcefield and which act on each atom are applied to the system of finite temperature, i.e., finite kinetic energy E_{kin} . Each of the N particles is assigned a random (Boltzmann) velocity vector $\dot{\mathbf{r}}_i$ so that the total kinetic energy of the system corresponds to the desired temperature T

$$E_{kin} = \sum_{i=1}^N \frac{1}{2} m_i \dot{\mathbf{r}}_i^2 = \frac{(3N - 6)}{2} k_B T \quad (5.4)$$

Here $(3N - 6)$ is the number of degrees of freedom and k_B is the Boltzmann constant. In the course of a simulation, integration of the Newtonian equations of motion

$$\mathbf{F}_i = -\nabla_{\mathbf{r}_i} U_i(\mathbf{r}_1, \dots, \mathbf{r}_N) = m_i \ddot{\mathbf{r}}_i \quad (5.5)$$

leads to a new velocity of each particle which can be extrapolated over the time step $\Delta t = 1 \text{ fs}$ of the simulation to determine the new coordinates \mathbf{r}_i . The force \mathbf{F}_i , acting on a particle i of mass m_i , results from the gradient of the potential energy U_i (see eq. 5.5) determined by the forcefield eq. 5.1. The choice of the time step Δt results from the consideration that the fastest vibration of the system should be sufficiently resolved. In a typical IR-spectrum, the C-H-bond shows a characteristic peak at $\lambda_{\text{C-H}} \approx 3000 \text{ cm}^{-1}$, which corresponds to an oscillation period of $\tau_{\text{C-H}} \approx 10 \text{ fs}$. The MD-simulations that were performed in this thesis using the Discover engine with the commercial COMPASS force field^{82, 83} of Accelrys Inc.

5.1.3 The Concept of Ensembles

In statistical thermodynamics, details of individual particles are usually not of great importance. On the contrary, for a realistic representation of thermodynamic behavior, the expectancy of observable properties are regarded. This may be achieved by taking the mean value with respect to time or as the average of a number of configurations. In molecular dynamics, the evolution of a system with respect to time is observed. Depending on the property under investigation, different *ensembles* are

evaluated, i.e., different state-variables are held constant to observe the behavior of others.

In the *microcanonical ensemble* the number of particles N , the total energy E and the volume of the simulation cell V are held constant. While keeping N and E constant is quite straightforward and needs no further explanation, the volume V of a system may be kept constant by periodic boundary conditions (see 5.1.4), forcing a particle that leaves the virtual simulation cell to enter on the opposite side by assigning the appropriate coordinates.

A *canonical ensemble* is referred to if N , V and the temperature T are kept constant. The easiest way to control the temperature is to directly scale the particle velocities $\dot{\mathbf{r}}_i$, whenever the system temperature T_{sys} leaves a predefined temperature window $T_0 \pm \Delta T$:

$$\dot{\mathbf{r}}_{i,\text{new}} = \dot{\mathbf{r}}_{i,\text{old}} \left(\frac{T_0}{T_{sys}} \right)^{1/2} \quad (5.6)$$

More refined methods like the Berendsen thermostat⁸⁴ are more commonly used because a temperature change per simulation time step leads to a more smooth progression of the temperature. In this work, molecular dynamics are applied to canonical ensembles as part of the equilibration steps in the packing procedure (paragraph 5.1.5) and referred to as *NVT-MD* (according to the state variables N , V and T that are kept constant).

If, at constant N and T , the pressure p is held constant instead of the volume V the ensemble is called *isothermal-isobaric*. The pressure is evaluated using the virial Ξ and kinetic energy $E_{kin} \propto Nk_B T$ based on centers of mass:⁸⁴

$$\Xi(t) = \frac{1}{2} \sum_{i < j} \mathbf{r}_{ij}(t) \mathbf{F}_{ij}(t) \quad (5.7)$$

It is controlled by changing the volume V of the simulation cell according to the relation

$$pV = Nk_B T + \frac{2}{3} \langle \Xi \rangle \quad (5.8)$$

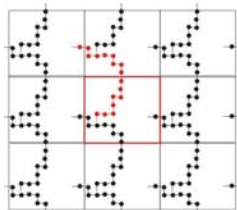
Molecular dynamics simulations of isothermal-isobaric ensembles (*NpT-MD*) are performed as final equilibration procedure of the packing models (see Section 5.1.5) and they constitute the core part of the integral dilation simulation which is described in detail in Section 5.2.3.

An ensemble of constant pressure, volume, temperature and chemical potential μ is called *grand canonical*. Here, the number of particles N is allowed to fluctuate. This is achieved by randomly inserting or deleting molecules. The chemical potential of the molecules within the matrix is balanced with a reference chemical potential, e.g. that of a surrounding gas phase at corresponding pressure and temperature. Using a Monte Carlo algorithm, a new configuration is energetically evaluated and accepted

if more favorable than the previous and otherwise rejected, allowing for thermal fluctuations using a temperature dependent Boltzmann factor (see also Section 5.2.2). Grand Canonical Monte Carlo (GCMC-) simulations are used in this work to calculate sorption equilibria on static packing models for several pressures (chemical potentials) at constant volume and temperature to determine concentration-pressure isotherms which are referred to as GCMC-isotherms (see Section 5.3.3). The GCMC-simulations were realized with the ‘Fixed Pressure’ MC algorithm of the Solid_Sorption module of the Cerius² package of Accelrys. The same procedure was also used to insert a specified number of penetrants for the integral dilation simulations by adjusting the chemical potential accordingly (see Section 5.2.3).

5.1.4 Periodic Boundary Conditions

An ensemble of some thousand atoms is large when regarded with respect to computing effort, but the resulting size of the simulation cell does not allow to calculate ‘bulk’ properties. The partial absence of nearest neighbors and the corresponding forces for atoms at and near the surface of the simulation cell falsifies results with



regard to bulk properties at this surface to volume ratio. The common way to avoid this problem is the application of three-dimensional periodic boundary conditions (3D-PBC). To this end, the cubic simulation cell is surrounded by identical copies of the original cell. Atoms at or near the surface of the original cell now interact with surface atoms of the surrounding replica. In the course of a simulation, if a molecule or atom

leaves the simulation cell through one wall, one of its replications enters the original cell at the opposite side of the wall. It should be noted that the boundary of the periodic box (wall) has no special significance other than defining the shape and orientation of the primitive cells of a periodic lattice. To save computing time and to avoid artifacts resulting from this forced periodicity, e.g. interaction of an atom with its own images or more than one image of other atoms in the replicated cells, the nonbonded interactions need to be cut off at a reasonable distance, which should not exceed one half of the edge-length of the simulation cell. Since the van der Waals interaction (eq. 5.3) decrease with the power of six of the distance, the error due to the cut-off distance can be neglected. For electrostatic interactions, groups of atoms, e.g. a methyl group ($-\text{CH}_3$), are collected into charge-groups which are assumed to be neutral to the outside and the interactions are calculated only within this group. Since in this thesis no electric charges (ions) are part of the simulations, a cut-off distance of 15 Å was used for the packing models whose edge-lengths are in all cases larger than 35 Å.

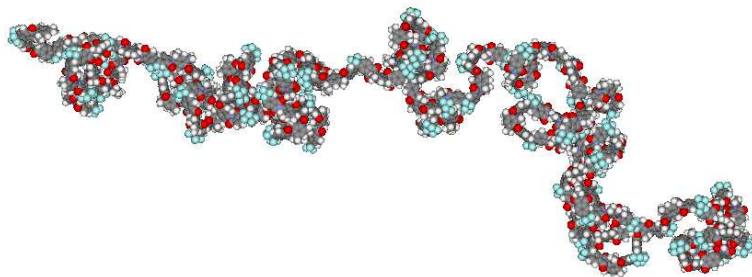


Figure 5.2: Template chain of PI4, containing 80 repeat units.

5.1.5 Packing Procedure

The detailed atomistic packing models that were investigated in this thesis were constructed following the basic packing and equilibration procedure that is based on the Theodorou-Suter method^{85, 86} and described in detail in reference [10]. Basis for the construction of packing models is an equilibrated repeat unit as depicted in Figures 4.1, 4.2 and 4.3. A head and a tail of the repeat unit are defined and a template chain is grown adding repeat units step by step and, as e.g. in the case of a $\text{CH}_2\text{-CH}_2$ - bond, choosing one of the favorable bond angles (cis, trans, gauche) at random, until a specified number of repeat units is connected to the polymer chain (see e.g. Fig.5.2). The ‘open’ bonds at each end of the chain are terminated by a hydrogen atom. The single template chain is subjected to energy minimizing using molecular mechanics (MM).

To obtain a packing model, a cubic simulation cell is defined such that the template chain confined to the volume of the simulation cell would yield a density of about 10 % of the experimental value. 400 small molecules (CO_2 or CH_4) are distributed at random positions within this simulation cell as obstacles. The low density and the obstacles within the cell prevent packing artifacts such as ring-catenations or -spearings in the following packing step. Using a random position within the simulation cell as starting point, the template chain is packed, atom by atom along the backbone of the chain, with 3D-PBC applied, i.e., if the chain ‘grows out’ of the simulation cell at one side, it appears at the opposite side (growing in). If an obstacle is hit during this procedure, a second choice of the available favorable angles is tried. If all of the available angles fail, the angle of the previous repeat unit is changed and the accretion reattempted.

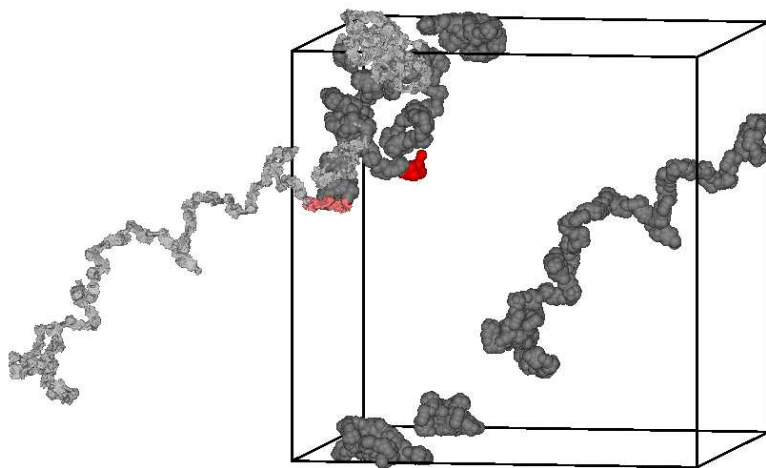


Figure 5.3: PI4 polymer chain in simulation cell of very low density with 3D-PBC applied (obstacles removed). Indicated in light red, the original chain (grey) leaves the simulation cell and the replica (red/dark grey) enters on the opposite side.

As a result, a packing model is obtained containing a number of obstacles and a polymer chain of a very low density which fulfills the periodic boundary conditions explained in Section 5.1.4. Figure 5.3 shows such a low density packing model with all obstacles removed. The light grey chain shows the complete chain. In dark grey, all atoms contained in the original simulation cell are displayed, demonstrating how replica of the light-grey chain enter and leave the simulation cell. At one position in the chain such behavior is marked in light-red (original chain) and red (replica).

To obtain a swollen model at an experimentally determined concentration of penetrants, most of the obstacles are deleted at random, leaving only the specified number which are then replaced by the desired penetrant species. The density is adjusted by scaling of the coordinates of all atoms and resizing the cell dimensions. It is obvious, that this compression is achieved by brute force: Therefore the nonbonded and torsional contributions to the forcefield (see eqns. 5.1) are turned on at a level of 1% and increased one by one to 100 % in several steps, performing minimizations (MM) and dynamics simulations (*NVT*-MD) in between.

The packing models are further equilibrated by stimulated annealing, several *NVT*-MD simulations at decreasing temperatures, typically starting above experimental glass transition. Finally an *NpT*-MD simulation of at least 1.3 ns is performed, allowing the volume to fluctuate. If the volume of the packing model is stable within thermal fluctuations, an adequate level of equilibration is reached and further analyses may be performed. Figure 5.4 shows an equilibrated swollen packing model of PI4 at the correct density. On the left hand side, the polymer chain is represented

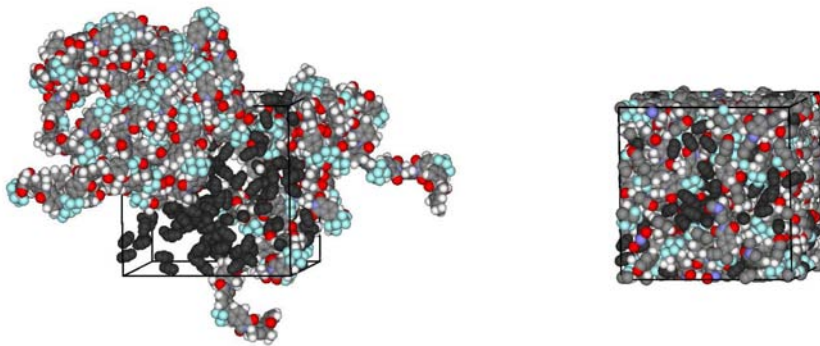


Figure 5.4: Equilibrated swollen packing model of 6FDA-TrMPD containing 156 molecules of CO_2 (*PI156*). Triatomic CO_2 molecules are colored in black. The polymer is represented as one chain (left) and as one cell (3D-PBC applied) (right).

as a continuous chain, while on the right side 3D-PBC are applied to show the space filling of the model. CO_2 molecules are depicted as black triatomic molecules. To obtain nonswollen models of the pure polymer, all penetrants are removed from the swollen model and the compression/ annealing/ equilibration treatment is performed as described above. The amorphous polymer packing models were constructed using the Theodorou-Suter method^{85, 86} as implemented in the `Amorphous_Cell` module.⁸⁷

5.2 Modeling Techniques

5.2.1 Free Volume Analysis

Several definitions of free volume in glassy polymers are employed in the literature,¹ depending on the method of evaluation or the subject under investigation. In this work, the *accessible* free volume based on the insertion of a test particle is used. To estimate the size distributions of *free volume elements* (FVEs), a recently developed computer program⁸⁸ was applied to the packing models. The free volume is derived by the superimposition of a fine grid over the cubic packing model. At every grid point a hard sphere is inserted as test particle. If the test particle overlaps with any atoms of the polymer matrix, which are also represented by hard spheres of van der Waals radii, the grid point is classified as ‘occupied’ (see red circle in Figure 5.5(a)). If there is no overlap (large green circle), the grid point is considered as ‘free’ and contributes to the free volume (green dots). Neighboring free grid points are collected into groups which represent individual holes. The grouping is done in two ways.^{88, 89} In the first approach (named V_{con} , con for connected), affiliation to a group is defined through next neighborhood: every point of a group has at least one next neighbor which is also member of this group.

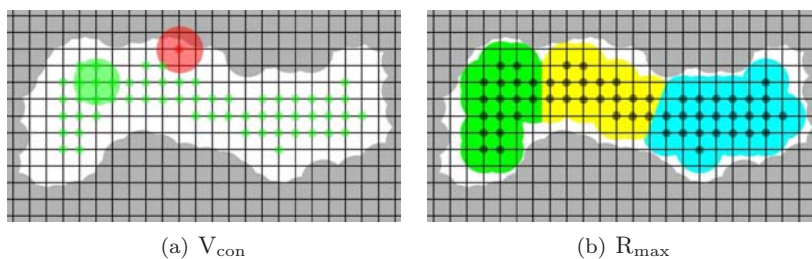


Figure 5.5: 2D-illustration of the *free volume* analysis: (a) The V_{con} -method groups free gridpoints, where the test-sphere (green) does not overlap the matrix (grey), according to next neighborhood (green dots). (b) The R_{max} -method further subdivides these groups by detecting constrictions (‘bottlenecks’, cf. text).

This approach identifies holes, which may be of complex shape and of large volume. In Figure 5.5(a) all gridpoints marked green contribute to one FVE according to the V_{con} method. In a second approach (named R_{max}) for every free grid point the distance to the nearest matrix atom is determined. By calculation of the gradient, the grid points are assigned to the nearest local maximum in this distance. The R_{max} -approach may divide larger free volume regions of elongated or highly complex shape into smaller, more compact regions (as illustrated in Figure 5.5(b)).

Figure 5.6 further illustrates the method for three dimensions: Atoms of the polymer matrix are colored grey. Only free gridpoints are shown, depicted as a small ball. The size of the test-particle is indicated by the transparent surface (green) around the marked free gridpoint (black) in the lower left corner. All free gridpoints that are shown belong to a single free volume element in the sense of the V_{con} method. Different coloring of the free gridpoints indicate connectivity according to the R_{max} method of grouping.

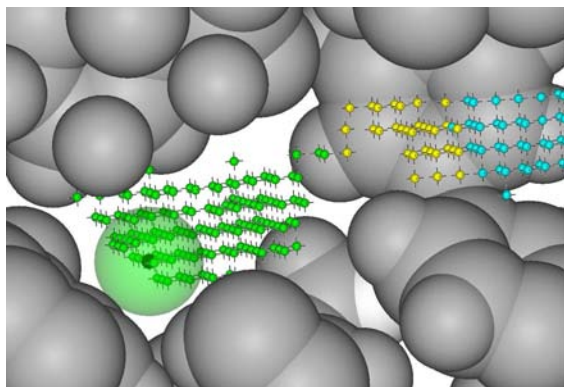


Figure 5.6:

Visualisation of the *free volume* analysis in three dimensions. One V_{con} -FVE is shown: Matrix atoms are grey, only free gridpoints are displayed and colored according to the R_{max} -method. The half-transparent test-sphere (green) is centered on the black grid-point.

Originally introduced to match better the situation in PALS* experiments, where the positronium probe can obviously not completely sample very large holes of complex topology,^{88, 89} the second approach also seems more adequate to depict the environment of a sorbed molecule:^{1, 2} An oblong hole that is constricted at some point would be regarded as a single hole by the V_{con} method (see e.g. Fig. 5.13). However, a penetrant molecule would have to jump an energy-barrier to pass this ‘bottleneck’ and therefore ‘see’ two separate sorption sites. By defining a hole according to the R_{max} method this separation would be recognized (Fig. 5.13). With the help of a small computer program, the gridpoints of a free volume element are assigned the volume of a cube of edge length according to the grid spacing; corrections are made for grid points that are at the surface of the FVE. The volumes of the grid points add up to the total volume of a free volume element. Results of the free volume analysis and a visualization of the Free Volume will be presented in Section 5.3.2.

5.2.2 Grand Canonical Monte Carlo Calculations

The atomistic packing models of the swollen and nonswollen state were used to calculate CO_2 - and CH_4 -sorption isotherms, assuming a static polymer matrix and therefore exclusively using the free volume elements of the matrix as sorption sites. This was carried out by Monte Carlo simulations of a Grand Canonical ensemble (GCMC). This well documented technique permits the calculation of phase equilibria between gas- and sorbate phase. The properties of the sorbed CO_2 (CH_4) molecules in the FVEs of the polymer matrix are calculated by statistic sampling of molecular configurations that are consistent with temperature and chemical potential of the penetrants. Assuming phase equilibrium, the chemical potential is calculated from the gas phase at the specified temperature and pressure using an adequate equation of state (here: Peng Robinson⁹³). For several pressures up to 50 bar, it is tried to add single penetrant molecules at random positions within the polymer matrix (overlaps with matrix atoms are not allowed), and consistent with the chemical potential of the (virtual) gas phase. The new configuration is energetically evaluated, compared to the previous configuration and accepted or rejected according to a temperature dependent fluctuation factor. In the same manner, a penetrant molecule is deleted from the configuration or translated or rotated within the configuration. This way the number of penetrants may fluctuate and after some million iterations the system reaches an equilibrium concentration of penetrants within the static polymer matrix which corresponds to the pressure of the penetrant gas phase. As a result, concentration pressure isotherms are obtained which are presented in Section 5.3.3. The insertion was realized with the ‘Fixed Pressure’ MC Algorithm of the Solid_Sorption module of the Cerius² package of Accelrys.

*Positron Anihilation Lifetime Spectroscopy, for a more detailed discussion in this context see ref. [1], for PALS data on PSU, PI4 and PIM-1 see refs. [90, 91], [64] and [66], respectively, and for a study relating PALS with the site distribution model see ref. [92].

5.2.3 Integral Dilation Simulation

In Section 4.5.2, the experimental results of integral sorption and dilation were presented. As already mentioned at the beginning of this chapter, the diffusion process of penetrants into the polymer matrix is too slow to be directly simulated with our modeling method. Therefore, our approach, also presented in ref. [2], is focused on the dilation only, bypassing the slow diffusion process by establishing the experimentally observed concentration within nonswollen static packing models by *insertion* of penetrants at adequate sites.

To this end, the general scheme to establish the experimentally determined concentration of penetrants within the packing models and to observe the induced dilation, comprises the following steps of insertion/dilation:

1. Insertion of as many of the specified number of penetrants as possible, using the Solid_Sorption tool described above.
2. Short *NVT*-MD run (20 ps) to obtain a ‘realistic’ velocity distribution at $T=308$ K.
3. Longer *NpT*-MD run (300 ps) allowing volume fluctuations (‘dilation’) consisting of two steps: (i) The first 20 ps are calculated with timesteps of 0.1 fs for better resolution and (ii) the following 280 ps with timesteps of 1.0 fs to save CPU time and to reduce the amount of data.
4. Deletion of all penetrants from the packing models.
5. Retry of insertion of the specified number of penetrants (steps 1.-3.).

The insertion was carried out by the ‘Fixed Loading’ MC algorithm of the Solid_Sorption module (cf. Appendix A). Due to differences in the concentration levels of the different gases and the initial free volume characteristics of the polymer matrix, the target gas concentration may be reached after a single insertion cycle (step 1.-3.), or multiple insertion cycles following the general scheme (step 1.-5.), as for example for PI4/CO₂. In this case, the dilation result is the sum of the observed dilation during the 300 ps *NpT*-MD run (step 3.), following each insertion step needed to reach the target concentration. To check the reversibility of the observed dilation, after the 300 ps of *NpT*-MD, (step 3.), the penetrants were deleted from a copy of the packing model and subsequently an *NpT*-MD simulation allowing volume fluctuations was carried out to see the ‘contraction’ behavior of the dilated packing models. All (dilation and contraction) *NpT*-MD-simulations were continued up to a total simulation time of 1.3 ns.

5.3 Modeling Results and Discussion

5.3.1 Detailed Atomistic Molecular Packing Models

In Section 5.1.5, the general packing and equilibration procedures that were applied in this work have been introduced. Using the input parameters that are compiled in Table 5.1 (on page 64), of each polymer and reference state (characterized by density and penetrant concentration) three[‡] packing models were obtained that showed reasonable agreement in characteristics with experimental specifications.

Polysulfone

The packing models of pure polysulfone,¹ named *PSU*,[‡] contain a single chain consisting of 94 repeat units (r.u.) as depicted in Figure 4.1, amounting to 5048 atoms within the cubic simulation cell of average edge length 38.6 Å. This corresponds to an average density $\rho_{\text{pure}} = 1.200 \text{ g/cm}^3$ of the *PSU* packing models, deviating from the experimentally specified value by about -3% . Figure 5.7 shows a representative slice of 5.5 Å thickness cut off one packing model for convenient visualization. All slices of one packing model per polymer and CO_2 -reference state may be viewed in Appendix A.3, Figures A.1-A.6. Since the swelling effect of CH_4 is small, no additional visualisations of CH_4 -swollen packing models are shown in this thesis.

For the CO_2 -swollen packing models of PSU at a pressure of 50 bar, the experimentally reached concentration level of $C_{\text{CO}_2} = 52.6 \text{ cm}^3/\text{cm}^3$ corresponds to the number of 80 CO_2 molecules per packing model (mpp) and were therefore named *PSU80*.² The experimentally obtained volume dilation of $\Delta V/V_0 = 6.5 \%$ corresponds to a density of $\rho_{\text{exp}} = 1.262 \text{ g/cm}^3$ of the binary system. On average, the packing models *PSU80* reached a density of $\rho_{\text{sim}} = 1.233 \text{ g/cm}^3$, i.e., 39.3 Å edge length of the simulation cell, agreeing quite well with the experimental specifications (-1.8%). A slice of 5.6 Å thickness of a *PSU80_m* packing model with CO_2 penetrants removed (index *m*)^b is depicted in Figure 5.8.

Experimental results specify a number of 35 CH_4 molecules per simulation cell of 38.9 Å ($\rho_{\text{exp}} = 1.242 \text{ g/cm}^3$) for the swollen PSU/ CH_4 system ($22.4 \text{ cm}^3/\text{cm}^3$). Packing and equilibration efforts resulted in *PSU35* models of average density $\rho_{\text{sim}} = 1.189 \text{ g/cm}^3$ (-4.2%). It should be noted, that the packing models of pure polysulfone (*PSU*) and CH_4 -swollen polysulfone (*PSU35*) were obtained by deleting CO_2 molecules from the *PSU80* models (and in the case of *PSU35* sufficient random replacement by CH_4 , see Section 5.1.5) and subsequent densification; therefore identical specifications

[‡]With the exception of *PSU80* and *PSU35*, the swollen models of PSU/ CO_2 and PSU/ CH_4 , respectively, where four packing models were used for all analyses.

[‡]Note that the packing models of the polymers are typeset in *italic*, whereas the ‘real’ material is abbreviated in normal font.

^bThe swollen packing models with removed penetrant molecules are marked by the index *m* as in *PSU80_m* to indicate that only the polymer matrix has been analysed.

regarding the number of chains and matrix atoms apply to all polysulfone packing models.

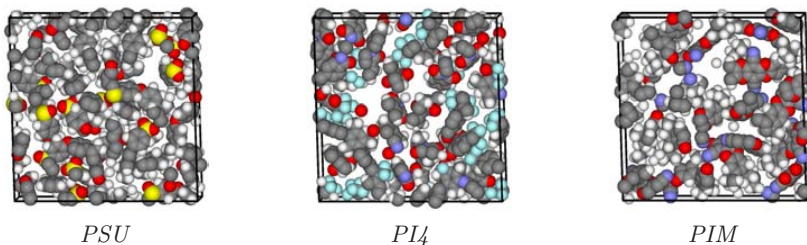


Figure 5.7: Representative slices of nonswollen packing models of *PSU*, *PI₄* and *PIM*. For more slices confer to Figures A.1, A.3 and A.5 in Appendix A.3.

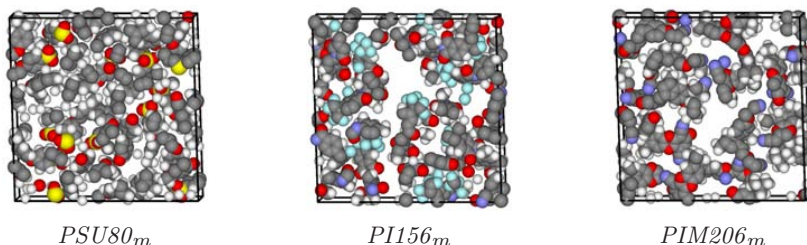


Figure 5.8: Representative slices of nonswollen packing models of *PSU80_m*, *PI156_m* and *PIM206_m*. For more slices confer to Figures A.2, A.4 and A.6 in Appendix A.3.

6FDA-TrMPD Polyimide (*PI₄*)

The packing models of the pure polyimide 6FDA-TrMPD, named *PI₄*, each contain a single chain of 80 repeat units (see Figure 4.2). The simulation cells of 38.8 Å average edge length consist of 4482 atoms, corresponding to an average density of $\rho_{\text{sim}} = 1.273 \text{ g/cm}^3$, showing a relatively high deviation from the target density (-5.8% , see also Section 5.3.2). A slice of the nonswollen packing model *PI₄* of 5.5 Å thickness is depicted in Figure 5.7.

The reference state for the CO_2 -swollen *PI₄* packing models was taken at 35 bar CO_2 pressure (see Section 4.5.1). The concentration of $105.6 \text{ cm}^3/\text{cm}^3$ corresponds to 156 molecules of CO_2 within the simulation cell at a dilation of $\Delta V/V_0 = 21.4 \%$. The obtained packing models were stable under NpT -equilibration at an average density of $\rho_{\text{sim}} = 1.359 \text{ g/cm}^3$ (edge length 39.8 Å), deviating by -5.8% from experimental specifications. Figure 5.8 shows a slice of the CO_2 -depleted packing model *PI156* (5.7 Å).

CH₄-swollen models were constructed meeting the experimentally determined concentration (69.4 cm³/cm³) and dilation (3.5 %) state at 50 bar CH₄ pressure. This corresponds to 76 CH₄ molecules in the *PI76* packing models, which reached an average packing density of $\rho_{sim} = 1.276 \text{ g/cm}^3$ (39.1 Å edge length), deviating by -4.9 % from the target density.

PIM-1

The property of *intrinsic microporosity* of the PIM-1 investigated in this work is a consequence of the rigid and contorted repeat unit (see Figure 4.3).⁶⁵ However, this rigidity also poses difficulties for the packing algorithm (section 5.1.5), slowing the process of finding a valid configuration of a single chain packed inside a simulation cell. It has proven to be more successful to pack a PIM-1 model as a number of smaller chains.⁹⁴ The packing models of the pure PIM-1 (named *PIM*) therefore contain 5 chains of 15 repeat units, i.e., 4145 atoms, within the simulation cell of average density $\rho_{sim} = 1.073 \text{ g/cm}^3$ (37.7 Å edge length), a deviation of -4.5 % to the experimental density. The slice of the *PIM* packing model presented in Figure 5.7 has a thickness of 5.4 Å.

Experimental sorption results at 45 bar CO₂ pressure correspond to 206 CO₂ molecules per packing model (150.1 cm³/cm³) for the swollen reference state of the PIM-1/CO₂ system.⁹⁵ The *PIM206* packing models reached an average density of $\rho_{sim} = 1.229 \text{ g/cm}^3$ (39.3 Å edge length), agreeing well with experimental specifications (-2.8 %). Figure 5.8 shows a 5.6 Å slice of a *PIM206_m* packing model.

The packing models of the swollen PIM-1/CH₄ reference state at 45 bar contain 95 molecules of CH₄ (69.4 cm³/cm³).⁹⁵ The density of the packing models $\rho_{sim} = 1.047 \text{ g/cm}^3$ deviates from the experimentally determined value (volume dilation of 7.5 %) by 4 %.

Table 5.1: Construction parameters of packing models.

polymer/gas	name	r.u. ^a	chains	atoms	p_{ref} bar	ρ_t^b g/cm ³	ρ_o^c g/cm ³	dev. %
PSU (pure)	<i>PSU</i>	94	1	5078	0	1.240	1.200	-3.1
PSU / CO ₂	<i>PSU80</i>			+240	50	1.262	1.233	-1.8
PSU / CH ₄	<i>PSU35</i>			+175	50	1.242	1.189	-4.2
PI4 (pure)	<i>PI4</i>	80	1	4482	0	1.352	1.273	-5.8
PI4 / CO ₂	<i>PI156</i>			+468	35	1.284	1.359	-5.8
PI4 / CH ₄	<i>PI76</i>			+380	50	1.342	1.276	-4.9
PIM-1 (pure)	<i>PIM</i>	15	5	4145	0	1.124	1.073	-4.5
PIM-1 / CO ₂	<i>PIM206</i>			+618	45	1.229	1.194	-2.8
PIM-1 / CH ₄	<i>PIM95</i>			+475	45	1.091	1.047	-4.0

^aNumber of repeat units.

^bTarget density.

^cObtained density.

5.3.2 Free Volume Analysis

In Section 5.2.1 the method of analyzing the *free volume* of a packing model by insertion of a testparticle was introduced. In the following, the results of this insertion method will be presented. All packing models of the pure polymers were analysed using a positronium sized test particle (1.1 Å radius) and a grid spacing of 0.5 Å. Two different approaches of group affiliation, V_{con} and R_{max} , were applied. That way, for each polymer, two size distributions of free volume elements (FVEs) were obtained. It is common in the literature to assign each volume V the radius of a volume-equivalent sphere (r.e.s.) $r = \sqrt[3]{V3/4\pi}$. The size distributions are displayed as the fractional free volume (FFV)

$$\text{FFV}_i = \frac{N_i(4/3\pi r_i^3)}{V_0} \quad (5.9)$$

where N_i is the number of FVEs found by the respective method within an interval $[r_i \pm 0.25 \text{ Å}]$, and V_0 is the analyzed volume of the nonswollen polymer. It should be noted that, strictly speaking it is a distribution of equivalent sphere radii, rather than a distribution of FVE volumes. In the same manner, the CO₂-swollen packing models were analyzed after removing all CO₂ molecules. The volume of the nonswollen polymer V_0 is also used for the FFV of the swollen models to emphasize on the increase in *free volume*. The swelling effect of the polymer/CH₄ systems was too small for the analysis to contrast the nonswollen models and therefore in this thesis, the focus of the *free volume* analysis will be on pure and CO₂-swollen packing models. In the following, for each polymer, swelling state and method of group affiliation the distributions are presented.

PSU and PSU80_m

Figure 5.9(a) shows the analysis results for the nonswollen and swollen polysulfone packing models *PSU* and *PSU80_m*. The distribution of the fractional free volume of the nonswollen packing models *PSU* shows that the free volume is distributed rather evenly among all sizes of FVEs found in the analysis. However, it should be kept in mind that for small sizes a larger number of individual FVEs is needed for the same fraction of the *free volume*. This will become more apparent when displayed as a number distribution of sorption site volumes as it is done in Section 6.2. No exceptionally large free volume elements have been detected in the packing models of pure polysulfone.

For the swollen models *PSU80_m* the shift to larger FVEs is apparent. The difference in area of the distributions may be viewed as a measure of the increase in *free volume* in *PSU* and *PSU80_m*. However, it should be kept in mind, that both distributions are based on the volume V_0 of the nonswollen packing models *PSU*, for better comparison. Besides the general shift to higher radii of equivalent spheres the tendency of smaller FVEs merging to larger elements of free volume can be observed.

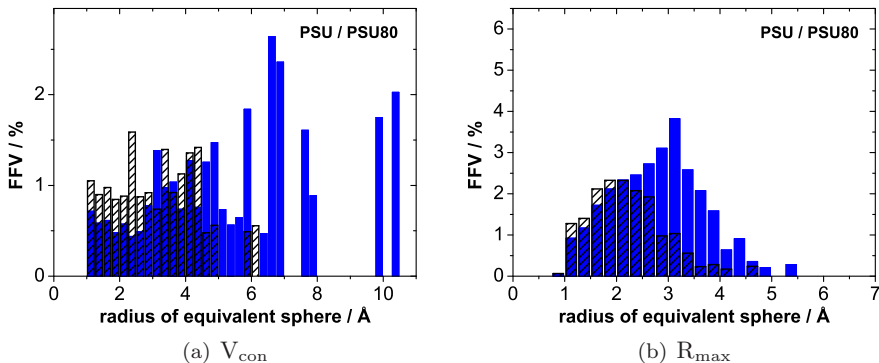


Figure 5.9: Fractional free Volume in nonswollen (hatched) and swollen (blue) models of PSU, as detected by a positronium sized sphere on a 0.5 Å grid. (a) FFV distribution according to the V_{con} -method and (b) after subdivision by the R_{max} -method.

In contrast to the *PSU* packing models, the swollen packing models also contain few rather large FVEs at around 10 Å radius, within the analysed volume. It should be noted that only two of these voids were detected in the three packing models of *PSU80_m*; however, at this size they contribute a rather large fraction to the free volume of the polymer. Figure 5.9(b) shows the result of the free volume analysis using the R_{max} -method. According to this method, group affiliation is not determined by a mere connectivity test, but also constrictions or ‘bottlenecks’ are detected (cf. Section 5.2.1). As a result, large volumes of complex shape, which would appear as one FVE according to the V_{con} -method, are divided into several FVEs of a more spherical shape. Consequently, more FVEs are detected and no particularly large ones are observed. Furthermore, the distribution of the fractional free volume now shows a distinct peak at around 2 Å r.e.s. for the *PSU* models. This peak is shifted to about 3 Å for the swollen *PSU80_m* packing models in addition to a gain in area, again indicating the increase in the amount of free volume.

PI4 and *PI156_m*

Figure 5.10(a) shows the results of the V_{con} -method applied to the nonswollen and swollen packing models of the polyimide *PI4*. For small radii of equivalent spheres, i.e., up to 6 Å, the size distribution of FVEs of the nonswollen *PI4* packing models appears similar to that of the *PSU* packing models: The fractional free volume is distributed evenly in that range and no peak is observed (see inlet of Figure 5.10). However, each individual packing model shows one rather large FVE in the range 11 Å to 14 Å, that contributes (due to its size) the main fraction to the free volume.

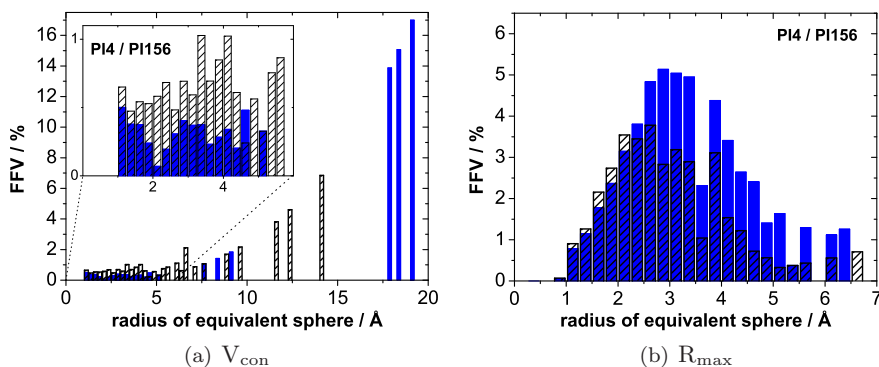


Figure 5.10: Fractional free Volume in nonswollen (hatched) and swollen (blue) models of PI4. (a) FFV distribution according to the V_{con} -method and (b) after subdivision by the R_{max} -method.

Upon swelling ($PI156_m$ packing models), the shift to larger FVEs is even more apparent than in PSU. Compared to the nonswollen $PI4$, only few percent of the FFV is organized in the small r.e.s. range, while the three large FVEs appear to make up for all the swelling of the polymer.

Again, the R_{max} analysis divides the large FVEs into smaller units (Figure 5.10(b)). Both, $PI4$ and $PI156_m$ packing models show a distinct peak structure in the FFV distribution (2.5 Å and 3 Å), and while the shift between $PI4$ and $PI156_m$ is not as pronounced as for the packing models of polysulfone, the broader shoulder to higher r.e.s. is more developed upon swelling, and area and larger radii attest a large free volume. It should be noted that this swelling state of $PI156$ serves as reference state at only 35 bar CO_2 pressure, in contrast to the packing models $PSU80$ and $PIM206$ (50 bar).

PIM* and *PIM206_m

The results of the free volume analysis (V_{con}) on the PIM packing models are shown in Figure 5.11(a). Only a small fraction of the free volume of the PIM packing models is present as more or less evenly distributed FVEs of small radii. On the contrary, most of the free volume (of each of the three individual PIM packing models) is located in one extraordinary large FVE with an equivalent sphere radius above 15 Å. As observed in PI4, the analysis of the $PIM206_m$ packing models shows that the swelling (gain of free volume) takes place in this large FVE and at the cost of smaller FVEs. It should be noted that the shift of the large FVEs to about 20 Å r.e.s. contributes to volume gain in the third power.

If ‘bottlenecks’ and constrictions are considered, as in the R_{max} analysis, the large FVEs of complex shape are divided into smaller units and a distribution of the FFV

is obtained that show peaks at 2.6 Å and 3 Å for the nonswollen and swollen models, respectively. Similar to $PI_4/PI156$, the peak of the swollen packing models $PIM206_m$ shows a broadened shoulder towards higher r.e.s. and an enlarged area, indicating the increase in free volume.

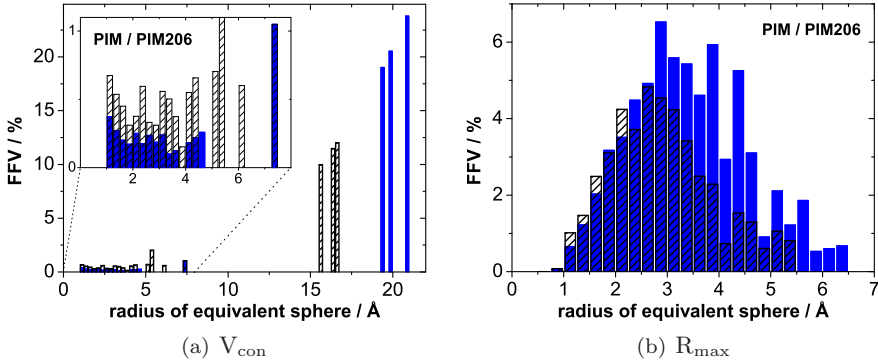


Figure 5.11: Fractional free Volume in nonswollen (hatched) and swollen (blue) models of PIM-1. (a) FFV distribution according to the V_{con} -method and (b) after subdivision by the R_{max} -method.

Free Volume Visualization

In the free volume analysis method of test particle insertion discussed above, a three-dimensional grid is superimposed on the simulation cell containing the packing model. At the coordinates of the overlap-free gridpoints, a sphere of testparticle-size may be inserted to visualize the free volume. However, looking at the packing model $PI156$ displayed in Figure 5.4 makes clear that it does not suffice to display the simulation cell as a whole, because the matrix molecules obstruct the view and the great number of holes interfere with each other if displayed together. To get a better impression, the simulation cell is cut into slices of about 5 Å thickness. For even better viewing, matrix atoms are displayed in ‘stick-style’ and are colored grey. It should be noted that due to the slicing process and to periodic boundary conditions some matrix atoms as well as FVEs appear fragmented or continue on the opposite side.

Figure 5.12 shows representative slices, cut out of one packing model of each polymer and reference state (nonswollen and CO_2 -swollen). In the top row, the FVEs of the PSU and $PSU80$ slices are visualized. Next to a number of small individual FVEs (orange^d), only few larger FVEs contribute to the *free volume* of the PSU -slice, and all FVEs are evenly distributed between the matrix atoms. The slice of the $PSU80$ packing model is shown on the right side.

^dIf necessary, the spheres are colored differently according to connectivity, to distinguish between individual FVEs. However, the colors green, red and purple *always* refer to *one single* FVE according to the V_{con} -method.

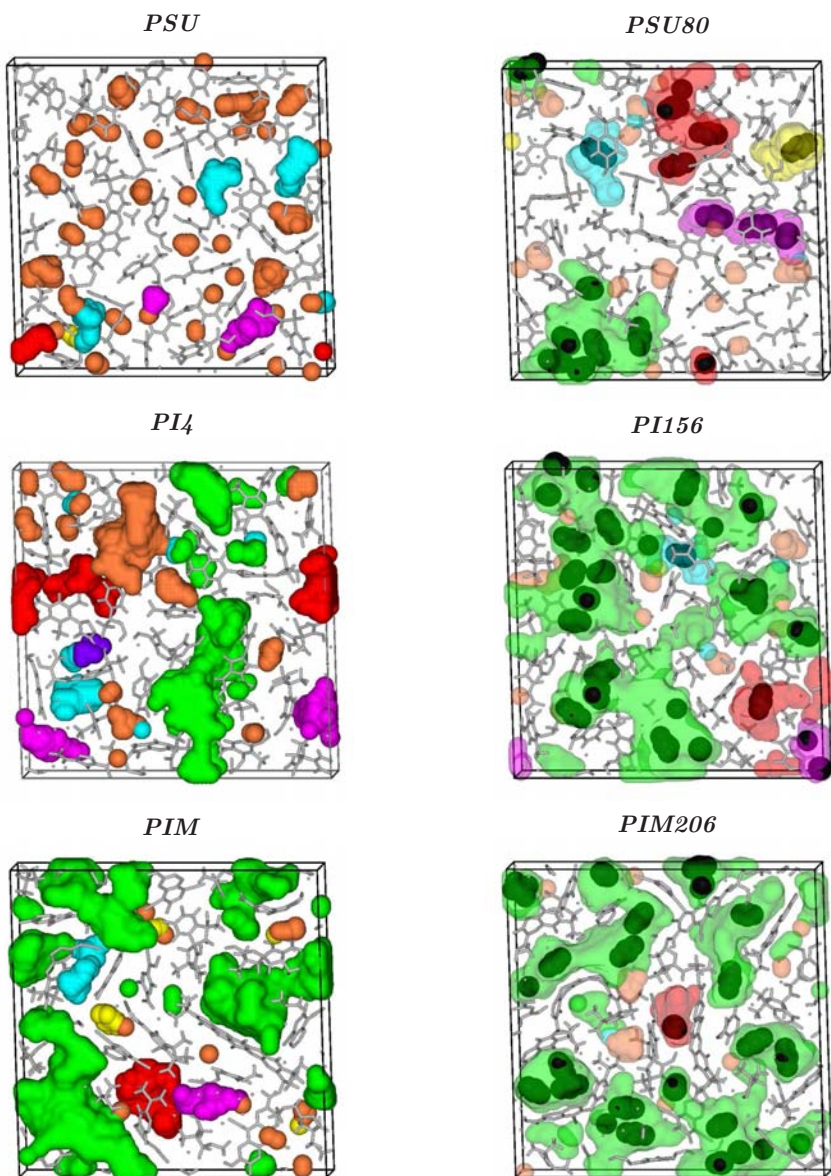


Figure 5.12: Slices of nonswollen (left) and swollen (right) packing models of PSU, PI4 and PIM-1. Green, red or purple color indicates one *single* FVE (associated free grid-points according to V_{con}), whereas other colors are used to mark individual FVEs. Matrix atoms are represented as grey ‘sticks’.

The FVEs are represented by semi-transparent surfaces, to permit the view on the CO₂ penetrant molecules, which are colored black. The shift to FVEs of larger size is easily noticeable. Obviously the larger FVEs contain more than one CO₂ molecule, supporting the employment of the R_{\max} -method when considering *sorption sites*. Figure 5.13 shows the purple FVE of the *PSU80* slice. On the left hand side, the V_{con} -FVE is shown in a wire-mesh representation, containing three CO₂ molecules. On the right side, the R_{\max} -FVEs are shown as solid surface representations. These are more compact and of a more spherical size than the V_{con} -FVEs and generally provide space for only one CO₂ molecule. It has to be noted that in this visualization the R_{\max} -FVEs overlap because the grid size is smaller than the testparticle radius.

The second row of Figure 5.12 shows the slices of *PI4* and *PI156*. For the nonswollen packing model the number of small FVEs is reduced in comparison to *PSU*. Large FVEs dominate the visualization. The largest FVE (colored green) spans the entire height of the simulation cell and continues through neighboring slices.[‡] This becomes even more pronounced in the slice of the swollen packing model *PI156*. As the quantitative analysis has shown (cf. Figure 5.10), most of the free volume of a single packing model is present in one individual FVE. The high complexity of the shape suggests the formation of a dendritic mesh of connected ‘holes’ in the polymer matrix, which could be thought of as a *void-phase*, as opposed to singular, disconnected and smaller FVEs as they are found in *PSU* (and *PSU80*). The majority of the CO₂ penetrants are contained within this *void-phase*, emphasizing its importance for penetrant sorption and transport.

In the bottom row of Figure 5.12, the visualization of FVEs of the *PIM* and *PIM206* slices is shown. Of the three nonswollen polymers, the *PIM* packing models contain the largest single FVEs, exhibiting equivalent sphere radii larger than 15 Å, which is not much less than those of the swollen *PI156* packing models. Accordingly, the *PIM*-slice shows a *void-phase* for the *PIM* packing models even in the nonswollen state. The corresponding FVE (colored green) expands wide over the plane of the slice and its fragmentation points at the three dimensional character of the expansion.[‡] Upon swelling to the *PIM206* reference state, this *void-phase* grows at the cost of smaller FVEs and dominates the appearance of the free volume, while losing none of its complexity in shape. As in *PI156*, the penetrant CO₂ are mainly located in the *void-phase*.

[‡]In this method of visualization, discontinuities within one FVE point to the continuance within a neighboring slice and reentry at another position into the shown slice. Likewise, ‘flat’ surfaces at the edge of the slice point to a FVE reaching across slices.

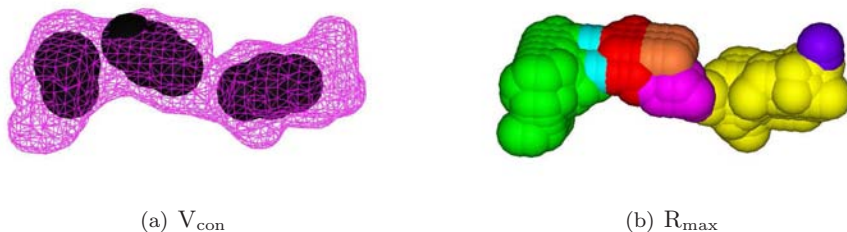


Figure 5.13: (a) Single FVE as analyzed by the V_{con} -method in *PSU80*. (b) Same FVE subdivided by the R_{max} -method.

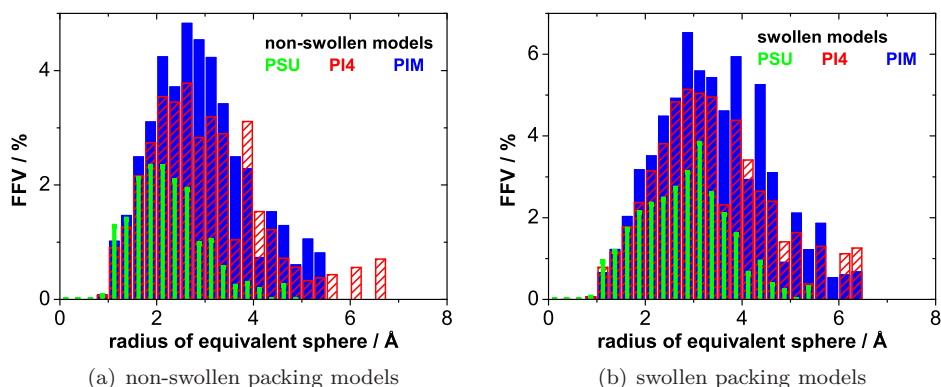


Figure 5.14: Fractional free volume distributions in nonswollen packing models of PSU, PI4 and PIM-1 and in the swollen packing models *PSU80_m*, *PI156_m* and *PIM206_m*, according to the R_{max} -method.

The results of the *free volume* visualization and analysis of the polymer packing models can be summarized as follows:

- M1) The *free volume* was successfully probed using a test particle insertion method. Two different approaches of group affiliation (V_{con} and R_{max}) yield diverse size distributions which allow the perception of *free volume* from different perspectives: While the V_{con} -method yields more information about the connectivity of *free volume*, the R_{max} -method resembles better the surrounding volume of sorbed penetrants.
- M2) The *fractional free volume* (FFV) detected by the V_{con} -method in nonswollen packing models is distributed rather evenly in size up to an equivalent sphere radius (r.e.s.) of about 8 Å. However, the *PI4* packing models each contain

one extraordinary large free volume element (FVE) and in the *PIM* models one FVE of highly complex shape contains the major fraction of the free volume (*void-phase*).

- M3) Upon swelling, all polymers tend to develop larger FVEs at the cost of smaller ones. While the *PSU80_m* packing models show FVEs of only moderate size, the *PI156_m* packing models exhibit a *void-phase* similar to all *PIM*/*PIM206* packing models.
- M4) The R_{\max} -method breaks up larger FVEs by considering ‘bottlenecks’. The size distributions of the FFV of all packing models exhibit a similar peak structure slightly increasing in peak position and width in the order $PSU < PI4 \lesssim PIM$, reflecting the expected amount of *free volume* present in each polymer, respectively (cf. Fig. 5.14(a)).
- M5) The swollen models of each polymer show a shift of the peak position towards larger FVEs. However, the shift between polymers is not as pronounced as for the nonswollen models (cf. Fig. 5.14(b)).
- M6) The R_{\max} -method divides the exceptionally large FVEs found by the V_{con} -method, including the *void-phase*, into smaller units that better represent ‘sorption sites’ for penetrant molecules.

5.3.3 Sorption Isotherms

In Section 5.2.2 the possibility to calculate concentration-pressure isotherms using Grand Canonical Monte Carlo (GCMC) simulations on static packing models was introduced. To this end, penetrants are inserted at adequate positions into the static matrix until an equilibrium is reached that is consistent with the chemical potential of a virtual gas phase at a given pressure and temperature (here: 308 K). Repeated calculation at several pressures leads to the sorption isotherms on static packing models. In the following, the results of the calculations are presented that were conducted for CO_2 and CH_4 on the nonswollen packing models and on the swollen packing models with removed penetrants. For each polymer, gas and swelling state, the GCMC sorption isotherm was calculated for all packing models. The results are presented as an average of the respective packing models with error bars indicating the standard deviation. Dual mode sorption fits were used to interpolate the simulated sorption data and fitparameters are compiled in Table 5.2.

Table 5.2: Dual Mode Sorption model parameters for GCMC-simulated sorption isotherms (see eq. 3.3).

<i>Model</i> /gas	$k_D/$ $\text{cm}^3/\text{cm}^3\text{bar}^{-1}$	$C'_H/$ cm^3/cm^3	$b/$ bar^{-1}
<i>PSU</i> /CO ₂	0.066	14.0	0.384
<i>PSU80_m</i> /CO ₂	0.113	45.2	0.815
<i>PSU</i> /CH ₄	0.076	9.40	0.176
<i>PSU35_m</i> /CH ₄	0.073	22.7	0.247
<i>PI4</i> /CO ₂	0.243	51.6	0.931
<i>PI156_m</i> /CO ₂	0.254	96.4	0.980
<i>PI4</i> /CH ₄	0.187	40.4	0.179
<i>PI76_m</i> /CH ₄	0.229	54.4	0.205
<i>PIM</i> /CO ₂	0.269	72.6	1.165
<i>PIM206_m</i> /CO ₂	0.321	121.9	0.815
<i>PIM</i> /CH ₄	0.195	53.3	0.183
<i>PIM95_m</i> /CH ₄	0.270	74.5	0.183

Simulated CO₂ and CH₄ sorption in Polysulfone

Figure 5.15(a) shows the calculated sorption isotherms for CO₂ on the packing models *PSU* (▼) and *PSU80_m* (▲) along with the experimentally measured sorption isotherm (□, cp. Fig. 4.10 on page 34). Dual mode sorption fits (represented as broken lines) were used to interpolate the data, and a circle indicates the experimental reference data used to construct the swollen packing models. Neither simulated GCMC-isotherm is able to represent the experimentally measured data over the full pressure range. The nonswollen *PSU* sorption isotherm compares well to experimental data at low pressures; however, after the initial increase, the calculated isotherm levels off rapidly at a pressure of about 5 bar, fairly underestimating experimental data at intermediate and high pressures. In contrast, the *PSU80_m* sorption isotherm increases rapidly at low pressures, overestimating the experimental data over the whole pressure range but agreeing well at the highest pressure. The flattening of the curve occurs at about the same pressure as for the *PSU* isotherm. This is an expected result. The GCMC calculations are performed with static packing models. No rearrangements of the polymer matrix may take place to better accommodate the CO₂ penetrants within the matrix; any swelling, elastic or relaxational, as it is observed in sorption induced dilation experiments (Section 4.5.2) or in the integral dilation simulations (Section 5.3.4), is excluded.

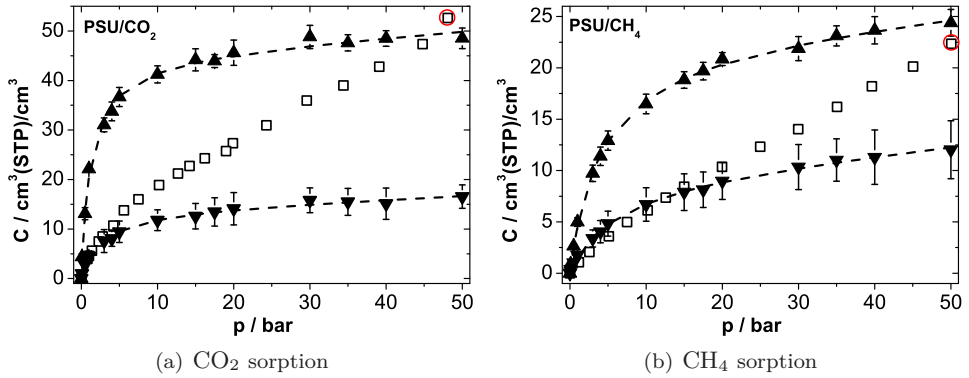


Figure 5.15: CO₂ (a) and CH₄ (b) GCMC isotherms calculated for nonswollen (▼) and swollen (▲) models of PSU. The high-pressure reference data taken from experimental measurement (□) are marked by a red circle.

Solely the ‘movement’, i.e., rotation or relocation of the penetrants by the GCMC insertion algorithm, may lead to a reduction of chemical potential of the ensemble and hence to further ‘sorption’. The simulated sorption may thus be regarded as a ‘hole filling’ process. The nonswollen packing models provide enough energetically favorable sorption sites in the beginning, agreeing with the experimental data rather well until at moderate concentrations most of the sorption sites are occupied and the sorption isotherm levels off. In contrast, the swollen packing models *PSU80_m* are at an artificially low density because they were constructed to provide space for the experimentally determined concentration at 50 bar CO₂ pressure, hence the overestimation. However, the agreement of the simulated sorption isotherms of the nonswollen packing models *PSU* and the fact that after removal of the CO₂ penetrants from the swollen packing models *PSU80*, the experimental concentration at the highest pressure is reached by way of Grand Canonical Monte Carlo simulations on the *PSU80_m*, can be regarded as a good result and a validation of the GCMC method in this context. A way to further improve this result is introduced in Section 6.1.

Figure 5.15(b) shows the GCMC-sorption isotherms for CH₄ on the nonswollen *PSU* packing models and the swollen *PSU35_m* packing models in the same fashion and using the same symbols for swollen, nonswollen and experimental data as Figure 5.15(a) for CO₂. Both isotherms show the same main features as already observed for CO₂ sorption: The isotherm of the nonswollen packing models agrees well with experimental data at low pressures and underestimates at high pressures. The isotherm of the swollen models *PSU35_m* overestimates the experimental sorption isotherm but for the highest pressure, where experimental and simulated concentration agree well.

Simulated CO₂ and CH₄ sorption in 6FDA-TrMPD

Figure 5.16(a) shows the simulated CO₂-sorption isotherms in the nonswollen *PI4* and swollen *PI156_m* packing models. Here, the reference pressure of 35 bar was selected from the experimental data due to technical reasons (cf. Section 4.5.1). All the same, the GCMC calculations were performed up to a pressure of 50 bar. This leads to the peculiarity that the sorption isotherm of the *PI156_m* packing models seems to underestimate extrapolated[‡] experimental data (■) in the high pressures range above the reference point. However, the agreement of experiment and model is excellent at the reference pressure itself, as should be expected. It is questionable if the extrapolation of *Dual Mode* sorption model results is feasible, however, the method was used here to illustrate the reasonably expected underestimation by the GCMC sorption isotherm of the static *PI156_m* packing models above the reference point.

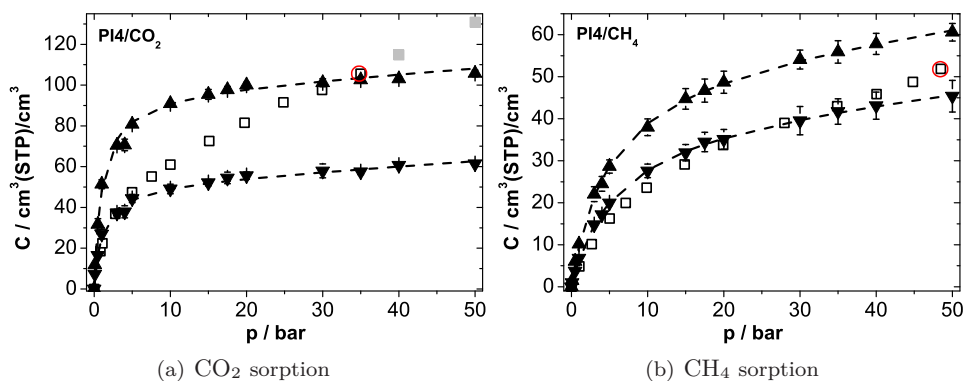


Figure 5.16: CO₂ (a) and CH₄ (b) GCMC isotherms calculated for nonswollen (▼) and swollen (▲) models of PI4.

The CH₄-sorption isotherms for the nonswollen and swollen packing models *PI4* and *PI35_m* are presented in Figure 5.16(b). Compared to the previous isotherms, the isotherm of the nonswollen packing model *PI4* follows the experimental data over a wide pressure range up to about 40 bar. The agreement between the experimental reference point at about 50 bar is satisfying, considering the noticeably smaller difference between isotherms for swollen and nonswollen packing models (by comparison with the previous isotherms).

[‡]By calculation of the concentration at 40 and 50 bar, using the DM parameters listed in Table 4.1 on page 36.

Simulated CO₂ and CH₄ sorption in PIM-1

In Figure 5.17(a) the CO₂ GCMC-sorption isotherms for the packing models of the polymer of intrinsic microporosity (PIM-1) are shown. The isotherm of the nonswollen *PIM* represents the low pressure range well, as expected. The *PIM206* packing models, on the other hand, do not seem to be able to take up as many penetrant molecules at 50 bar as the models were constructed for, understating the experimental data at the reference point. It should be noted that at 35 bar, where experimental and GCMC isotherms cross, the agreement is merely coincidental and should not be compared with that of the CO₂-PI4 isotherm in Figure 5.16, where a reference state at 35 bar was chosen.

The CH₄-PIM-1 isotherms are presented in Figure 5.17(b). Again, the isotherms of the nonswollen packing models *PIM* represent the experimental data in the low pressure range up to 5 bar quite well and underestimate at higher pressures.

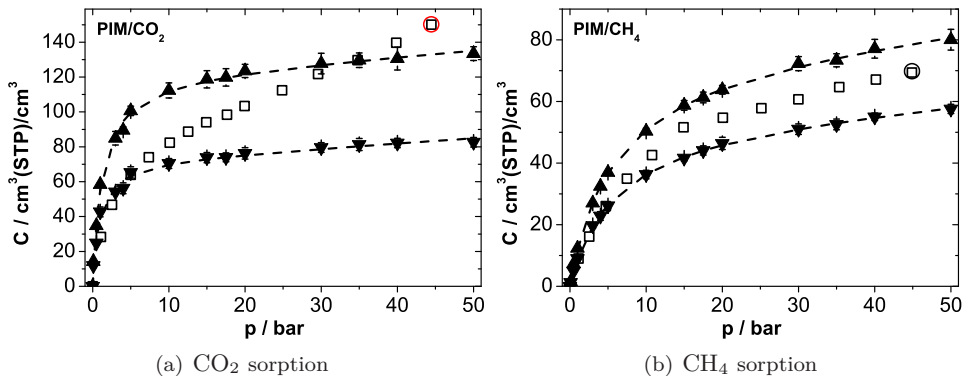


Figure 5.17: CO₂ (a) and CH₄ (b) GCMC isotherms calculated for nonswollen (▼) and swollen (▲) models of PIM-1.

As was the case for *PI4*-CH₄ (Figure 5.16(b)), the swollen packing models *PIM95_m* take up slightly more penetrants than the model was built for. However, the deviation is within acceptable limits, considering the concentration difference between swollen and nonswollen packing models at the reference pressure. It is obvious from Figures 5.15 to 5.17), that the CH₄ isotherms in all three polymers do not level off as rapidly as do the CO₂-sorption isotherms. This could be due to the fact, that none of the CH₄ isotherms reach a concentration level at which the respective CO₂-isotherm levels off, implying that the polymer matrix still provides enough space in the *free volume* for further sorption of penetrants without the need for rearrangement or relaxation of the polymer chain (dilation).

Continuing the summary on page 71, the modeling results of the concentration-pressure isotherms calculated by GCMC simulations at 35 °C on nonswollen and swollen packing models for CO₂ and CH₄ can be resumed as follows:

- M7) The GCMC sorption isotherms that were calculated for nonswollen and swollen packing models of three polymers and two gases are in good agreement to the experimental data within the pressure range of the respective reference state, validating the method of calculating isotherms using GCMC simulations.
- M8) Outside the respective pressure ranges, the observed underestimation of experimental data for the nonswollen packing models can be explained by the impossibility of the polymer matrix to relax stresses which may be induced by the insertion of penetrants.
- M9) The sorption isotherms of swollen packing models overestimate the experimental data in low and intermediate pressure ranges. This may be understood using the simple picture of a hole filling process in low density packing models that provide enough free volume to accommodate large concentrations of penetrants.
- M10) In general, the calculated CH₄-isotherms seem to level off less rapidly with increasing pressure than do the CO₂-isotherms, suggesting that not all possible ‘sorption sites’ are occupied at the highest simulated pressure.

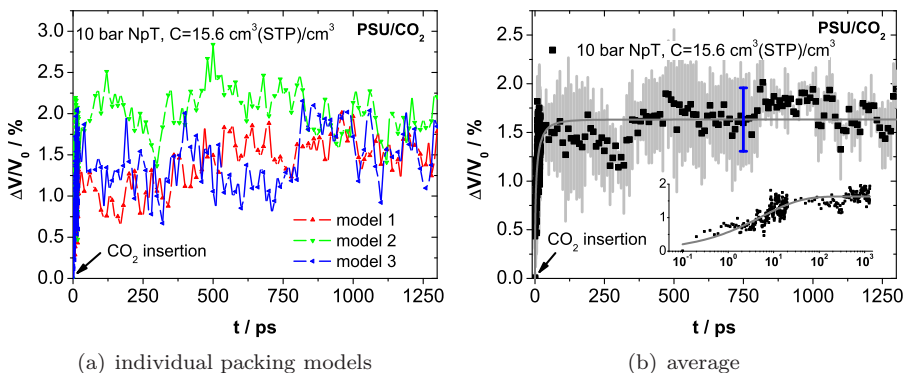


Figure 5.18: Simulated CO₂ induced dilation of *PSU*. (a) Dilation is shown for all 3 packing models. (b) The average is shown (■) with resulting standard deviation (grey bars), the mean standard deviation (blue) and an arbitrary fit (—) to emphasize the kinetics (inlet on logarithmic time scale).

5.3.4 Integral Dilation Simulation

In Section 4.5.2 the results of the experimental integral-sorption measurements were presented. The experimental values for the (quasi-) equilibrium concentration at 10 bar gas pressure that are listed in Table 4.2 (p. 46), were converted to the number of the respective penetrant molecules per packing model to construct the loaded packing models and perform the simulations of integral dilation as described in Section 5.2.3. After sufficient repetition of the insertion steps (see p. 61) and a short NVT -MD run (=at fixed volume), the packing models were equilibrated in an NpT -MD run at 10 bar and 35 °C, allowing the volume of the initially nonswollen packing models *PSU*, *PI4* and *PIM* to adjust to the respective penetrant load.

The result of the volume dilation for the three individual packing models of *PSU*/CO₂ is shown in Figure 5.18(a). Even though there are considerable fluctuations in the volume of a simulation cell and some discrepancies between individual packing models, a distinct volume dilation can be clearly recognized. For better clarity, the average of the three packing models is taken and depicted in Figure 5.18(b). The grey shadow at each timestep denotes the standard deviation. The mean of the standard deviation with respect to time, taking all data points into account, is displayed as a blue error bar, which is set arbitrarily to 750 ps and which is positioned on the grey line. This grey line is the result of a fit to an arbitrarily chosen exponential function. The inset of Figure 5.18(b) shows the averaged data and the fit curve on a logarithmic time scale to emphasize the fact that the dilation is following some kinetics rather than appearing instantly. However, the absolute parameter values of the fit and the exact nature of the fit function will not be discussed beyond this general statement.

In the following, the resulting volume dilation of each polymer/gas-system is presented

as the average of the three respective packing models versus simulation time, along with the contraction after removal of the penetrants. The error bar indicates the mean standard deviation of the averaging procedure as detailed above, to provide a measure of the deviation while preserving the lucidity of the Figures.

Simulated dilation of *PSU*

Figure 5.19(a) shows the dilation (■) and contraction (□) of the *PSU* packing models after insertion/removal of CO_2 penetrants. The simulation cell expands rapidly upon insertion (i.e., upon starting the *NpT*-MD simulation), levels off after a few picoseconds and settles, within thermal fluctuations, at a volume dilation of $\Delta V \approx 1.6\%$ (data listed in Table 5.3 on page 80). To check the reversibility of the observed dilation effect, the penetrants were removed from a copy of the dilated mixed ensemble at 300 ps. For this depleted packing model, the *NpT*-MD simulation was continued at 1 bar.

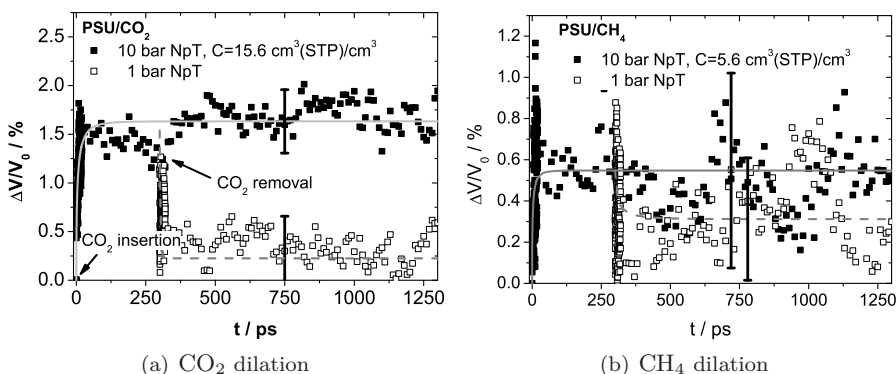


Figure 5.19: Simulated gas induced dilation (■) and contraction (□) after insertion/removal of penetrants into the *PSU* packing models (average) and subsequent *NpT*-MD simulation. The mean standard deviation is indicated by a black error bar centered on the fit-curve.

The depleted model shows nearly immediate contraction down to a level off about 25 % of the dilation effect. Over the remaining simulation time a slight tendency of further contraction can be ascertained, resulting in a recovery of the dilation effect of 88 %. It should be noted that the individual packing models behave different, two recovering to the original volume while one of the models only marginally contracts. The three packing models are expected to show slightly different behavior within the range of usual thermal fluctuations. However, deviations in the fraction of the free volume as well as the local free volume distribution will lead to further discrepancies between the packing models that are loaded with the same number of penetrant molecules.

Figure 5.19(b) shows the average dilation and contraction of the CH_4 loaded and depleted *PSU* packing models. Because the concentration level of CH_4 is quite low at a pressure of 10 bar, the dilation effect is also rather small. The contraction of the packing models upon removal of the penetrants is even less pronounced. Again the packing models behave differently, one recovering to an even smaller volume than the original while two do not show a clear contraction trend. It is worth to note that the dilation effect of *PSU*/ CH_4 reaches only the magnitude to which the *PSU*/ CO_2 packing models contract rapidly and then show very slow trends of contraction. In view of this, the observed indistinct response of the matrix to the removal of the CH_4 molecules might be expected.

Table 5.3: Data for simulated integral dilation.

polymer/ gas	C / mpp	$\Delta V/V_0$ / %	recovery %	V_p / cm^3/mol
<i>PSU</i> / CO_2	25	1.63	88	23.5
<i>PSU</i> / CH_4	9	0.55	43	21.9
<i>PI4</i> / CO_2	120	3.80	104	10.5
<i>PI4</i> / CH_4	31	0.57	96	6.0
<i>PIM</i> / CO_2	130	2.94	79	6.6
<i>PIM</i> / CH_4	55	0.57	32	3.0

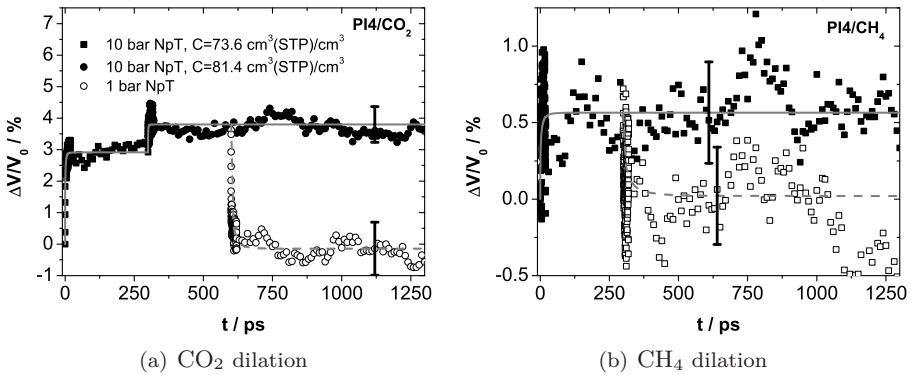


Figure 5.20: Simulated gas induced dilation (■) and contraction (○) of *PI4*. Note that a second insertion step (●) is needed to reach the specified concentration of CO_2 (a).

Simulated dilation of *PI4*

In the *PSU*/ CO_2 and *PSU*/ CH_4 systems presented above, the insertion algorithm of the Solid_Sorption module was able to find non-overlapping sorption sites within the polymer matrix for all penetrant molecules needed to match the experimental concentration, i.e., only one insertion-cycle (step 1. to 3.) was needed. In the case of *PI4*/ CO_2 , step 1. yielded a concentration of $C = 73.6 \text{ cm}^3/\text{cm}^3$, that is, 109 CO_2 molecules per packing model (mpp), and a second insertion cycle (step 4. and 5.) was needed to reach the experimentally determined concentration of $C = 81.4 \text{ cm}^3/\text{cm}^3$ (120 mpp). The result of the volume dilation of both steps is shown in Figure 5.20(a). After a first rapid step of volume dilation, a smaller second rapid dilation step is observed following the second insertion step. To check the stability of the first step, the initial MD-simulation was continued to 1.3 ns containing the initial amount of penetrants (not shown). Both the first and the second CO_2 -induced dilation are completely reversible on a short time scale, as the contraction behavior of the depleted packing models after removal of the penetrants shows (not shown for the first dilation step in Fig. 5.20(a)).

In the case of *PI4*/ CH_4 again only one insertion cycle was needed to load the packing models with the experimentally specified number of molecules of 31 mpp. The dilation result of the subsequent *NpT*-MD simulation is shown in Figure 5.20(b). Similarly to the *PSU*/ CH_4 system, the dilation effect of methane in *PI4* is not very pronounced. However, after removal of the CH_4 molecules, the volume dilation completely recovers to the original volume within very short time, in contrast to the results for polysulfone but in accordance to the CO_2 induced dilation in *PI4*. Within the range of the usual volume fluctuations, all three packing models show this behavior.

Simulated dilation of *PIM*

Figure 5.21(a) shows the dilation and contraction of the *PIM* packing model after insertion and removal of the CO_2 molecules, respectively. Despite the rather large number of 130 mpp, only one insertion step was necessary to prepare the mixed ensembles according to the experimentally determined specification ($95 \text{ cm}^3/\text{cm}^3$). The *PIM* packing models dilate at a relatively slow rate, when compared to *PSU* or *PI4*, and although the CO_2 content of *PIM* is the largest, the volume dilation does not exceed the dilation of the first insertion step of *PI4*. This might be expected considering that only one insertion step was needed, which suggests the presence of a sufficient number of possible sorption sites within the *free volume*. The contraction upon removal of the CO_2 molecules is incomplete (79 % recovered). However, as the large error bar indicates, the individual models behave different. As in the *PSU*/ CO_2 contraction, two of the packing models virtually recover to their original volume, while one packing model does not show a distinct contraction.

CH_4 induced dilation of the *PIM* packing models is shown in Figure 5.21(b). In contrast to *PIM*/ CO_2 , the dilation occurs as fast as for all previously shown packing

models. Interestingly, the volume dilation that is induced by CH_4 is nearly the same for all three polymers ($\sim 0.5\%$).

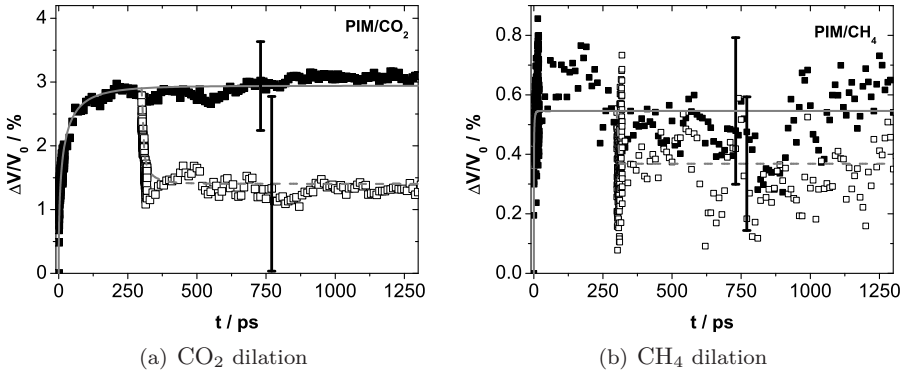


Figure 5.21: Simulated gas induced dilation (■) and contraction (□) of *PIM*.

Upon removal of the 55 CH_4 molecules only minor contraction is observed. By way of fitting the data, it can still be determined that 32 % of the dilation is recovered, although a large error needs to be considered.

Table 5.3 on page 80 lists the partial molar volumes (PMV) V_p that were calculated from the ratio of induced dilation and CO_2 and CH_4 concentration in the polymer packing models, respectively, using equation 2.14. For both penetrants an increasing PMV is observed with decreasing amount of fractional free volume. The partial molar volumes will be discussed in more detail in Section 6.3.

The results of the simulated integral dilation of nonswollen packing models by insertion of penetrants and subsequent NpT equilibration can be summarized as follows:

- M11) It was shown that a distinct volume dilation induced by penetrants may be simulated using the presented approach.
- M12) In all cases the dilation appeared very rapidly but clearly following some kinetics on a time scale of a few picoseconds. Only *PIM*/ CO_2 showed a timescale of a few hundred picoseconds.
- M13) The dilation was shown to be mainly recoverable on the same timescale. However, only the *PI4* packing models contracted to the original volume and especially the CH_4 loaded models exhibit large relative errors.
- M14) While results M11) and M12) fit into the concept of elastic wave propagation as suggested in the beginning of this chapter, result M13) implies relaxational processes which are also part of the dilation.

M15) The partial molar volumes of CO₂ and CH₄ order as $PSU > PI4 > PIM$, as would be expected from the calculated fractional free volume (cf. Section 4.1).

In the following chapter, the results of the experimental chapter and those of this chapter are subject to a combined analysis and comparison, including a further discussion of the phenomenological models and further insights to aspects of the *free volume*.

6 Combined Discussion

In Sections 4.5 and 5.3 the results of the experimentation and simulation efforts were presented, respectively. In some cases, where input of the other was needed, the connection between ‘real’ and ‘virtual’ experiment has already been established and some of the results from phenomenological analysis have been shown along with the experimental results to allow a direct comparison with the data. However, primarily the immediate results have been shown and were discussed independent of each other. To comply with the objective of this work, that is, to combine experiment, phenomenological model and detailed atomistic molecular modeling, in this chapter the results will be interpreted and discussed in direct comparison. For convenience, some of the results that have been presented in the preceding chapters are shown again, introducing varying ways of presentation.

6.1 Sorption Isotherms

In Section 5.3.3 the results of the Grand Canonical Monte Carlo (GCMC) simulations for two gases and nonswollen and swollen packing models of three polymers were presented in the form of sorption isotherms. For all systems investigated, the simulated data compared well with the experimentally obtained data, provided that only the pressure range of the reference state is regarded. However, the simulated data of the intermediate pressure range is not in agreement with experimental data. As stated in Section 5.3.3, this result is anticipated because of the resemblance of the GCMC calculations on static packing models with a ‘hole-filling’ process. To be able to describe the experimental data in the intermediate pressure range, the continuous swelling of the polymer matrix must be taken into account. The concept of preswollen packing models was especially designed to avoid time and resource consuming simulation methods. To approximate the sorption behavior at intermediate pressures, it is therefore proposed to implement a transition between the sorption isotherm of the nonswollen and the swollen packing model. The most obvious difference between both reference states is the density of the polymer matrix (depleted of penetrants). In the phenomenological model ‘Non-Equilibrium Thermodynamics of Glassy Polymers’

(NET-GP¹⁹, see Section 3.2), the density change of the matrix is assumed to be linear with pressure (equation 3.24 on page 19). Adopting this supposition and further assuming a linear relationship between density and concentration as well, a simple transition between the isotherms of the nonswollen and swollen packing models can be achieved mathematically:

$$C(p) = \left(1 - \frac{p}{p_{sw}}\right) \cdot C_{no}(p) + \frac{p}{p_{sw}} \cdot C_{sw}(p) \quad (6.1)$$

Here, $C_{no}(p)$ indicates the calculated sorption isotherms of the nonswollen (index *no*) packing model, and $C_{sw}(p)$ indicates the isotherm of the swollen model (index *sw*), as they are represented by the respective Dual Mode sorption fits (cf. Table 5.2). Using the pressure of the swollen reference state p_{sw} as basis, equation 6.1 introduces the concentration $C(p)$ as a linear weighted average of nonswollen and swollen isotherm, giving the former full weight at zero pressure while at p_{sw} only the latter contributes.

Figure 6.1(a) shows the result of the transition (solid line) from the nonswollen to the swollen GCMC isotherm that were calculated for CO₂ in polysulfone (broken lines). The experimental data (\square) is represented excellently over the whole pressure range.

Figure 6.1(b) confirms the usefulness of the method for methane in PSU. While the transition overestimates the experimental data a little, the shape of the isotherm could be improved. Also note the difference in scales of Figures 6.1 (a) and (b), enhancing the deviation in the latter Figure.

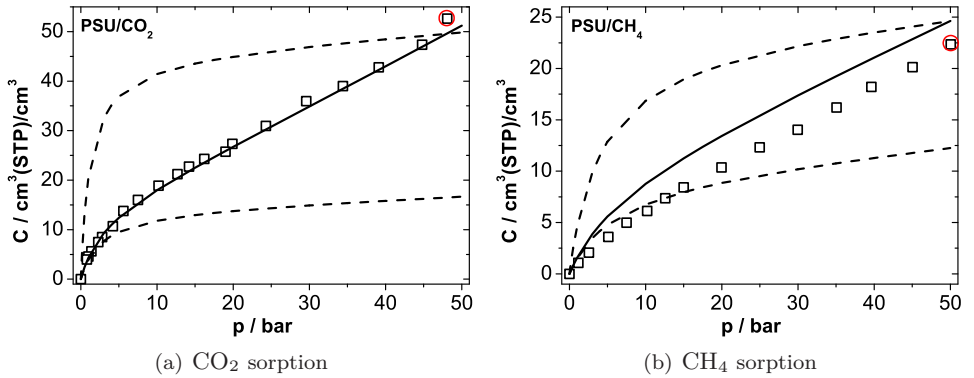


Figure 6.1: Model representation of experimental sorption data (\square) of CO₂ (a) and CH₄ (b) in PSU by linear transition (—) of GCMC isotherms for swollen and nonswollen packing models (- - -). A red circle indicates the reference data for the swollen model.

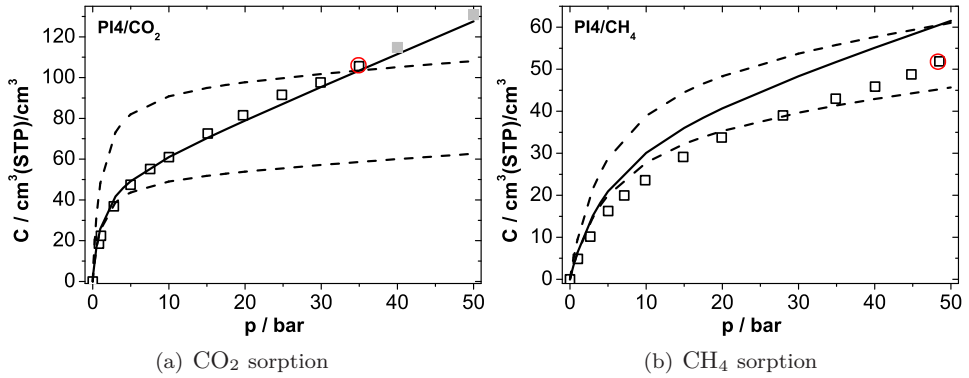


Figure 6.2: Model representation of experimental sorption data (\square) of CO₂ (a) and CH₄ (b) in PI4 by linear superposition (—) of GCMC isotherms for swollen and nonswollen packing models (- -). The linear transition covers also the extrapolation of experimental data (\blacksquare) beyond the reference state (red mark) of CO₂/PI4 (cf. text).

Figure 6.2 shows the transition of CO₂ and CH₄ sorption isotherms calculated for PI4. Again, the experimental data, especially for the CO₂ isotherm, are represented very well. Sorption isotherms in glassy polymers are known to show an upward curvature at high pressures in some cases,⁹⁶ which is why the agreement to the extrapolated experimental data (cp. Fig. 5.16) beyond the reference state should not be overrated. However, it also shows that the method is capable to afford reasonable first approximation predictions. The CH₄ transition isotherm exceeds experimental data, but the shape could be improved as before.

Figure 6.3 shows the transition isotherms for CO₂ and CH₄ in PIM-1. As already stated in Section 5.3.3, the GCMC isotherm of the swollen packing models *PIM206_m* does not reach the concentration of the experimental reference state. Consequently, the transition isotherm underestimates the experimental data. However, the agreement is still very satisfactory, as is the agreement of the transition of the methane isotherms from *PIM* to *PIM95_m*.

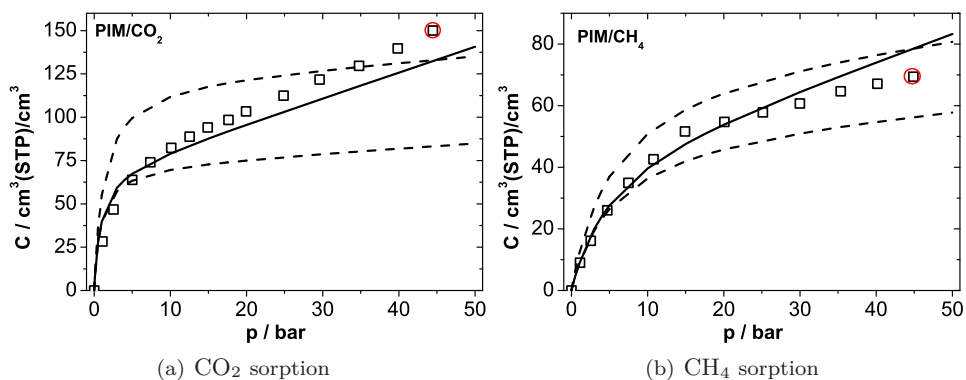


Figure 6.3: Model representation of experimental sorption data (\square) of CO₂ (a) and CH₄ (b) in PIM-1 by linear superposition (—) of GCMC isotherms for swollen and nonswollen packing models (---).

Comparison with NET-GP

The GCMC isotherm transitions that were presented in the previous paragraph have been achieved by building a packing model for a nonswollen and a swollen reference state, respectively, relying on experimental density data. In principle, packing models could be built for several pressure steps and the linear transition performed between each step, refining the method. This corresponds exactly to the procedure of the NET-GP phenomenology presented shortly in Section 3.2. Based on experimental density data, a linear swelling factor k_s describes the density change of the polymer matrix (eq. 3.24 on page 19). For each pressure step, i.e., chemical potential of the gas phase, the equilibrium chemical potential of penetrant gas can be calculated from pure component parameters, statistical considerations of possible configurations of the components on the lattice and parameters of the latter, including the density as an order parameter.

Figure 6.4(a) shows the prediction of CO₂ and CH₄ sorption in PSU as calculated by the NET-GP model using a swelling factor of $k_{st} = 1.461 \text{ \%}/\text{MPa}^{-1}$ calculated from the total dilation (cf. Figure 4.14(b) and Table 3.1) and the pure component data of reference [54] and Table 3.1. For CO₂ (solid line) the experimental data at larger pressures is overestimated, while NET-GP yields an excellent prediction for CH₄ sorption (broken line).

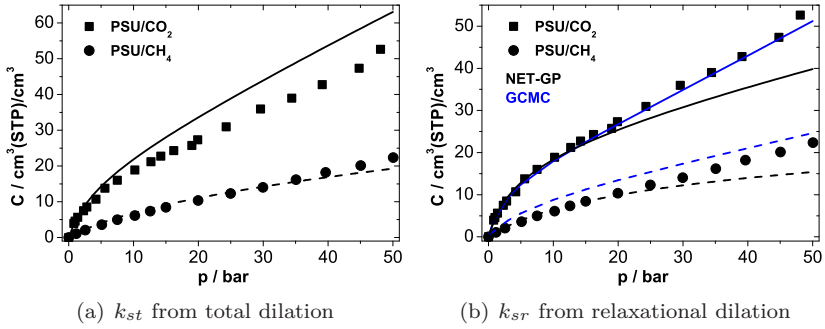


Figure 6.4: NET-GP sorption predictions for CO_2 (—) and CH_4 (- -) in PSU. (a) Swelling coefficient calculated from total dilation data (k_{st}) and (b) from relaxational fraction (k_{sr}), including the linear transitions of the GCMC isotherms (blue).

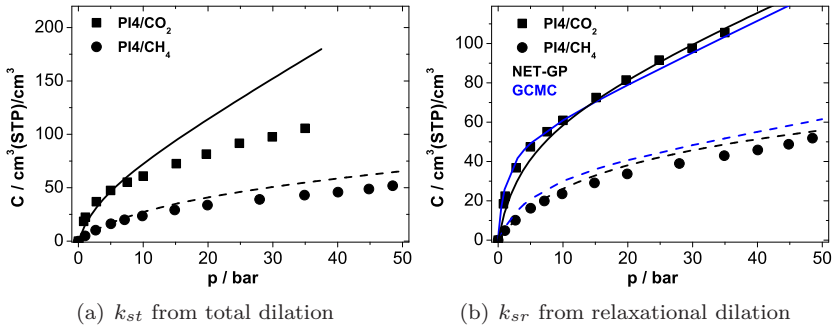


Figure 6.5: NET-GP sorption predictions for CO_2 and CH_4 in PI4.

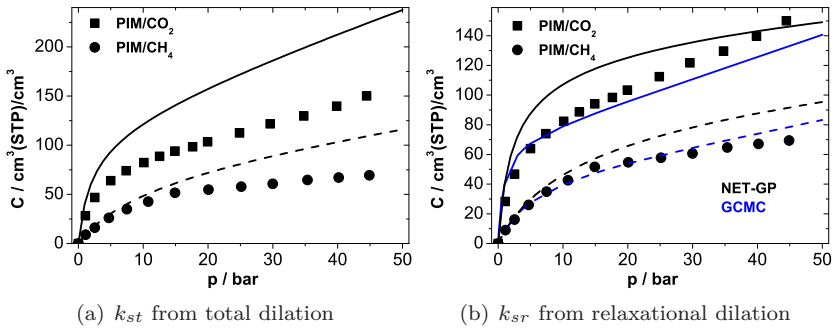


Figure 6.6: NET-GP sorption predictions for CO_2 and CH_4 in PIM-1.

Looking at the prediction for CO₂ in PI4 (Fig. 6.5(a)), the overestimation of experimental data is even larger, while the prediction for CH₄ in PI4 is still acceptable. The predictions for CO₂ and CH₄ in PIM-1, however, are not satisfying, both isotherms being largely overestimated (Figure 6.6(a)).

The single one parameter emanating from this work that affects the calculation is the swelling factor k_s , fitted from the dilation data. It is indeed possible to obtain excellent fits of the sorption data by adjusting k_s . However, if done that way, the predicted dilation exceeds the experimental dilation data in all cases equally unsatisfying. To improve the result, it is useful to review how the polymer density influences the behavior of the NET-GP model: As stated in Section 3.2, a polymer of N r -mers is considered, ‘each mer occupying a lattice site of molar volume v^* ’. Since the volume of a ‘mer’, meaning one mobile unit of the polymer, is a constant, the size of a lattice site remains fixed as well. Thus the model implies that volume changes of the polymer are effected by an increase in the number of lattice sites (N_r , cf. equation 3.6) rather than their volume v^* .

From the kinetic analysis of the experimental data (section 4.4) two different types of dilation processes can be distinguished and separately quantified. The *elastic* fraction stems from the picture of a misfit between penetrant and sorption site, dilating the surrounding matrix *reversibly*. Clearly, no generation of new ‘lattice sites’, i.e. increase of *free volume* would be expected by this process.

That leaves the *relaxational* fraction of dilation. Here, the polymer matrix relaxes the stresses induced by penetrant sorption by rearranging mobile subunits of the polymer chain. This process can certainly be connected to the generation of *free volume* and is in fact known as *conditioning*.⁹⁷ Based on this in some respect admittedly speculative notion, the swelling factors k_s of the polymer/gas systems were obtained by linearly fitting the experimental data of the *relaxational* fraction of dilation only, resulting in swelling factors $k_{sr} < k_{st}$ (Table 3.1, p. 20).

If these swelling factors are applied, predictions for sorption of CO₂ and CH₄ in PSU result, that are displayed in Figure 6.4(b). For convenient comparison to the simulated GCMC calculations the respective isotherms are included as solid blue lines. Using the swelling coefficient k_{sr} resulting from relaxational dilation data, the sorption capacity of PSU is predicted to be considerably lower, now underestimating the experimental data. The representation of experimental data in the intermediate pressure range (10 to 20 bar) could be remarkably improved. On the other hand, the prediction of the CH₄ sorption isotherm by the NET-GP model is somewhat impaired. An obvious improvement of the prediction is achieved for the CO₂ isotherm in PI4, shown in Figure 6.5(b). The NET-GP model relying on relaxational dilation input excellently matches experimental sorption data. No worsening of the CH₄ sorption prediction is observed; on the contrary, the lower relaxational swelling coefficient k_{sr} even provides for a slight improvement. The grand overestimation of CO₂ and CH₄ sorption in PIM-1 is corrected by the relaxational swelling coefficient (Figure 6.6(b)). However, a stronger curvature results in an unsatisfactory representation of the data in the intermediate

pressure region for CO₂, and some residual overestimation is still observed for CH₄ at large pressures.

The transition isotherms of the GCMC simulations are included for easy comparison in all Figures 6.4(b) to 6.6(b). In general, the transition isotherms give an equally good or better representation of the experimental data than do the isotherms calculated by the NET-GP model. But while the simulations depend on density data as well as on concentration data for construction of the packing models at the reference state, the NET-GP phenomenology relies on input on swelling (and pure component data) only, to yield a concentration-pressure isotherm that is purely predictive in nature. All things considered, both methods provide rather good descriptions of experimental sorption data for the gases and polymers investigated in this work.

Table 6.1: Swelling coefficients used for NET-GP sorption prediction.

polymer gas	PSU		PI4		PIM-1	
	CO ₂	CH ₄	CO ₂	CH ₄	CO ₂	CH ₄
k_{st} [%/MPa] ^a	1.461	0.249	6.371	0.758	3.961	1.761
k_{sr} [%/MPa] ^b	0.584	0.042	2.378	0.210	0.490	0.519

^aObtained from linear fit through total dilation data.

^bObtained from linear fit through relaxational fraction of dilation data.

6.2 Free Volume Distributions

In Section 3.3 the phenomenology of the *site distribution* (SD) model was introduced, which provides the means to determine a size distribution of Gaussian form by way of analyzing the sorption and dilation data of gases in glassy polymers. The curves of the fitting procedure have already been presented along with the experimental data on two gases and three polymers in Section 4.5. In this section the Gaussian size distribution of sorption sites are to be discussed and compared with the size distributions obtained by the free volume analysis of detailed atomistic molecular packing models that were presented in Section 5.3.2, albeit in a different exposition.

Performing the least square fit of eqs. 3.44 and 3.48 (see page 23) to the experimental sorption and dilation data (*diffusive/elastic* fraction), ultimately leads to the parameters V_{h0} and σ_v , i.e., center and width, that characterize the Gaussian size distribution of the *free volume* of the investigated polymers, respectively. The parameter values are listed in Table 6.2. To obtain reasonable values for the number of sorption sites N_0 , the *free volume* analysis of the nonswollen packing models was consulted. In Section 5.2.1 it was already argued, that in view of the high geometric complexity of large *free volume elements* (FVEs) as determined by the V_{con} -method, the R_{max} -method would be preferred to obtain a size distribution of FVEs that pass as sorption sites in terms of the SD model. One further adjustment was made, namely the exclusion of FVEs with volumes smaller than the positronium-sized probe-sphere. It is inherent in the method of analysis to exhibit the greatest uncertainties for small volumes, where the dimensions of the volume are comparable to the grid spacing. Furthermore, it is an artifact of the calculation algorithm to yield undersized volumes if the number of free grid points is small. Therefore, for the determination of the number of sorption sites N_0 , all FVEs of volumes not larger than that of the probe-sphere were assumed to be ‘bottlenecks’ (potential diffusion paths), rather than sorption sites, and excluded. This procedure may appear somewhat arbitrary, however, the resulting values listed in Table 6.2 are well within the range of the estimates made by Kirchheim⁵⁶ and therefore it seems an adequate approach to determine the number of sorption sites individually.

Table 6.2: Site distribution model parameters.

polymer / gas	V_g^a / cm^3/mol	G_0 / kJ/mol	σ_G / kJ/mol	V_{h0} / cm^3/mol	σ_V / cm^3/mol	N_0 / $10^{21}/\text{cm}^3$
PSU /CO ₂	46.1	17.5	10.5	21.0	6.4	4.9
PSU /CH ₄	52.2	20.7	8.6	27.7	7.8	4.9
PI4 /CO ₂	46.1	14.7	14.4	13.8	3.7	6.6
PI4 /CH ₄	52.2	18.8	11.6	26.3	10.4	6.6
PIM-1/CO ₂	46.1	13.1	13.5	14.5	8.8	7.8
PIM-1/CH ₄	52.2	18.4	13.8	18.5	11.8	7.8

^a‘Dynamic volume’ of penetrant,⁶¹ cf. eq. 2.15 on page 10.

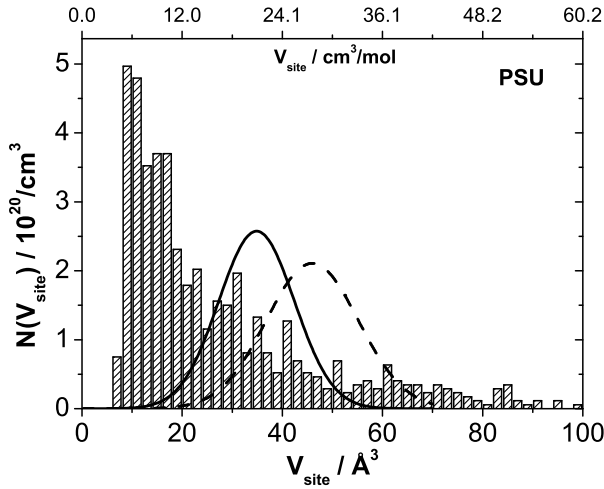


Figure 6.7: Number distribution of FVE volumes (R_{\max}) in *PSU* packing models and Gaussian distribution of sorption sites obtained from SD fit to CO_2 (—) and CH_4 (---) sorption and dilation data.

PSU

Figure 6.7 shows the results of the SD analysis of sorption and dilation data of CO_2 and CH_4 in *PSU*, that is, the Gaussian size distributions of free volume in *PSU*, along with the R_{\max} distribution of FVEs of the nonswollen packing models *PSU*. In principle, it is the same distribution as in Figure 5.9(b) (hatched columns), yet with the aforementioned exclusion of the smallest FVEs and this time the distribution is displayed as a *number*-distribution of FVE-volumes, as opposed to the fractional free volume distribution of radii of volume equivalent spheres. Noticeably, by this last point, the rather symmetrical shape of the distribution in Figure 5.9(b) is stretched to the large volume range. In fact, for convenient comparison with the Gaussian size distributions, the R_{\max} -volume distribution is only shown up to a volume of 100 Å³; several larger FVEs exist only in small numbers and hence do not contribute to the shape of the distribution.[‡] The size distribution of FVEs detected by the R_{\max} -method in nonswollen *PSU* packing models does not resemble a Gaussian shape. The number distribution is increasing from large volume tail until a sharp cutoff that is due to the exclusion of smallest volumes. Since the detection of smaller and smaller FVEs depends on the probe- as well as the grid-size, it has to be presumed that this sharp peak could

[‡]Although it has to be mentioned that these contribute considerably to the *fractional* free volume, due to their large size.

be pushed to smaller volumes, while increasing in intensity. Likewise, increasing the probe-size would shift the peak to larger volumes at the cost of the number of FVEs detected. The choice of a positronium-sized test-sphere is a reasonable compromise, meeting the detection limit of PALS experiments while maintaining the ability to map geometries of the FVEs.

The Gaussian size distribution of the *free volume* in PSU, as established by the SD model using CO₂ and CH₄ sorption and dilation data, are displayed in Figure 6.7 as a solid and broken line, respectively. In theory, both distributions should coincide. Instead, the CH₄ data yields a distribution that is shifted to larger volumes. The message of this outcome is that obviously CH₄ induces less dilation in PSU than would be expected from its ‘dynamic volume’[‡] $V_g = 52 \text{ cm}^3/\text{mol}$, given that the assumptions made by the SD-model hold and the CO₂ data yield the ‘correct’ distribution. In fact, this was assumed by Gotthardt et al.,⁵⁹ who used the dynamic volume of CH₄ as fit-parameter to adjust equation 3.48 to experimental dilation data induced by methane in Bisphenol-A-Polycarbonate (BPA-PC). A value of $V_g = 71.7 \text{ Å}^3$ ($43.2 \text{ cm}^3/\text{mol}$) resulted using the size distribution in BPA-PC obtained from CO₂ sorption and dilation data and its dynamic volume of 76.7 Å^3 ($46.2 \text{ cm}^3/\text{mol}$). This qualitatively corresponds to the shift in the distribution observed in Figure 6.7: In terms of the mechanical point of view assumed by the SD model, dilation is caused by the misfit between penetrant and ‘hole’ volume ($V_g - V_h$, eq. 3.35, p. 22). However, to stay consistent within this work, the ‘dynamic volumes’ of only one reference for both gases were used,⁶¹ and the procedure of fitting the data was not modified. In addition to the uncertainties regarding the dynamic volumes of the penetrants, the SD model assumes a spherical geometry of the penetrants and concentration-independent interaction other than that of elastic nature. Especially in the case of CO₂, this may not be the case at higher concentrations, despite the exclusive usage of *diffusive/elastic* fraction of sorption and dilation data. In view of these simplifications, the agreement between both Gaussian size distributions within a few Ångstrom is still acceptable.

For all the differences in shape, center and width of the Gaussian distributions shown in Figure 6.7 with the R_{max} -distribution of FVEs of detailed atomistic packing models, the accordance within the same order of magnitude can be counted as a success. For their comparison, it has to be kept in mind that, while the SD model is derived from considerations of the above- T_g *dynamics* (cf. eq. 3.25, p. 21), the volume analysis is performed on the *static* atomistic model of polysulfone. Moreover, continuum mechanics and idealized spherical shapes are assumed in the SD model, whereas the volumetric analysis does not distinguish between geometrical shapes. But large volumes detected by model analysis may well be narrow in one or two dimensions and not necessarily accommodate penetrant molecules as well as would spherical holes of the same volume.

[‡]That is, the partial molar volume of the penetrant in rubbery polymers or liquids, cf. Section 2.14.

PI4

Similar observations as for the size distributions in PSU can be made for PI4, as shown in Figure 6.8. Using the methane data, the Gaussian distribution is shifted and considerably broadened. However, recalling the quality of the fits to the data (Figure 4.14 on page 41), one is lead to believe that in this case the distribution derived from CO₂ data is less reliable. The unexpectedly low center ($V_{h0}(\text{PI4}) < V_{h0}(\text{PSU})$, cf. Table 6.2 on page 91) adds to that suspicion. In PI4, a larger fraction of *free volume* (18.7 %) than in PSU (13.5 %) is present (see Section 4.1). If, as the result of the R_{\max} -analysis on *PI4* suggests, this is at least in part due to the presence of larger sorption sites, there should be a smaller misfit and hence less dilation. The opposite is observed, and for this reason the SD model yields a low value for V_{h0} . The main features of the FVE distribution agree with those of *PSU* as could be expected from Figure 5.10(b) (p. 67). Again, sorption sites in the same order of magnitude resulted from both, molecular simulation and SD analysis.

PIM-1

Figure 6.9 shows the results of the *free volume* analysis of the R_{\max} -method and SD analysis in PIM-1. The mismatch between the Gaussian distributions obtained from CO₂ and CH₄ data is smaller than for PSU and PI4. The distributions are rather broad, and on first sight the agreement to the distribution of FVE sizes seems better than for the other polymers. However, like in *PI4*, the distribution of FVEs in *PIM* exhibits a long tail towards large volumes which seems not to be detected by the SD model, where the size distribution is determined making use of the ratio of experimental sorption and dilation.

Possible Limits of the Model

Although the agreement of the size distributions as determined by packing model analysis and by SD analysis of polymer/gas-systems is satisfying, being within the same order of magnitude, the question remains why the trend of the size distributions of FVEs towards a higher number of large volumes for *PI4* and *PIM* in comparison to *PSU* (cf. Fig. 5.14(a)) is not reflected by the position of the centers of the Gaussian size distributions, displayed together in Figure 6.10.

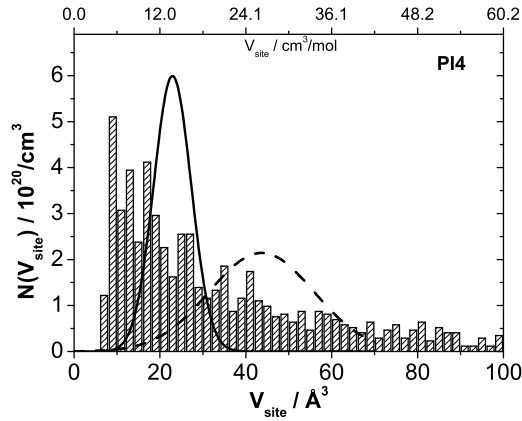


Figure 6.8: Size distribution (R_{\max}) of FVEs in *PI4* packing models and Gaussian distribution of sorption sites obtained from SD fit to CO_2 (—) and CH_4 (- -) sorption and dilation data.

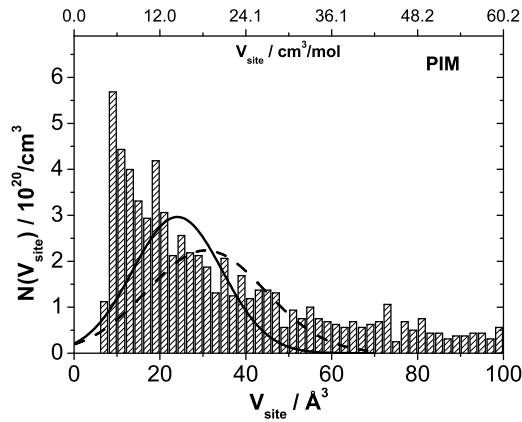


Figure 6.9: Size distribution (R_{\max}) of FVEs in *PIM* packing models and Gaussian distribution of sorption sites obtained from SD fit to CO_2 (—) and CH_4 (- -) sorption and dilation data.

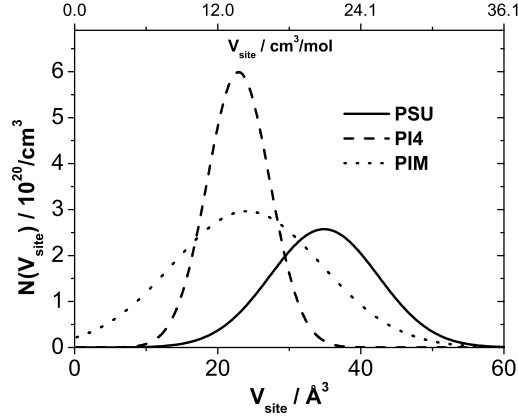


Figure 6.10: Gaussian distributions of sorption sites obtained from SD fit to CO₂ sorption and dilation data in PSU (—), PI4 (---) and PIM-1 (····).

Since experimental PALS data suggest the same trend (equivalent sphere radii of 2.9 Å for PSU,⁹¹ 4.0 Å for PI4,⁶⁴ and 4.8 Å for PIM-1,⁹⁸) as the *free volume* analysis of packing models, a closer look at the SD model seems appropriate to resolve the question. The center of the Gaussian size distribution V_{h0} is the result of a fit of equation 3.48 to experimental dilation data:

$$\Delta V/V_0 = \int_{-\infty}^{\infty} [V_g - V_h(G)] C(G) dG$$

As a result of equation 3.47, which states that large sorption sites have the lowest sorption energy G , and the fact that integration in eq. 3.48 starts at low energies, the mathematics of the SD model implies that penetrants of volume V_g occupy the largest volumes V_h first, dilation setting-in once the misfit $[V_g - V_h(G)]$ is positive. This assumption may not be correct. The step by step insertion of penetrants that was performed to calculate sorption isotherms in the nonswollen polymer packing models, provides the means to actually analyse which of the FVEs present in a packing model are occupied by the ‘first’ 10 CO₂ molecules. To account for complex shapes even the R_{\max} -method does not cancel out, the FVEs were characterized by the radius of the largest sphere that would fit into an FVE without overlap. As it turns out, the FVEs that are occupied first in the GCMC procedure exhibit an equivalent sphere radius of 1.9 ± 0.3 Å in all *PSU* packing models, 2.2 ± 0.3 Å in *PI4* and 2.4 ± 0.3 Å in *PIM*. However, the largest volumes present in the polymer packing models range from 2.4 Å to 1.9 Å in *PSU*, 3.9 Å to 2.9 Å in *PI4* and 3.2 Å to 2.7 Å in *PIM*. While in the *PSU* packing models the FVEs that are occupied first range among the largest that are available, clearly for *PI4* and *PIM* this is not the case.

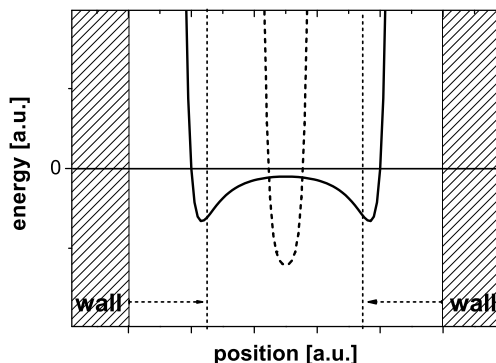
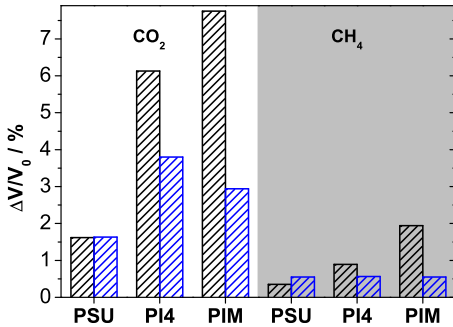


Figure 6.11: Sketch of the adsorption potential of a molecule between the two walls of a slitpore (—). If the distance between the walls is reduced (\cdots) to a finite distance, the potential minimum is optimized ($- -$).

This train of thought is supported by the behavior of a slit-pore potential. Here, the potential Φ_{sp} of a molecule between two rigid walls is examined in one dimension. The commonly used 10–4 potential is sketched out in Figure 6.11 for two distances.⁹⁹ Without going into further detail, Fig. 6.11 illustrates that the potential exhibits a local minimum close to the walls of the slit-pore. This minimum is optimized when the walls are at a finite distance.

Related to the matter at hand, this means that, deviant from the mathematics of the SD model, where large sorption sites are occupied first because of the little or absent elastic energy contribution, in reality penetrants may occupy sorption sites first, where such a minimum distance to the polymer matrix in all directions is given, i.e., where a maximum of ‘constructive’ interaction between penetrant molecule and matrix can be achieved. In the case of PSU this would not effect the SD analysis much, since the ‘preferred size’ of the FVEs coincides more or less with the largest available FVEs. However, if, as the analysis of the packing models of *PI4* and *PIM* suggests, the largest sites present in these two polymers are left unoccupied in favor of smaller sorption sites, at low concentration levels of penetrants a dilation would be observed that is similar to polysulfone. This dilation, in addition to a high number of sorption sites N_0 would then be ‘mathematically’ misinterpreted by the SD model, yielding undersized Gaussian distributions. Incidentally, the Gaussian distributions obtained for *PI4* and *PIM* center in the same volume range, lending more support to the hypothesis that the SD model is ‘blind’ to oversized volumes.

**Figure 6.12:**

Gas induced volume dilation in polymers (black) and corresponding dilation in polymer packing models (blue).

6.3 Integral Dilation

In Section 4.5.2 the results of the experimentally observed volume dilation induced by integral gas sorption were presented. Using the experimental sorption data, non-swollen packing models of each polymer were prepared containing the specified number of penetrant molecules. The resulting volume dilation of the simulation cell in a subsequent NpT -MD simulation were presented in Section 5.3.4. Figure 6.12 summarizes the data that were listed in Tables 4.2 and 5.3 (see pages 46 and 80).

In all six cases, the polymer matrix responds to the sorption and accordingly to the insertion of penetrants with a volume dilation. This volume dilation, which seems to be instantaneous upon sorption of a penetrant in the corresponding experiments, appears to follow a kinetics in the corresponding simulation experiments that is not possible to resolve in the experimental setups used in this work. The absolute value of the dilation effect found by detailed atomistic molecular dynamics simulation deviates from the experimentally obtained values by not more than a factor of three. Upon removal of the penetrants, all polymer/gas systems were shown to contract. But while in the experiments the contraction is complete, showing only a slower diffusion kinetics as is expected for desorption, all packing models except for *PI4* show a residual volume dilation after equilibrating the depleted packing models. Considering the limited size of the packing models and the difference in time scales of experiment (minutes) and modeling (picoseconds) of more than 10 orders of magnitude, these results can be regarded as being in rather satisfying agreement to the experimental data.

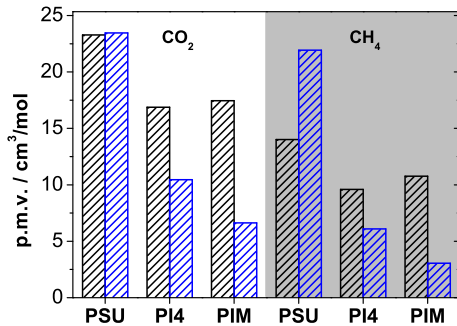


Figure 6.13:

Partial molar volume of CO₂ and CH₄ in polymers (black) and corresponding PMV in polymer packing models (blue).

All polymer/gas systems were investigated at the same pressure of the respective penetrant gas. Since the concentration levels are quite different, it is instructive to relate concentration and dilation effects. In Section 2.3 the concept of the *partial molar volume* (PMV) was outlined and equation 2.14 was offered as a practical means to calculate the PMV V_p of a penetrant from experimental concentration (change in penetrant number Δn_i) and dilation data:

$$V_p = \frac{\Delta V}{\Delta n_i}$$

In Figure 6.13 the PMVs of CO₂ and CH₄ in the three polymers are displayed as they were calculated from experimental integral sorption and dilation data and calculated from the simulated integral dilation of polymer packing models (see Tables 4.2 and 5.3 on pages 46 and 80).

It was already noted in Section 4.5.2, that the experimental results order as PSU > PIM-1 \gtrsim PI4, despite the expectation that the calculated *free volume* (Bondi)³⁵ suggests PSU > PI4 > PIM-1 for the concentration levels reached in the experiment. The latter order is actually found in the simulated integral dilation. However, both simulated dilation effects of PI4 and PIM are considerably lower (about 60 % and 40 %, respectively) than in the corresponding experiments. Two aspects have to be considered in regard to this difference:

(1) The densities of the PI4 and PIM packing models deviate from the experimental densities by -6 % and -5 %, while those of the PSU packing models deviate only by -3 %. The negative sign of the deviation suggests a larger fractional free volume in the packing models than in the ‘real’ samples and hence a smaller dilation effect should be observed. However, a rough estimate shows that the difference in fractional free volume between packing model and ‘real’ sample amounts to +34 % for PI4 and

+25 % for *PIM*. Due to the smaller fractional free volume in polysulfone, the relatively smaller deviation of the obtained density still amounts to +25 % for the *PSU* packing models. These values actually suggest for the simulated dilation of *PSU* to show some deviations as well; however, no such effects can be observed in this case. Also, in the discussion of the *site distribution* model in the previous section evidence was presented that large sorption sites are not occupied first in the simulation and it is therefore not clear that the surplus of *free volume* necessarily leads to the observed deviation in dilation behavior. In any case, it should be noted, that an improvement of the density of the *PI4* and *PIM* packing models would probably lead to an improvement of the dilation results as well, qualitatively emphasizing the simulated dilation effect.

Although it cannot be ruled out for the density deviations to contribute to the deviations in dilation, another approach is possible in order to explain the ‘incomplete’ dilation of the *PI4* and *PIM* packing models which was presented in reference [3]:

(2) The larger deviation of the dilation values of *PI4* and *PIM* in comparison to the very good results for *PSU* may be explainable in terms of the stiffness of the respective repeat units. As was explicated in reference [3], polysulfone has a higher density of flexible, i.e., more or less rotatable bonds along the polymer chain than the polyimide *PI4* does (cf. Fig. 4.1). Therefore e.g. rearrangements of phenylene rings are more easily possible than in *PI4*. In *PI4*, bulky side groups, like the $-\text{CF}_3$ groups, or the methyl-groups in ortho-position to the imide group, represent additional hindrances to local reorientation of groups (cf. Fig. 4.2). Besides the considerably higher glass transition temperature of *PI4*, compared to *PSU*, this reasoning was supported by an analysis of the rotational mobilities of selected bond angles in *PSU* and *PI4* packing models (see Appendix A.4)³ as well as the mean square displacement of backbone atoms of (*PSU*>*PI4*).^{1, 63} The absence of a glass transition at temperatures well above that of *PI4* and a supposedly even more rigid polymer matrix insinuates that the same reasoning should apply to *PIM-1* as well, even if no such thorough investigations for *PIM-1* were committed in the course of this work.

Assuming the second explanation to be the main reason for the deviations between experiment and modeling, the incomplete dilation of *PI4* and *PIM* packing models could be interpreted as the result of an *anelastic* contribution to the dilation on a time scale that is well below the resolution limit of the experimental setups used in this work, while being fast enough to be detected within the nanoseconds of simulation time only in the case of *PSU*. Anelastic relaxation behavior in glassy polymers was investigated by Boyd et al.⁴⁵ and related to secondary relaxation processes (β -relaxation) that may well match the intermediate time scales between experiment and modeling. However, extensive investigations of relaxation spectra as well as further simulations would be necessary to unambiguously correlate these processes.

Partial Molar Volume and Hole Volumes

The partial molar volumes can be further used to gain information about the localized free volume. Equation 3.35, which was introduced in the context of the *site distribution* model, connects the partial molar volume V_p of individual penetrants via their ‘dynamic volume’ V_g with the volume of the occupied ‘hole’ V_h :

$$V_p = \text{const}(V_g - V_h)$$

Assuming $\text{const} = 1$ and the ‘dynamic volumes’ $V_g = 46.2 \text{ cm}^3/\text{mol}$ and $V_g = 52 \text{ cm}^3/\text{mol}$ for CO_2 and CH_4 , respectively, as was done in the SD analysis, the average site volumes of the *occupied* sorption sites result from the partial molar volumes shown in Figure 6.13 that can be expressed as the radii of volume equivalent spheres. Figure 6.14 shows the resulting values for the three investigated polymers.

A slight trend may be discerned towards the occupation of larger hole volumes in the case of CH_4 compared to CO_2 , and larger sites seem to be occupied in the different polymers, taking on the order $\text{PSU} < \text{PI4} < \text{PIM-1}$ for both penetrants, however, the differences are rather small. Recalling the discussion of the SD model in the previous section, the values of 1.9 \AA^3 , 2.2 \AA^3 , and 2.4 \AA^3 were evaluated for the FVEs occupied by the first 10 CO_2 molecules in *PSU*, *PI4* and *PIM* packing models, respectively. Given the higher concentration level of penetrants in the integral dilation experiments and simulations, the observed increase is expected, because increasing elastic contribution to the sorption energy upon occupation of smaller and smaller sites will eventually make the occupation of larger-than-optimum sites more ‘favorable’.

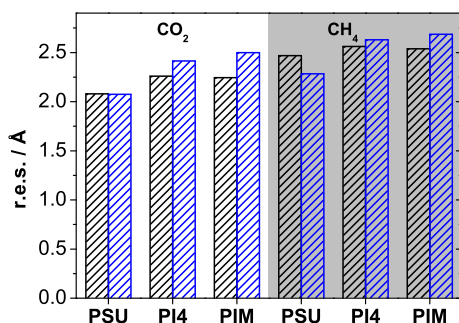
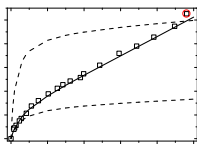


Figure 6.14:

Average equivalent sphere radii (r.e.s.) of sorption sites occupied by CO_2 and CH_4 in polymers (black) and polymer packing models (blue).

7 Synopsis

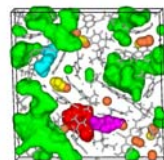
Summary Sorption and dilation characteristic of three polymers (PSU, PI4 and PIM-1) in contact with two gases (CO_2 and CH_4) have been investigated utilizing experimental characterization methods, techniques of detailed atomistic molecular modeling and theoretical data analysis. Differential sorption and dilation isotherms were recorded up to gas pressures of 50 bar and were kinetically analyzed. The resulting diffusive/elastic fractions of the isotherms were subjected to an analysis by means of the *site distribution* (SD) model, yielding well agreeing fits and resulting in parameters of Gaussian size distributions of the localized *free volume* of each polymer.



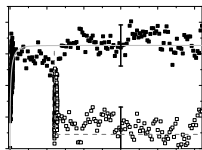
The density and concentration data at the minimum and maximum pressure of each sorption and dilation isotherm were chosen as reference states to construct detailed molecular packing models of the nonswollen and swollen state of each polymer/gas system. Grand Canonical Monte Carlo simulations

(GCMC) were performed to obtain simulated sorption isotherms for the nonswollen and swollen state, respectively, and a linear transition with pressure was proposed that agrees excellently with the experimental data. The close resemblance to the *Non Equilibrium Thermodynamics of Glassy Polymers* (NET-GP) model was identified and results compared to the sorption predictions of the model, using both, the total and the relaxational fraction of the experimental dilation isotherms to obtain the swelling factor needed for this purpose.

A thorough analysis and visualization of the *free volume* was conducted on the static packing models of the pure polymers, revealing separated *free volume elements* (FVEs) for PSU and PI4, whereas PIM exhibits large FVEs of highly complex shape that were denominated as a *void phase*, taking up the main portion of the *fractional free volume* (FFV). The same analysis on the CO_2 -swollen packing models showed that PI4 developed a similar *void phase* upon swelling (PI156) while no such change could be observed in swollen PSU models (PSU80) at the investigated dilation levels. The size distributions of FVEs according to the R_{max} -method in nonswollen models were found to be of the same order of magnitude as Gaussian size distributions obtained by SD analysis of experimental data. Differences in shape were discussed to be a matter of the dynamic/static viewpoint of the experimental



and modeling technique, respectively. Possible limits of the SD model regarding the occupation sequence of sorption sites have been pointed out for PI4 and PIM-1.



Integral sorption and dilation measurements were carried out at 10 bar pressure for all polymer/gas systems. The dilation was recognized as an elastic process on the time scale of the experiments. The sorption data were used as input to prepare nonswollen yet penetrant-loaded packing models which showed reasonably agreeing dilation in subsequent NpT -MD simulations. The deviation towards lower dilation in *PI4* and *PIM* as well as the incomplete recovery of the dilated *PSU* and *PIM* packing models were attributed to anelastic relaxations in the time range intermediate to experiment and simulation. The partial molar volumes of the two penetrant gases within the respective polymers were related to the volume of occupied sorption sites using the ‘dynamic volume’ of the penetrants.

Conclusions The experimental investigation of the phenomena associated with gas sorption and dilation in glassy polymers demands a considerable effort of time and resources. The prospect of assessing the properties of polymer/gas systems by examination of detailed atomistic molecular packing models, selecting only the most promising materials for further investigation, seems a reasonable presumption, given the progress in computing power and availability of CPU time is sustained. However, the large gap of several orders of magnitude in system size and time scales between experiment and simulation will not be bridged by capacity and speed alone. Methods are called for that combine experiment and simulation and make possible a deeper understanding of the mechanisms that govern sorption and dilation in polymer/gas systems.

In this work, several approaches were presented that address this apparent incompatibility of experiment and simulation. Since the relaxational swelling of the polymer matrix that is observed at elevated concentration levels of penetrants, is orders of magnitudes too long to directly simulate the respective molecular dynamics in reasonable time and effort, representative reference states were evaluated experimentally and packing models constructed according to the specifications. Even though this method is still dependent on experimental input, the successful description of experimental sorption data using a transition between GCMC isotherms of nonswollen and swollen model validates both, the quality of the molecular models and the general approach, which is further backed up by its resemblance to the well established NET-GP model. In addition, the *free volume* analysis of nonswollen and swollen packing models revealed fundamental differences in the structure of the free volume of the investigated polymers in their initial and swollen states. In the recently developed new class of *Polymers of Intrinsic Microporosity* (PIM), the existence of a *void phase* could be detected and quantified. The visualization showed the *void phase* as a large fraction of the free volume of highly complex shape that is loosely connected and penetrates far reaches of the simulation cell. This sort of structure is present in *PI4* only in the swollen state and not at all in the investigated *PSU* reference states. Certainly,

this *void phase* plays an important role in sorption and transport characteristics of penetrant gases that have yet to be studied.

Some disagreement was encountered concerning the size distributions of FVEs and the Gaussian distributions obtained via the SD model. Although generally of the same order of magnitude, which already can be clearly counted as a success given the disparate conditions of the two approaches, the Gaussian distributions suggested a different trend concerning the center of the distribution. Here, the tool of detailed molecular modeling provided the means to put model assumptions to the test, exposing possible limits or weaknesses of the model with respect to polymers that exhibit sorption sites of large volume. However, the elastic response of the matrix to the insertion of penetrants could successfully be simulated. Furthermore the SD model is able to describe the experimental sorption and dilation data quite well, if the kinetic analysis and its results are consistently implemented, that is, if the diffusive/elastic fraction is used exclusively. To a certain extent, this lends some credibility to the perception of the processes involved as established by the SD model.

In experimental measurements of gas induced dilation as they were studied in this work, sorption is necessarily associated with the diffusion of the penetrant gas. The method of inserting penetrant molecules in a nonswollen packing model to observe the dilation effect in NpT -MD simulations avoids the ‘slow’ process of diffusion with respect to simulation time and thus allows the comparison to the experiment, with quite satisfying agreement. Although some deviation remains, the results obtained in this work point at the existence of possible short-time relaxations or anelastic reactions of the polymer matrix that are specific to each polymer. However, the successful secondary insertion of CO_2 molecules into the dilated PI_4 matrix and the fact that the isotherms of the nonswollen models show good agreement to the experimental isotherms in the low pressure region, shows that in principle, no experimental input may be needed to record concentration/dilation isotherms that compare to the elastic fraction of experimental dilation.

Outlook In this work methods of analysis of the sorption and dilation phenomena in polymer/gas systems were presented that combine experiment, theory, and simulations. Even though promising results could already be achieved, further efforts are necessary to add extra confirmation and to answer the questions that were raised in the course of this work. In the context of the integral dilation simulation anelastic processes were surmised that account for the ambiguous behavior of the packing models. The rough analysis of bond angle rotations for PSU and PI_4 packing models that was conducted as a scouting experiment in the course of this work (see Section 6.3 and Appendix A.4), should be refined and extended to PIM packing models, along with the analysis of the dynamic mechanical or dielectric spectra of the ‘real’ counterparts, to confirm or disprove the conjecture. As already mentioned in the previous paragraph, the notion of simulating sorption *and* dilation by alternately loading (GCMC) and equilibrating (NpT -MD) a nonswollen packing model provides an intriguing way

to record diffusive/elastic concentration- and dilation-pressure isotherms independent of experimental input.

A follow-up on these encouraging new ways of comparison of laboratory experiments and molecular modeling, to further converge the respective boundary conditions and to reconcile them with the assumptions made by phenomenological models, is recommended to improve the compatibility of the results and thereby ensure targeted material design in the future.

Bibliography

- [1] M. Heuchel, M. Böhning, O. Hölck, M. R. Siegert, and D. Hofmann. Atomistic Packing Models for Experimentally Investigated Swelling States Induced by CO₂ in Glassy Polysulfone and Poly(ether sulfone). *Journal of Polymer Science Part B: Polymer Physics*, 44(13):1874–1897, 2006.
- [2] O. Hölck, M. R. Siegert, M. Heuchel, and M. Böhning. CO₂ Sorption Induced Dilation in Polysulfone: Comparative Analysis of Experimental and Molecular Modeling Results. *Macromolecules*, 39(26):9590–9604, 2006.
- [3] O. Hölck, M. Heuchel, M. Böhning, and D. Hofmann. Simulation of Experimentally Observed Dilation Phenomena during Integral Gas Sorption in Glassy Polymers. *Journal of Polymer Science Part B: Polymer Physics*, 46(1):59–71, 2008.
- [4] D. L. Tomasko, H. B. Li, D. H. Liu, X. M. Han, M. J. Wingert, L. J. Lee, and K. W. Koelling. A Review of CO₂ Applications in the Processing of Polymers. *Industrial and Engineering Chemical Research*, 42(25):6431–6456, 2003.
- [5] A. F. Ismail and W. Lorna. Penetrant-Induced Plasticization Phenomenon in Glassy Polymers for Gas Separation Membrane. *Separation and Purification Technology*, 27(3):173–194, 2002.
- [6] H. Q. Lin, E. Van Wagner, B. D. Freeman, L. G. Toy, and R. P. Gupta. Plasticization-Enhanced Hydrogen Purification using Polymeric Membranes. *Science*, 311(5761):639–642, 2006.
- [7] I. Kikic, F. Vecchione, P. Alessi, A. Cortesi, F. Eva, and N. Elvassore. Polymer Plasticization using Supercritical Carbon Dioxide: Experiment and Modeling. *Industrial and Engineering Chemical Research*, 42(13):3022–3029, 2003.
- [8] J. Ulrich, H. G. Brion, and R. Kirchheim. The Influence of Sorption of Small Molecules on the Yield Stress of Glassy Polymers. *Polymer*, 40(7):1807–1814, 1999.

-
- [9] A. Pasricha, G. Wing, O. Kumar, M. Tuttle, and K. Seeler. Effect of CO₂ Sorption and Desorption on the Creep Response of Polycarbonate. *Polymer Engineering and Science*, 45(12):1639–1644, 2005.
- [10] D. Hofmann, L. Fritz, J. Ulbrich, C. Schepers, and M. Böhning. Detailed-Atomistic Molecular Modeling of Small Molecule Diffusion and Solution Processes in Polymeric Membrane Materials. *Macromolecular Theory and Simulations*, 9(6):293–327, 2000.
- [11] G. K. Fleming and W. J. Koros. Dilation of Polymers by Sorption of Carbon-Dioxide at Elevated Pressures. 1. Silicone-Rubber and Unconditioned Polycarbonate. *Macromolecules*, 19(8):2285–2291, 1986.
- [12] D. R. Paul. Gas Sorption and Transport in Glassy Polymers. *Berichte der Bunsen-Gesellschaft-Physical Chemistry Chemical Physics*, 83(4):294–302, 1979.
- [13] D. Raucher and M. D. Sefcik. Sorption and Transport in Glassy Polymers - Gas Polymer Matrix Model. *ACS Symposium Series*, 223:111–124, 1983.
- [14] J. S. Vrentas and C. M. Vrentas. Sorption in Glassy Polymers. *Macromolecules*, 24(9):2404–2412, 1991.
- [15] G. G. Lipscomb. Unified Thermodynamic Analysis of Sorption in Rubbery and Glassy Materials. *AIChE J.*, 36(10):1505–1516, 1990.
- [16] Y. Mi, S. Zhou, and S. A. Stern. Representation of Gas Solubility in Glassy Polymers by a Concentration Temperature Superposition Principle. *Macromolecules*, 24(9):2361–2367, 1991.
- [17] R. G. Wissinger and M. E. Paulaitis. Molecular Thermodynamic Model for Sorption and Swelling in Glassy Polymer-CO₂ Systems at Elevated Pressures. *Industrial and Engineering Chemical Research*, 30(5):842–851, 1991.
- [18] R. M. Conforti, T. A. Barbari, P. Vimalchand, and M. D. Donohue. A Lattice-Based Activity-Coefficient Model for Gas Sorption in Glassy Polymers. *Macromolecules*, 24(11):3388–3394, 1991.
- [19] F. Doghieri and G. C. Sarti. Nonequilibrium Lattice Fluids: A Predictive Model for the Solubility in Glassy Polymers. *Macromolecules*, 29(24):7885–7896, 1996.
- [20] I. C. Sanchez and R. H. Lacombe. Statistical Thermodynamics of Polymer-Solutions. *Macromolecules*, 11(6):1145–1156, 1978.
- [21] Y. Tsujita. Gas Sorption and Permeation of Glassy Polymers with Microvoids. *Progress in Polymer Science*, 28(9):1377–1401, 2003.
- [22] A. C. Newns. The Sorption and Desorption Kinetics of Water in a Regenerated Cellulose. *Transactions of the Faraday Society*, 52(11):1533–1545, 1956.

- [23] A. J. Erb and D. R. Paul. Gas Sorption and Transport in Polysulfone. *Journal of Membrane Science*, 8(1):11–22, 1981.
- [24] J. S. Chiou, Y. Maeda, and D. R. Paul. Gas Permeation in Polyethersulfone. *Journal of Applied Polymer Science*, 33(5):1823–1828, 1987.
- [25] J. S. Wang and Y. Kamiya. Concurrent Measurements of Sorption and Dilation Isotherms and Diffusivity for Polysulfone Membrane Carbon-Dioxide System. *Journal of Membrane Science*, 98(1-2):69–76, 1995.
- [26] J. S. Wang, Y. Kamiya, and Y. Naito. Effects of CO₂ Conditioning on Sorption, Dilation, and Transport Properties of Polysulfone. *Journal of Polymer Science Part B: Polymer Physics*, 36(10):1695–1702, 1998.
- [27] J. S. McHattie, W. J. Koros, and D. R. Paul. Gas-Transport Properties of Polysulfones. 1. Role of Symmetry of Methyl-Group Placement on Bisphenol Rings. *Polymer*, 32(5):840–850, 1991.
- [28] Y. Kamiya, T. Hirose, K. Mizoguchi, and Y. Naito. Gravimetric Study of High-Pressure Sorption of Gases in Polymers. *Journal of Polymer Science Part B: Polymer Physics*, 24(7):1525–1539, 1986.
- [29] M. Böhning. *Untersuchungen der Gaspermeationseigenschaften von Polymeren und dabei auftretender Wechselwirkungs- und Quellungsphänomene*. Dissertation, Technical University Berlin, 1997.
- [30] J. D. Wind, S. M. Sirard, D. R. Paul, P. F. Green, K. P. Johnston, and W. J. Koros. Relaxation Dynamics of CO₂ Diffusion, Sorption, and Polymer Swelling for Plasticized Polyimide Membranes. *Macromolecules*, 36(17):6442–6448, 2003.
- [31] P. M. Budd. Putting Order into Polymer Networks 1. *Science*, 316(5822):210–211, 2007.
- [32] G. B. McKenna and S. L. Simon. The Glass Transition: Its Measurement and Underlying Physics. In S. Z. D. Cheng, editor, *Applications to Polymers and Plastics*, volume 3 of *Handbook of Thermal Analysis and Calorimetry*, book chapter 2. Elsevier Science B.V., 2002.
- [33] P. Ehrenfest. Phase Conversions in a General and Enhanced Sense, Classified According to the Specific Singularities of the Thermodynamic Potential. *Proceedings of the Koninklijke Akademie Van Wetenschappen Te Amsterdam*, 36(1/5): 153–157, 1933.
- [34] L. H. Sperling. *Introduction to Physical Polymer Science*. Wiley-Interscience, New York, 2001.
- [35] A. Bondi. *Physical Properties of Molecular Crystals, Liquids and Glasses*. Wiley, New York, 1968.

-
- [36] G. Maier. Gas Separation with Polymer Membranes. *Angewandte Chemie-International Edition*, 37(21):2961–2974, 1998.
- [37] T. Visser, G. H. Koops, and M. Wessling. On the Subtle Balance between Competitive Sorption and Plasticization Effects in Asymmetric Hollow Fiber Gas Separation Membranes. *Journal of Membrane Science*, 252(1-2):265–277, 2005.
- [38] P. Pekarski and R. Kirchheim. On the Sorption of Gas Mixtures by Polymer Glasses. *Journal of Membrane Science*, 152(2):251–262, 1999.
- [39] J. Crank. *The Mathematics of Diffusion*. Oxford Science Publications, New York, 2. edition, 1975.
- [40] J. D. Eshelby. The Continuum Theory of Lattice Defects. In F. Seitz and D. Turnbull, editors, *Solid State Physics*, pages 79–144. Academic Press, 1956.
- [41] W. Flügge. *Viscoelasticity*. Blaisdell Publishing Company, Waltham, 1967.
- [42] A. R. Berens and H. B. Hopfenberg. Diffusion and Relaxation in Glassy Polymer Powders. 2. Separation of Diffusion and Relaxation Parameters. *Polymer*, 19(5):489–496, 1978.
- [43] M. Wessling, I. Huisman, T. Vanderboomgaard, and C. A. Smolders. Dilation Kinetics of Glassy, Aromatic Polyimides Induced by Carbon-Dioxide Sorption. *Journal of Polymer Science Part B: Polymer Physics*, 33(9):1371–1384, 1995.
- [44] C. Zener. *Elasticity and Anelasticity of Metals*. The University of Chicago Press, Chicago, 1948.
- [45] R. H. Boyd, M. E. Robertsson, and J. F. Jansson. The Nature of the Non-Linear Anelasticity of Glassy Polymers. *Journal of Polymer Science Part B: Polymer Physics*, 20(1):73–81, 1982.
- [46] I. Böhm, H. G. Brion, and R. Kirchheim. Effect of dissolved small molecules on the mechanical relaxation behavior of polycarbonate. *Polymer*, 41(17):6613–6617, 2000.
- [47] D. T. Punsalan. *A Sorption and Dilation Investigation of Amorphous Glassy Polymers and Physical Aging*. Dissertation, University of Texas at Austin, 2001.
- [48] Y. Kamiya, T. Hirose, Y. Naito, and K. Mizoguchi. Sorptive Dilation of Polysulfone and Poly(ethylene-terephthalate) Films by High-Pressure Carbon-Dioxide. *Journal of Polymer Science Part B: Polymer Physics*, 26(1):159–177, 1988.
- [49] G. C. Sarti and F. Doghieri. Predictions of the Solubility of Gases in Glassy Polymers based on the NELF Model. *Chemical Engineering Science*, 53(19):3435–3447, 1998.

- [50] F. Doghieri and G. C. Sarti. Predicting the Low Pressure Solubility of Gases and Vapors in Glassy Polymers by the NELF Model. *Journal of Membrane Science*, 147(1):73–86, 1998.
- [51] M. G. Baschetti, F. Doghieri, and G. C. Sarti. Solubility in Glassy Polymers: Correlations through the Nonequilibrium Lattice Fluid Model. *Industrial and Engineering Chemical Research*, 40(14):3027–3037, 2001.
- [52] I. C. Sanchez and R. H. Lacombe. Elementary Molecular Theory of Classical Fluids - Pure Fluids. *Journal of Physical Chemistry*, 80(21):2352–2362, 1976.
- [53] F. Doghieri. Non Equilibrium Package. Internet download, 2002. Diffusion in Polymers Research Group, DICMA, University of Bologna, <http://serwebdicma.ing.unibo.it/polymers/nelfexcnew.zip>.
- [54] M. G. De Angelis, G. C. Sarti, and R. Doghieri. NELF Model Prediction of the Infinite Dilution Gas Solubility in Glassy Polymers. *Journal of Membrane Science*, 289(1-2):106–122, 2007.
- [55] M. G. De Angelis. Chemical Engineering-Department, University of Bologna, Italy. Personal Communication, 2007.
- [56] R. Kirchheim. Sorption and Partial Molar Volume of Small Molecules in Glassy Polymers. *Macromolecules*, 25(25):6952–6960, 1992.
- [57] R. Kirchheim. Partial Molar Volume of Small Molecules in Glassy Polymers. *Journal of Polymer Science Part B: Polymer Physics*, 31(10):1373–1382, 1993.
- [58] F. Bueche. Segmental Mobility of Polymers Near Their Glass Temperature. *Journal of Chemical Physics*, 21(10):1850–1855, 1953.
- [59] P. Gotthardt, A. Gruger, H. G. Brion, R. Plaetschke, and R. Kirchheim. Volume Change of Glassy Polymers by Sorption of Small Molecules and its Relation to the Intermolecular Space. *Macromolecules*, 30(25):8058–8065, 1997.
- [60] S. Kanehashi and K. Nagai. Analysis of Dual-Mode Model Parameters for Gas Sorption in Glassy Polymers. *Journal of Membrane Science*, 253(1-2):117–138, 2005.
- [61] D. S. Pope, I. C. Sanchez, W. J. Koros, and G. K. Fleming. Statistical Thermodynamic Interpretation of Sorption Dilation Behavior of Gases in Silicone-Rubber. *Macromolecules*, 24(8):1779–1783, 1991.
- [62] Polymer User Guide. MSI/Accelrys Inc., San Diego, 1996. Synthia Section.
- [63] M. Heuchel, D. Hofmann, and P. Pullumbi. Molecular Modeling of Small-Molecule Permeation in Polyimides and its Correlation to Free-Volume Distributions. *Macromolecules*, 37(1):201–214, 2004.

-
- [64] J. Kruse, J. Kanzow, K. Ratzke, F. Faupel, M. Heuchel, J. Frahn, and D. Hofmann. Free Volume in Polyimides: Positron Annihilation Experiments and Molecular Modeling. *Macromolecules*, 38(23):9638–9643, 2005.
- [65] P. M. Budd, E. S. Elabas, B. S. Ghanem, S. Makhseed, N. B. McKeown, K. J. Msayib, C. E. Tattershall, and D. Wang. Solution-Processed, Organophilic Membrane Derived from a Polymer of Intrinsic Microporosity. *Advanced Materials*, 16(5):456–459, 2004.
- [66] P. M. Budd, N. B. McKeown, and D. Fritsch. Free Volume and Intrinsic Microporosity in Polymers. *Journal of Materials Chemistry*, 15(20):1977–1986, 2005.
- [67] P. M. Budd, K. J. Msayib, C. E. Tattershall, B. S. Ghanem, K. J. Reynolds, N. B. McKeown, and D. Fritsch. Gas Separation Membranes from Polymers of Intrinsic Microporosity. *Journal of Membrane Science*, 251(1-2):263–269, 2005.
- [68] K. Heinrich. GKSS Research Center, Geesthacht, Germany. Personal Communication, 2006.
- [69] M. Böhning and J. Springer. Sorptive Dilation and Relaxational Processes in Glassy Polymer Gas Systems - I. Poly(sulfone) and Poly(ether sulfone). *Polymer*, 39(21):5183–5195, 1998.
- [70] T. Hirose, K. Mizoguchi, and Y. Kamiya. Dilation of Polyethylene by Sorption of Carbon-Dioxide. *Journal of Polymer Science Part B: Polymer Physics*, 24(9):2107–2115, 1986.
- [71] R. G. Wissinger and M. E. Paulaitis. Swelling and Sorption in Polymer-CO₂ Mixtures at Elevated Pressures. *Journal of Polymer Science Part B: Polymer Physics*, 25(12):2497–2510, 1987.
- [72] Y. Kamiya, Y. Naito, K. Terada, K. Mizoguchi, and A. Tsuboi. Volumetric Properties and Interaction Parameters of Dissolved Gases in Poly(dimethyl siloxane) and Polyethylene. *Macromolecules*, 33(8):3111–3119, 2000.
- [73] S. Shenoy, D. Woerdeman, R. Sebra, A. Garach-Domech, and K. J. Wynne. Quantifying Polymer Swelling Employing a Linear Variable Differential Transformer: CO₂ Effects on SBS Triblock Copolymer. *Macromolecular Rapid Communications*, 23(18):1130–1133, 2002.
- [74] D. H. Liu, H. B. Li, M. S. Noon, and D. L. Tomasko. CO₂-induced PMMA Swelling and Multiple Thermodynamic Property Analysis using Sanchez-Lacombe EOS. *Macromolecules*, 38(10):4416–4424, 2005.
- [75] V. I. Bondar, Y. Kamiya, and Y. P. Yampolskii. On Pressure Dependence of the Parameters of the Dual-Mode Sorption Model. *Journal of Polymer Science Part B: Polymer Physics*, 34(2):369–378, 1996.

- [76] P. Goldreich, S. Mahajan, and S. Phinney. Order of Magnitude Physics: Understanding the World with Dimensional Analysis, Educated Guesswork, and White lies. Internet Communication, 1999. <http://www.inference.phy.cam.ac.uk/sanjoy/oom/book.pdf>.
- [77] D. Hofmann, J. Ulbrich, D. Fritsch, and D. Paul. Molecular Modelling Simulation of Gas Transport in Amorphous Polyimide and Poly(amide imide) Membrane Materials. *Polymer*, 37(21):4773–4785, 1996.
- [78] A. Einstein. Elementary Theory of the Brownian Motion. *Zeitschrift für Elektrochemie und Angewandte Physikalische Chemie*, 14:235–239, 1908.
- [79] W. Paul and G. D. Smith. Structure and Dynamics of Amorphous Polymers: Computer Simulations Compared to Experiment and Theory. *Reports on Progress in Physics*, 67(7):1117–1185, 2004.
- [80] D. N. Theodorou. Principles of Molecular Simulation of Gas Transport in Polymers. In Y. Yampol’skii, I. Pinnau, and B. D. Freeman, editors, *Materials Science of Membranes for Gas and Vapor Separation*, book chapter 2. Wiley, 2006.
- [81] A. Hinchliffe. *Molecular Modelling for Beginners*. Wiley, 2003.
- [82] H. Sun and D. Rigby. Polysiloxanes: Ab Initio Force Field and Structural, Conformational and Thermophysical Properties. *Spectrochimica Acta Part A-Molecular and Biomolecular Spectroscopy*, 53(8):1301–1323, 1997.
- [83] D. Rigby, H. Sun, and B. E. Eichinger. Computer Simulations of Poly(ethylene oxide): Force Field, PVT Diagram and Cyclization Behaviour. *Polymer International*, 44(3):311–330, 1997.
- [84] H. J. C. Berendsen, J. P. M. Postma, W. F. Vangunsteren, A. Dinola, and J. R. Haak. Molecular-Dynamics with Coupling to an External Bath. *Journal of Chemical Physics*, 81(8):3684–3690, 1984.
- [85] D. N. Theodorou and U. W. Suter. Detailed Molecular-Structure of a Vinyl Polymer Glass. *Macromolecules*, 18(7):1467–1478, 1985.
- [86] D. N. Theodorou and U. W. Suter. Atomistic Modeling of Mechanical Properties of Polymeric Glasses. *Macromolecules*, 19(1):139–154, 1986.
- [87] Polymer User Guide. MSI/Accelrys Inc., San Diego, 1996. Amorphous Cell Section.
- [88] D. Hofmann, M. Heuchel, Y. Yampolskii, V. Khotimskii, and V. Shantarovich. Free Volume Distributions in Ultrahigh and Lower Free Volume Polymers: Comparison between Molecular Modeling and Positron Lifetime Studies. *Macromolecules*, 35(6):2129–2140, 2002.

-
- [89] D. Hofmann, M. Entrialgo-Castano, A. Lerbret, M. Heuchel, and Y. Yampol'skii. Molecular Modeling Investigation of Free Volume Distributions in Stiff Chain Polymers with Conventional and Ultrahigh Free Volume: Comparison between Molecular Modeling and Positron Lifetime Studies. *Macromolecules*, 36(22):8528–8538, 2003.
- [90] B. D. Malhotra and R. A. Pethrick. Positronium Annihilation Studies of Polycarbonate, Polyethersulfone and Polysulfone. *European Polymer Journal*, 19(6):457–459, 1983.
- [91] J. P. Yuan, H. Cao, E. W. Hellmuth, and Y. C. Jean. Subnanometer Hole Properties of CO₂-Exposed Polysulfone Studied by Positron Annihilation Lifetime Spectroscopy. *Journal of Polymer Science Part B: Polymer Physics*, 36(17):3049–3056, 1998.
- [92] J. Bohlen, J. Wolff, and R. Kirchheim. Determination of Free Volume and Hole Number Density in Polycarbonates by Positron Lifetime Spectroscopy. *Macromolecules*, 32(11):3766–3773, 1999.
- [93] D. Peng and D. B. Robinson. New 2-Constant Equation of State. *Industrial & Engineering Chemistry Fundamentals*, 15(1):59–64, 1976.
- [94] M. Heuchel, D. Fritsch, P. M. Budd, N. B. McKeown, and D. Hofmann. Atomistic Packing Model and Free Volume Distribution of a Polymer with Intrinsic Microporosity (PIM-1). *Journal of Membrane Science*, submitted, 2007.
- [95] M. Heuchel. GKSS Research Center, Teltow, Germany. Personal Communication, 2006.
- [96] R. Paterson, Y. Yampol'skii, P. G. T. Fogg, A. Bokarev, V. Bondar, O. Ilinich, and S. Shishatskii. IUPAC-NIST Solubility Data Series 70. Solubility of Gases in Glassy Polymers. *Journal of Physical and Chemical Reference Data*, 28(5):1255–1450, 1999.
- [97] G. K. Fleming and W. J. Koros. Carbon-Dioxide Conditioning Effects on Sorption and Volume Dilation Behavior for Bisphenol-A-Polycarbonate. *Macromolecules*, 23(5):1353–1360, 1990.
- [98] R. Lima de Miranda, J. Kruse, K. Rätzke, F. Faupel, D. Fritsch, V. Abetz, P. M. Budd, J. D. Selbie, N. B. McKeown, and B. S. Ghanem. Unusual Temperature Dependence of the Positron Lifetime in a Polymer of Intrinsic Microporosity. *Physica Status Solidi (RRL)*, 1(5):190–192, 2007.
- [99] F. Rouquerol, J. Rouquerol, and K. Sing. *Adsorption by Powders and Porous Solids*. Academic Press, 1999.

A Appendix

A.1 Abbreviations

3D-PBC	3-dimensional boundary conditions
CPU	Central Processing Unit
DM	Dual Mode
DGC	Density Gradient Column
DSC	Differential Scanning Calorimetry
FFV	Fractional Free Volume
FFE	Free Volume Element
GCMC	Grand Canonical Monte Carlo
LF	Lattice Fluid Theory
MC	Monte Carlo
MM	Molecular Mechanics
MD	Molecular Dynamics
NET-GP	Non-Equilibrium Thermodynamics of Glassy Polymers
PALS	Positron Annihilation Lifetime Spectroscopy
PI4	6FDA-TrMPD, Polyimide 4
PIM	Polymer of Intrinsic Microporosity
PMV	Partial Molar Volume
PSU	Polysulfone
r.e.s.	Radius of Equivalent Sphere
SD	Site Distribution
STP	Standard Temperature and Pressure

A.2 Selected Notations

symbol	meaning	unit
b	affinity constant (DM)	cm^3/mol
C	concentration	$\text{cm}^3(\text{STP})/\text{cm}^3$
C'_H	Langmuir capacity (DM)	bar^{-1}
D	diffusion coefficient	cm^2/s
f	scaling factor for Langmuir dilation (DM)	
G_0	center of sorption-energy distribution (SD)	kJ/mol
k_D	Henry solubility (DM)	$\text{cm}^3/\text{cm}^3\text{bar}^{-1}$
k_{st}	swelling coeff. of total dilation (NET-GP)	MPa^{-1}
k_{sr}	swel. coeff. of relax. dilation (NET-GP)	MPa^{-1}
N_0	molar number of sorption sites (SD)	mol^{-1}
p^*	characteristic pressure (NET-GP)	MPa
ρ^*	characteristic density (NET-GP)	g/cm^3
ρ_0	density of pure polymer	g/cm^3
ρ_o	obtained density	g/cm^3
ρ_t	target density	g/cm^3
σ_G	width of sorption-energy distribution (SD)	kJ/mol
σ_V	width of size distribution (SD)	cm^3/mol
T^*	characteristic temperature (NET-GP)	K
V_0	initial volume of polymer	cm^3/mol
ΔV	volume change of polymer	cm^3/mol
V_g	'dynamic volume' of penetrant	cm^3/mol
V_h	volume of sorption site (SD)	cm^3/mol
V_{h0}	center of size distribution (SD)	cm^3/mol
V_p	partial molar volume of penetrant	cm^3/mol
V_{id}	volume of ideal gas (STP)	cm^3/mol

A.3 Slices of Packing Models

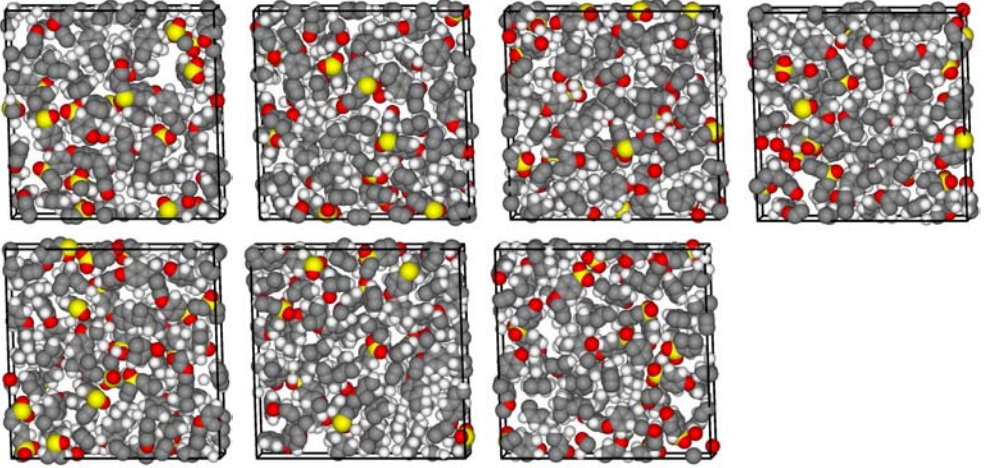


Figure A.1: Slices of one packing model *PSU*, thickness 5.5 \AA and edge length 38.6 \AA .

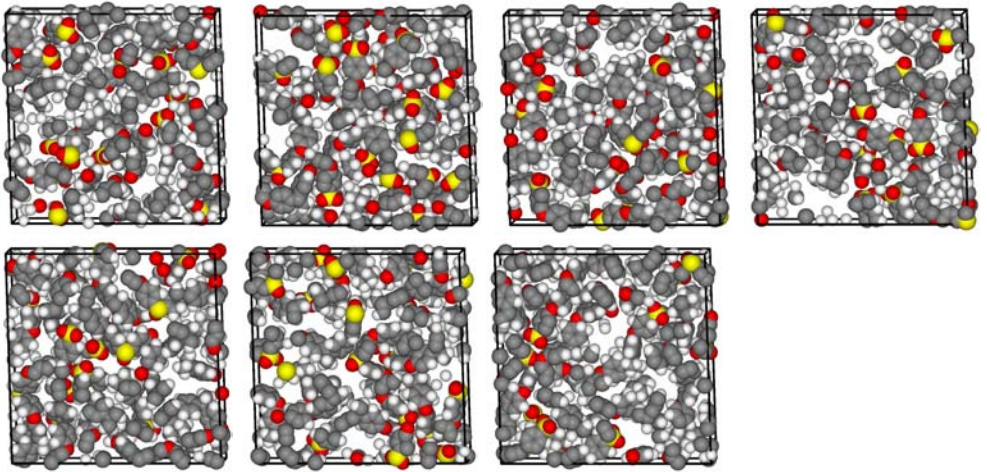


Figure A.2: Slices of one packing model *PSU80*, thickness 5.6 \AA and edge length 39.3 \AA .

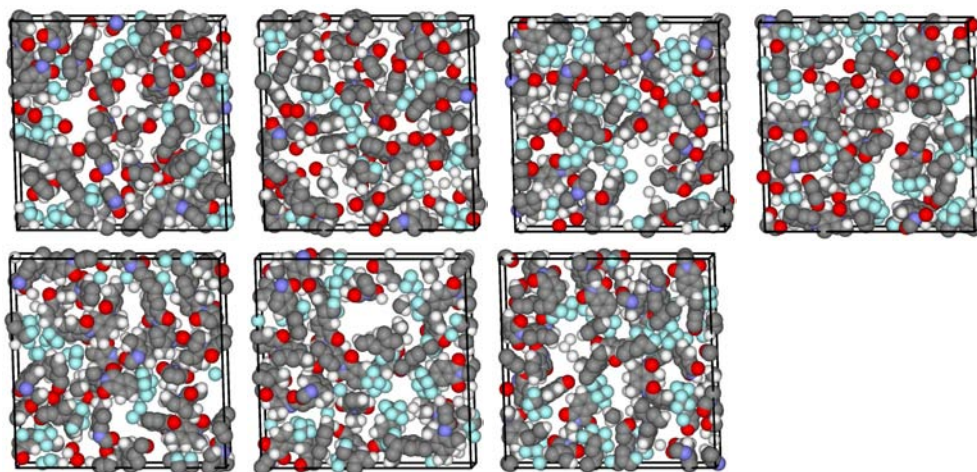


Figure A.3: Slices of one packing model *PI4*, thickness 5.5 Å and edge length 38.8 Å.

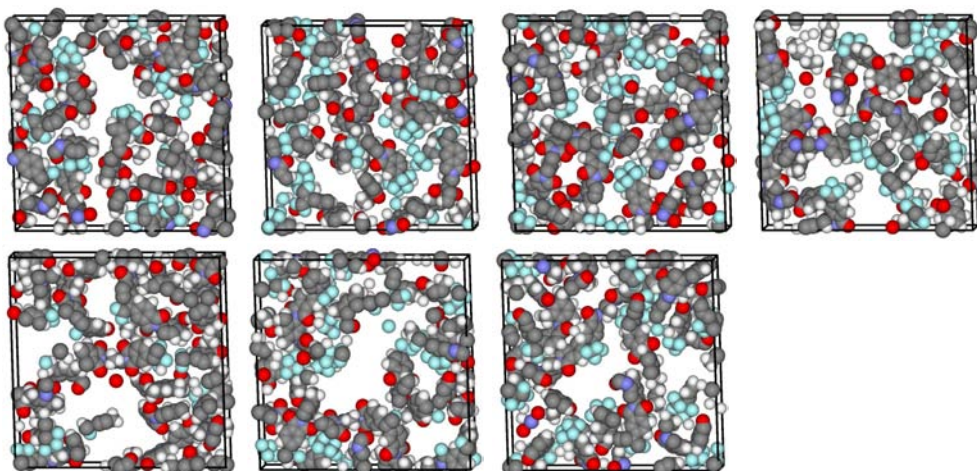


Figure A.4: Slices of one packing model *PI156*, thickness 5.7 Å and edge length 39.8 Å.

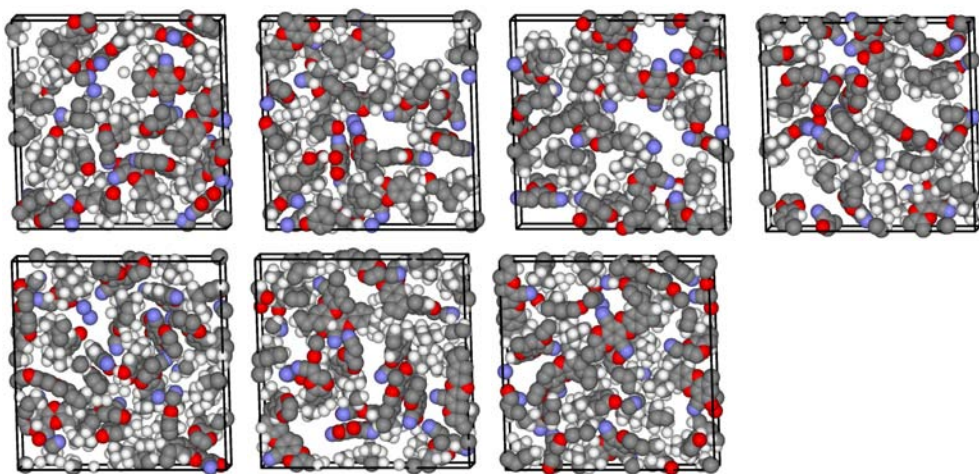


Figure A.5: Slices of one packing model *PIM*, thickness 5.4 Å and edge length 37.7 Å.

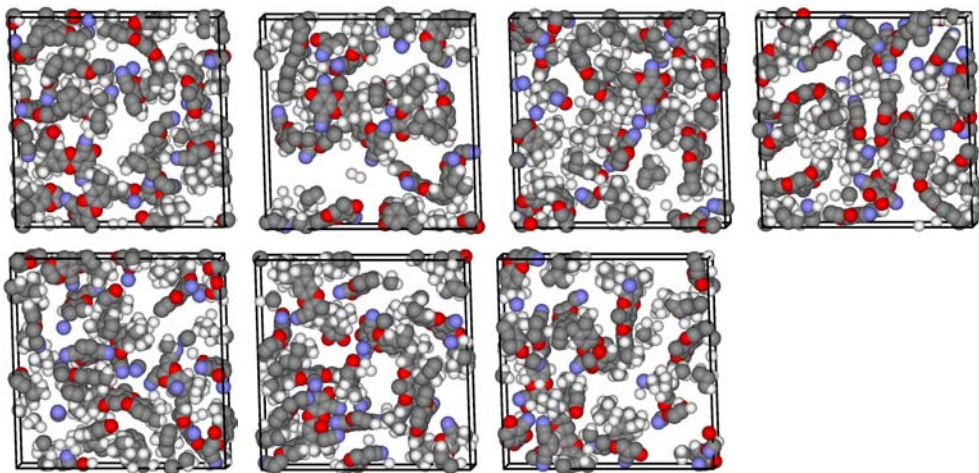


Figure A.6: Slices of one packing model *PIM206*, thickness 5.6 Å and edge length 39.3 Å.

A.4 Rotation Analysis of Bond Angles

To support the qualitative difference of backbone flexibility of the two polymers a rough analysis of dihedral angle rotations was carried out as a ‘scouting’ experiment (the analyzed bonds are indicated by arrows in Figure A.8 (a) and (b)).³ For one packing model of PI4 Figure A.7(a) shows individually for all 80 repeat units (y-axis) of a PI4 backbone chain the change of the dihedral angle for one of the two most ‘flexible’ bonds $\text{--C--C}(\text{CF}_3)_2\text{--}$, during an NpT-MD run of 1000 ps (x-axis) of the pure matrix at 1 bar bulk pressure. Each dot in the graph represents a state where the dihedral angle has changed more than 60° with respect to its initial value at $t = 0$. The value of 60° was chosen to distinguish significant changes from thermal fluctuations.

Four lines parallel to the x-axis can be observed, which represent ‘stable’ changes in dihedral angle which then last over the remaining simulation time. Figure A.7(b) shows a similar plot for a bond $\text{--C--C}(\text{CH}_3)_2\text{--}$ in each of the 94 repeat units (y-axis) of a PSU backbone chain. In comparison to PI4, two observations can be made. There is a larger number of ‘stable’ changes of dihedral angle, and the ‘life time’ of these is in average shorter (reverse-rotations to the initial angle are marked in green). The PSU repeat unit contains eight bonds which are capable of rotation. Of these, the one chosen for the analysis presented in Figure A.7(b), is the least flexible. The repeat unit of PI4 contains four bonds capable of rotation, of which the one indicated in Figure A.8(a) is one of the two more flexible (analysis presented in Fig. A.7(a)). These two bonds were chosen for the comparison to emphasize the difference in mobility of the two polymer backbones. The findings support the statement that the backbone of PSU is more flexible in comparison to PI4. See also reference [3].

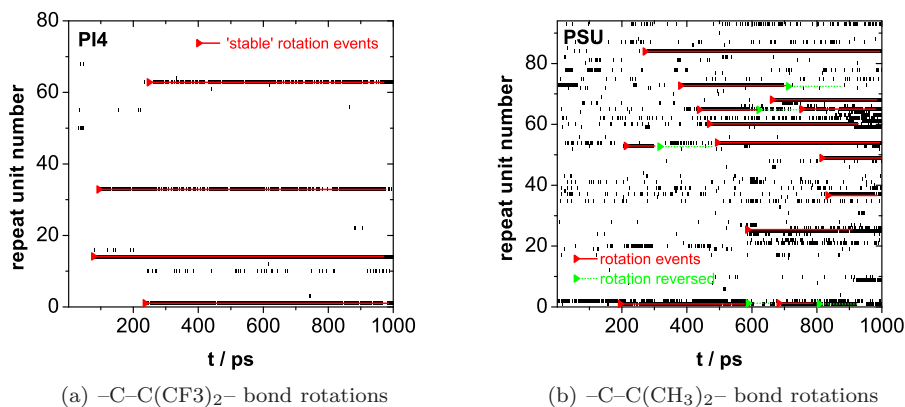


Figure A.7: Visualization charts of dihedral angle rotation events in PI4 (a) and PSU (b). The most flexible angle of each repeat unit (y-axis) was chosen for PI4, and the least flexible one (capable of rotation) for PSU (see Fig. A.8). Changes in dihedral angle ($>60^\circ$) in comparison to the value at $t = 0$ that are 'stable' with respect to simulation time (x-axis), appear as lines parallel to the x-axis. To guide the eye, lines were added to mark some of the rotation events that are considered 'stable' (red). In PSU, some of the bonds rotate back to the initial bond angle (marked green) within the simulation time.

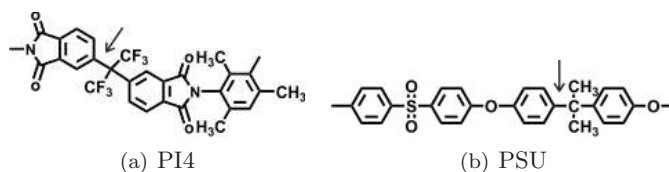


Figure A.8: Chemical structure of (a) 6FDA-TrMPD polyimide (PI4) and (b) poly(sulfone) (PSU). Arrows indicate the analyzed dihedral bonds.

Danksagung

Diese Arbeit ist das Ergebnis eines gemeinsamen Projektes, und ich bin einer Reihe von Leuten zu Dank verpflichtet, die mich bei der Fertigstellung unterstützt haben.

Ich danke Herrn Prof. Dr.-Ing. M. H. Wagner, der sich bereit erklärt hat, diese Arbeit seitens der TU Berlin zu betreuen und zu begutachten.

Prof. Dr. Dieter Hofmann hat sich ebenfalls zur Begutachtung der Arbeit bereit erklärt und stand mir mit seiner Modelling Gruppe des Instituts für Polymerforschung (GKSS, Teltow) in allen Fragen des Simulierens hilfreich zur Seite. Insbesondere die von ihm zur Verfügung gestellten PIM-1 Packungsmodelle haben die Abrundung der Untersuchungen ermöglicht.

Besonderer Dank gilt meinen beiden fachlichen Betreuern Dr. Martin Böhning (BAM) und Dr. Matthias Heuchel (GKSS), die das Projekt bei der Deutschen Forschungsgemeinschaft (DFG) beantragt haben und sich viel Zeit genommen haben, die einzelnen Schritte und Ergebnisse meiner Arbeit mit mir zu diskutieren. Ihre Erfahrungen und Vorarbeiten sowohl hinsichtlich detailliert atomistischer MD-Simulation als auch experimenteller Charakterisierung glasiger Polymere haben wesentlich zum Gelingen dieser Arbeit beigetragen.

Ich danke der DFG für die finanzielle Unterstützung im Rahmen der gemeinsamen Projekte [He2108/2-1] und [Bo1921/1-1], sowie der Bundesanstalt für Materialforschung und -prüfung (BAM), die mich auch im Rahmen ihres Doktorandenprogramms finanziert hat. Ich danke auch Herrn Prof. Dr. J. F. Friedrich (BAM VI.5) und Herrn Dr.-Ing. W. Mielke (BAM VI.3), die sich diesbezüglich für mich eingesetzt haben.

In der Arbeitsgruppe von Priv. Doz. Dr. Andreas Schönhals habe ich mich sowohl fachlich als auch persönlich sehr gut aufgehoben gefühlt. Meine Kollegen Dr. Hao Ning, Diana Labahn und Dr. Harald Goering haben viel zu der angenehmen Arbeitsatmosphäre beigetragen. Auch habe ich mich bei meinen häufigen Besuchen in Teltow in der Kaffeerunde der Modelling Gruppe immer willkommen gefühlt.

Ich danke Dr. Jörg Frahn (GKSS) für die Synthese des Polyimids PI4 und Kathleen Heinrich und Dr. Detlev Fritsch (GKSS) für die Herstellung von PIM-1. Dr. Martin R. Siegert (GKSS) verdanke ich die Ergebnisse der Bindungswinkelanalyse.

Dr. Maria Grazia De Angelis vom Chemical Engineering-Department der Universität von Bologna hat mir beim Verständnis des NET-GP Modells entscheidend weitergeholfen und mir die nötigen Parameter zur Verfügung gestellt.

Mit Andrea Pfitzner konnte ich über die Vorzüge von \LaTeX schwärmen und die Probleme des Layouts lösen.

Auf Annettes Rückhalt und insbesondere ihre Geduld während des Endspurts konnte ich jederzeit vertrauen. Für die Ablenkung zur richtigen Zeit waren unsere Kinder Jorid und Piet zuständig, und meine Mutter hat geholfen die Ablenkung zur unrechten Zeit abzuwenden. Meinen Spaß an der Physik verdanke ich meinem Vater, Physiker und Pädagoge, und ich wünschte, er hätte das noch erleben können.

Lebenslauf

Name: Ole Hölck
Geboren: 06.06.1972 in Kiel
Staatsangehörigkeit: deutsch
Familienstand: verheiratet, 2 Kinder

1978–1979: Hardenberg-Schule in Kiel
1980–1982: Claus-Rixen-Schule in Altenholz
1982–1992: Kieler-Gelehrten-Schule in Kiel
1988–1989: Prosser Highschool, Washington State, USA
Mai 1992: Abitur

Sept.1992–Nov. 1993: Zivildienst

Okt. 1994–Nov. 2000: Physikstudium,
Georg-August-Universität Göttingen
Okt. 1996 Vordiplom Physik
Okt. 1998–Sept.2000: Diplomarbeit am Institut für Materialphysik:
*Aufbau einer Vibrating Reed Anlage zur Untersuchung
der Inneren Reibung kleiner Moleküle in Polymeren
Gläsern*
Betreuer: Prof. Dr. R. Kirchheim

Nov. 2000: Diplom im Studiengang Physik

Jan. 2001–Sept.2003: Wissenschaftl. Hilfskraft, Inst. f. Materialphysik

Feb. 2004–Nov. 2007: Wissenschaftlicher Mitarbeiter der Bundesanstalt
für Materialforschung und -prüfung
Feb. 2004–Nov. 2007: Dissertation:
Gas Sorption and Swelling in Glassy Polymers